ISTANBUL TECHNICAL UNIVERSITY ★ GRADUATE SCHOOL

ADSORPTION OF SHIP-BORNE OIL POLLUTION USING COMPOSITE MATERIALS

M.Sc. THESIS

Noor Khader Hussain HUSSAIN

Department of Disaster and Emergency Management

Disaster Management Programme

JANUARY 2024

ISTANBUL TECHNICAL UNIVERSITY ★ GRADUATE SCHOOL

ADSORPTION OF SHIP-BORNE OIL POLLUTION USING COMPOSITE MATERIALS

M.Sc. THESIS

Noor Khader Hussain HUSSAIN
(801201045)

Department of Disaster and Emergency Management

Disaster Management Programme

Thesis Advisor: Prof. Dr. Didem SALOGLU DERTLI
Thesis Co-Advisor: Assoc. Prof. Dr. Ahmet Alper AYDIN

JANUARY 2024

ISTANBUL TEKNİK ÜNİVERSİTESİ ★ LİSANSÜSTÜ EĞİTİM ENSTİTÜSÜ

GEMİ KÖKENLİ PETROL KİRLİLİĞİNİN KOMPOZİT MALZEMELERLE GİDERİLMESİ

YÜKSEK LİSANS TEZİ

Noor Khader Hussain HUSSAIN
(801201045)

Afet Yönetimi Enstitüsü

Afet ve Acil Durum Yönetimi Ana Bilim Dalı

Tez Danışmanı: Prof. Dr. Didem SALOĞLU DERTLİ
Eş Danışman: Doç. Dr. Ahmet Alper AYDIN

OCAK 2024

Noor Khader Hussain HUSSAIN, an M.Sc. student of ITU Graduate School student ID 801201045, successfully defended the thesis/dissertation entitled "ADSORPTION OF SHIP-BORNE OIL POLLUTION USING COMPOSITE MATERIALS", which she prepared after fulfilling the requirements specified in the associated legislations, before the jury whose signatures are below.

Thesis Advisor :	**Prof. Dr. Didem SALOGLU DERTLI** Istanbul Technical University	.....
Co-advisor :	**Assoc. Prof. Dr. Ahmet Alper AYDIN** Istanbul Technical University	.....
Jury Members :	**Assoc. Prof. Dr. Nalan ERDOL AYDIN** Istanbul Technical University	.....
	Assoc. Prof. Dr. Ahmet TURAN Yeditepe University	.....
	Assist. Prof. Dr. Berrin SAYGI YALCIN Yalova University	.....

Date of Submission : 17 December 2023
Date of Defense : 19 January 2024

To my mother, siblings and friends

FOREWORD

This thesis and the research behind it would not have been possible without the extraordinary support of my supervisor Prof.Dr. Didem SALOGLU DERTLI and my co-supervisor Assoc.Prof.Dr. Ahmet Alper AYDIN whose enthusiasm, knowledge and keen interest in detail have inspired and kept my work on track from the first real beginning of this thesis to the list of references.

In addition, I would like to extend my thanks and appreciation to the Istanbul Technical University who without their support via the scientific research project numbered MYL-2022-43705, this thesis wouldn't have seen the light.

Also, I would like to extend my thanks to all my professors from The Disaster Management Institute for their neverending support during the master's degree program.

Finally and most importantly, I would be remiss in not mentioning my family, and friends. Their faith in me has kept my morale and motivation high throughout the course of writing my thesis.

December 2023

Noor Khader Hussain HUSSAIN
(Mechanical Engineer)

TABLE OF CONTENTS

Page

ABBREVIATIONS

ASTM : American Society for Testing and Materials

BCE : Before Common Era

BET : Brunauer-Emmett-Teller

BJH : Barrett–Joyner–Halenda

BSE : Backscattered Electrons

CAS : Chemical Abstracts Service

CCS : Cold Cranking (Viscosity) Simulator

CFR : Cooperative Fuel Research

DIN : Deutsches Institut für Normung (German institute for standardization)

DSC : Differential Scanning Calorimetry

DTG : Derivative Thermogravimetry

EDS : Energy Dispersive Spectroscopy

EDXA : Energy Dispersive X-Ray Analysis

EPA : Environmental Protection Agency

FTIR : Fourier Transform Infrared

HFO : Heavy Fuel Oil

ICDD : The International Centre For Diffraction Data

IR : Infrared

ITOPF : The International Tanker Owners Pollution Federation Limited

LEL : Lower Explosive Limit

LEPH : Light Extractable Petroleum Hydrocarbons

MPAS : Millipascal-Seconds

NAF : Non-Aqueous Fluids

NIR : Near-Infrared

NOAA : The National Oceanic and Atmospheric Administration

PAH : Polyaromatic Hydrocarbons

PHC : Petroleum Hydrocarbon

PMCC : Pensky-Martens Closed Cup

PPM : Parts Per Million

SBF **:** Simulated Body Fluid

SBM **:** Synthetic Based Mud

SE **:** Secondary Electrons

SEM **:** Scanning Electron Microscope

TGA **:** Thermogravimetric Analysis

TSSA **:** The Turkish Straits Sea Area

UEL **:** Upper Explosive Limit

UNCTAD **:** United Nations Conference on Trade and Development

UV **:** Ultraviolet

VPH **:** Volatile Petroleum Hydrocarbons

WBF **:** Water-Based Fluids

XRD **:** X-ray Diffraction

SYMBOLS

q_e	: Adsorption capacity at equilibrium (mg/g)
q_m	: Maximum adsorption capacity. (mg/g)
q_t	: Adsorption capacity at a given time (mg/g)
C_e	: Solution adsorbate concentration at the moment of equilibrium (mg/g)
C_o	: Initial adsorbate concentration in solution (mg/g)
V	: Volume of solution (ml)
m	: Amount of adsorbent (mg)
K_L	: Surface bonding energy
R_L	: Separation factor
K_F	: Relative adsorption capacity constant (L/g)
1/n	: Surface heterogeneity
A_T	: Temkin isotherm equilibrium binding constant (L/g)
b_T	: Temkin isotherm constant
B	: Heat of Adsorption constant
Q	: The maximum amount of adsorbate per unit mass of the adsorbent (mol/g)
T	: Temperature (K)
ε	: Dubinin-Radushkevich constant
E	: The average free energy value (kJ/mol)
k_{p1}	: The pseudo-first-order rate constant (min^{-1})
k_{p2}	: The pseudo-second-order rate constant (min^{-1})
k_{id}	: The velocity coefficient ($mg.g^{-1}.min^{-1}$)
α	: Adsorption rate
D_c	: The intra-crystalline diffusivity
R	: The particle radius
t	: The reaction time (h)
β	: Adsorption energy constant
R^2	: Correlation coefficient

LIST OF TABLES

Page

LIST OF FIGURES

Page

ADSORPTION OF SHIP-BORNE OIL POLLUTION USING COMPOSITE MATERIALS

SUMMARY

Due to the low cost of maritime shipping, petroleum is often transported by sea which withholds various health, safety, and environmental concerns due to the potential risk of oil spills that might occur throughout the transportation process and although oil enters the seas in many ways, oil tankers and general shipping vessels account for a serious percentage of the total oil spilled in water. The Istanbul and Canakkale Straits are among the busiest and the most dangerous maritime routes, mostly caused by energy transportation, after the Strait of Malacca between the Indian Ocean and the Pacific Ocean. Considering the risks occurred by the geophysical structure of the Bosphorus, it is inevitable to develop an effective treatment and response method to treat and control oil spills using synthetic adsorbents in order to minimize the damage to our ecosystem and protect water quality. The first part of the present thesis has included examining the dimension of ship-borne oil pollution hazards and their causes in the Istanbul Strait. The second part of the thesis consists of the synthesized gum arabic- maltodextrin and aerogel composite material. In order to determine the structural, thermal, morphological, and surface-cross-sectional properties of these synthesized composite materials, FTIR, TGA, DSC, XRD, SEM, and BET analyses was performed. In the third part of the thesis, the adsorption of ship-borned oil using the synthesized materials was investigated and different adsorption isotherms and kinetic parameters were determined.

GEMİ KÖKENLİ PETROL KİRLİLİĞİNİN KOMPOZİT MALZEMELERLE GİDERİLMESİ

ÖZET

Deniz taşımacılığının düşük maliyeti nedeniyle, petrol genellikle deniz yoluyla taşınmakta ve bu durum petrol taşımacılığı süreci boyunca meydana gelebilecek olası petrol sızıntısı riski nedeniyle çeşitli sağlık, güvenlik ve çevresel tehditleri beraberinde getirmektedir. Petrol denizlere birçok yolla girmesine rağmen, petrol tankerleri ve genel nakliye gemileri suya dökülen tüm petrolün ciddi bir yüzdesini oluşturmaktadır. İstanbul ve Çanakkale Boğazları, Hint Okyanusu ile Pasifik Okyanusu arasındaki Malakka Boğazı'ndan sonra, çoğunlukla enerji taşımacılığından kaynaklanan en işlek ve en tehlikeli deniz yolları arasında yer almaktadır. İstanbul Boğazı'nın jeofiziksel yapısının yarattığı riskler göz önünde bulundurulduğunda, boğazlardaki petrol sızıntısının ekosistemimize en az zarar vermesini sağlamak ve su kalitesini korumak için sentetik adsorbanlar kullanarak petrol sızıntılarını arıtmak ve kontrol altında tutmak amacıyla etkili bir arıtma ve müdahale yöntemi geliştirme ihtiyacı kaçınılmazdır.

Sunulan tez çalışmasının ilk bölümünde İstanbul Boğazı'nda gemi kaynaklı petrol kirliliği tehlikelerinin boyutları ve nedenleri incelenmiştir.

Tezin ikinci bölümü sentezlenen Arap zamkı, maltodekstrin ve aerojel kompozit malzemesinin eldesinden oluşmuştur. Sentezlenen kompozit malzemelerin yapısal, termal, morfolojik ve yüzey-kesit özelliklerini belirlemek için FTIR, TGA, DSC, XRD, SEM, ve BET analizleri yapılmıştır.

Tezin üçüncü bölümünde, sentezlenen malzemeler ile gemi kökenli petrol adsorpsiyon ile giderimi incelenmiş, farklı adsorpsiyon izotermi ve kinetik parametreleri belirlenmiştir.

Sunulan tez, sentezlenen malzemelerin ve potansiyel uygulamalarının kapsamlı analizi olarak dört ayrı aşamaya ayrılmıştır. Her aşama, sentezlenen malzemelerin ve potansiyel uygulamalarının derinlemesine anlaşılmasına katkıda bulunmaya odaklanmıştır.

İlk aşamayı oluşturan hazırlık ve sentez sürecinde aerojel, maltodekstrin ve arap zamkının farklı yüzdelerde karıştırılarak üç farklı numune sentezlenmiştir.

İkinci aşamada, sentezlenen malzemelerin pratik adsorpsiyon uygulamaları incelenmiştir. 1 saat, 3 saat, 5 saat, 8 saat ve 24 saatlik beş farklı zaman aralığında adsorpsiyon çalışmaları üç tekrarlı olarak gerçekleştirilmiştir. Sentezlenen malzemelerin deniz suyundan petrol adsorpsiyonu etkinliği üzerine zamanın etkisi ve adsorpsiyon kapasiteleri belirlenmiştir.

Üçüncü aşamada, sentezlenen kompozit malzemelerin kapsamlı bir karakterizasyonu yapılmıştır. Yapısal, termal, morfolojik ve yüzey-kesit özelliklerini belirlemek için FTIR, TGA, DSC, XRD, SEM ve BET analizleri de dahil olmak üzere çeşitli analitik

teknikler kullanılmıştır. Bu karakterizasyon testleri, sentezlenen malzemelerin fiziksel ve kimyasal yapısını anlamayı sağlamıştır.

Dördüncü aşama, Langmuir, Freundlich, Temkin ve Dubinin-Radushkevich modellerini kullanarak sentezlenen malzemelerin adsorpsiyon davranışını saptamak amacıyla adsorpsiyon izoterm modellerini içermektedir. Ayrıca, yalancı birinci mertebe, yalancı ikinci mertebe, Elovich ve Weber Morris adsorpsiyon kinetik modelleri kullanılarak adsorpsiyon kinetiği de bu aşamada incelenmiştir. Bu çok yönlü yaklaşımlar, işlevsel olarak deniz suyundan petrol adsorpsiyon mekanizmalarını anlamayı sağlamıştır.

Saf aerojel karakterizasyon sonuçları incelendiğinde, bir dizi önemli yapısal özellik ortaya çıkmıştır. Yapılan FT-IR analizi, Si-O-Si bağlarının simetrik gerilme titreşimlerini ve serbest Si-OH gruplarının gerilme titreşimlerini açıkça göstermiştir. Sentezlenen saf aerojel, 800 °C'ye kadar termal kararlılık göstermiştir. 100 ile 150 µm ve 0,5 ile 10 µm arasında değişen açık ve küçük gözeneklere sahip olduğu görülmüştür. Bu sonuçlar saf aerojelin başarılı bir şekilde sentezlendiğinin kanıtı olarak ifade edilebilir.

Saf arap zamkının FT-IR ile karakterizasyonunda, glukozid halkasını temsil eden belirgin absorpsiyon bantları ve çeşitli gerilme ve eğilme titreşimlerini temsil eden absorpsiyon bantları gözlenmiştir.

Benzer şekilde, saf maltodekstrinin FT-IR ile karakterizasyonu, O-H gerilme titreşimleri ve lipid C-H gerilme titreşimleri ile uyumlu pikleri göstermiştir.

Sunulan tez çalışmasında maltodekstrin, arap zamkı ve aerojelin farklı oranlarda birleştirilmesi ile sentezlenen S1, S2 ve S3 numuneleri tekil olarak sahip olunan karakteristik pikleri üzerinde taşıdığından, sentezlerin başarılı şekilde yapıldığına kanıt olarak kabul edilmiştir.

Termal gravimetrik analiz, S1, S2 ve S3 örneklerinin bozulma aşamalarına dair önemli veriler sağlamıştır. Sentezlenen tüm numunelerde 200 °C ile 380 °C arasında kütlesel kayıplar olduğu ve 500 °C'de tüm numuneler için yaklaşık %80'lik bir kütle kaybının olduğu açıkça görülmüştür. Diferansiyel termogravimetrik eğrileri, örnekler arasındaki bozulma hızlarındaki çeşitliliği vurgulamış ve S1'in en düşük ve S3'ün ise en yüksek bozulma hızları sergilemiştir.

X-ışını kırınımı sonuçları, SiO2'nin amorf matrisini temsil eden bir desen göstermiştir. Ham aerojelin sentezlenen malzemeler içindeki oranının düşük olması nedeniyle, Si-O kristalin piki S1, S2 ve S3 numunelerinin XRD desenlerinde gözlenmemiştir.

Taramalı elektron mikroskobu sonuçları, aerojel ve arap zamkının maltodekstrine başarılı bir şekilde entegre edildiğini göstermiş, yüksek büyütme görüntülerinin aerojellerin numunelerin yüzeyinde nokta benzeri bir görünüm ile izlenmesi başarılı bir sentezin kanıtı olarak ortaya konmuştur.

BET analizi, saf aerojel, S1, S2 ve S3 örneklerinin yüzey alanlarını aydınlatarak aerojel > S3 > S2 > S1 sıralamasını öne çıkarmıştır. Yüzey alanlarındaki belirlenen bu hiyerarşi, S2 ve S3'ün daha büyük yüzey alanlarını ve büyük bağlama boşlukları/siteleri nedeniyle petrol adsorpsiyonunda önemli bir verim artışına katkıda bulunabileceğini açığa çıkarmıştır.

Adsorpsiyon çalışmaları kapsamında S1-0.25, S1-0.5 ve S1-1.0 numuneleri için belirli zamanlardaki adsorpsiyon yüzdeleri incelenmiştir. S1-0.25'in 3 saat boyunca artan bir adsorpsiyon yüzdesine sahip olduğu, S1-0.5 ve S1-1.0'ın ise 24 saat boyunca yüksek

adsorpsiyon yüzdelerine ulaştığı ve 5 ve 24 saat civarında ise belirgin artışlar gösterdiği saptanmıştır.

Adsorpsiyon izoterm çalışmaları, sentezlenen malzemelerin adsorpsiyon davranışına dair önemli fikirler ortaya koymuştur. RL ayrılma faktörleri, petrol giderimi için Langmuir izoterm modelinin uygulanabilirliğinin Freundlich modeline göre daha düşük olduğunu göstermiştir. S1-0.25, S1-0.5, S1-1.0, S2-0.25, S2-0.5, S2-1.0, S3-0.25, S3-0.5 ve S3-1.0 için RL ayırma faktörleri sırasıyla 0,2857, 0,1667, 0,0909, 0,4384, 0,2807, 0,1633, 0,3933, 0,2448 ve 0,1395 olarak saptanmıştır. Tüm numuneler için RL ayırma faktörleri $0 < RL < 1$ aralığında olduğundan, Langmuir izoterm modelinin sentezlenen numunelerin tamamı için uygun olduğu belirlenmiştir. Ancak, R2 değerlerine göre korelasyon katsayıları dikkate alındığında, Langmuir izoterm modelinin sadece S1 için uyum sağladığı söylenebilir.

S1, S2 ve S3 için hesaplanan karakteristik 1/n heterojenlik faktörleri, Freundlich izoterm modelinin her üç numune için de uygunluğu göstermiştir. Freundlich izoterm modelinin uygunluğunu adsorpsiyon kapasiteleri ve R2 korelasyon katsayılarının yüksekliği belirlemiştir. S1, S2 ve S3 için 1/n heterojenlik faktörleri sırasıyla 0,2983, 0,8383 ve 0,602 olarak hesaplanmıştır. Heterojenlik faktörünün her üç numune için de 0 ile 1 arasında olduğu göz önüne alındığında, Freundlich izoterm modelinin sentezlenen malzemelerle petrol adsorpsiyonunu açıklamak için uygun olduğu anlamına gelmektedir. KF değerleri S1, S2 ve S3 için sırasıyla 2,4519 g/g, 38,282 g/g ve 16, 2032 g/g ve R2 korelasyon katsayıları 0,9995, 0,8368, 0,9188 olarak bulunmuştur. Korelasyon katsayılarının 0,83-0,99 arasında değişmesi, Freundlich izoterm modelinin Langmuir izoterm modeline göre adsorpsiyon mekanizmasını daha iyi açıkladığını göstermiştir.

Temkin izoterm modelinin S1, S2 ve S3 numunelerine uygulanması, bu modelin Freundlich izoterm modeline göre daha düşük korelasyon katsayıları ile daha az uyumlu olduğunu göstermiştir. Temkin modelinin özellikle S2 numunesi için en az uygun olduğunu vurgulamıştır.

Sunulan tez çalışmasında yalancı birinci dereceden, yalancı ikinci dereceden, Elovich ve Weber Morris modellerini kullanarak yapılan adsorpsiyon kinetiği çalışmaları, yalancı birinci dereceden kinetik modeli için 0,81 ila 0,99 arasında değişen yüksek R2 korelasyon katsayılarını göstermiştir. Ancak deneysel ve modelsel adsorpsiyon denge kapasiteleri arasındaki önemli farklar, bu modelin adsorpsiyon hızını ve parametrelerini açıklamada yetersiz olduğunu göstermiştir.

Sentezlenen S1, S2 ve S3 numuneleri için yalancı ikinci mertebeden kinetik modelin uygun olduğu yüksek R2 değerleri ile saptanmıştır.

Elovich modelinin düşük korelasyon katsayıları ile ilişkilendirilmesi, kemisorpsiyonunun ana adsorpsiyon mekanizması olmadığını göstermiştir.

Weber-Morris iç tanecik difüzyonu, sentezlenen poröz adsorbanlardaki adsorbat moleküllerinin gözeneklere difüzyonunu tanımlayan bir kinetik model olup, S3 için farklı kütle transfer mekanizmalarını ifade eden iki ayrı lineer aşama ile gösterilmiştir.

Sunulan tez çalışmasında İstanbul Boğazı'nda gemi kaynaklı petrol kirliliği tehlikelerinin adsorpsiyon yöntemi ile giderimi aerojel, maltodekstrin ve arap zamkı ile sentezlenen numuneler kullanılarak başarılı şekilde gerçekleştirilmiştir. Sentezlenen malzemelerin yapısal, termal, morfolojik ve adsorptif özelliklerine dair yapılan detaylı deneysel çalışmalar, İstanbul Boğazı'ndan alınan ve petrol sızıntısı içeren su numunelerinden petrol adsorpsiyon potansiyeli için umut verici özellikler

olduğunu ortaya koymuştur. Sentezlenen aerojel, maltodekstrin ve arap zamkı kombinasyonu numuneler ile etkili bir petrol adsorpsiyonu yapılmış ve çalışmanın ilgili aşamalarında gerçekleştirilen kapsamlı karakterizasyon ve analiz çalışmaları ile sağlanan temel adsorpsiyon mekanizmalarının detayları belirlenmiştir.

1. INTRODUCTION

Throughout the last 100 years, the share of petroleum and petroleum products in meeting energy demand has increased due to the impact of industrialization and urbanization around the globe. The growing industrialization around the world has made petroleum-based materials integrated into every part of human life (Yurdun, 2018; García-Borboroglu et al., 2008; Akpan & Akpan, 2012; Speight, 2014). For that reason, petroleum is often transported miles away from wells and refineries' locations. Due to the low cost of maritime shipping, petroleum is often transported by sea which withholds various health, safety, and environmental concerns due to the potential risk of oil spills that might occur throughout the transportation process (Matekenya & Ncwadi, 2022; García-Borboroglu et al., 2008). Accidents experienced during the overseas transportation of oil by tankers and negligence in ship management are identified as the two main causes of petroleum-related water pollution. The vast majority of this pollution is manmade and although oil enters the seas in many different ways, oil tankers and general shipping vessels account for a serious percentage of the total oil spilled in water (Chilvers et al., 2021).

The Turkish Straits Sea area (TSSA) which consisted of the Istanbul Strait, the Sea of Marmara, and the Canakkale Strait is one of the most important routes of oil transportation, mainly from the Black Sea, including Khazar Sea, to the Mediterranean Sea. The Istanbul and Canakkale Straits are among the busiest and the most dangerous maritime routes, mostly caused by energy transportation, after the Strait of Malacca between the Indian Ocean and the Pacific Ocean. The TSSA, especially for the last 20 years, turned into one of the most important and key statuses of shipping of the world seaborne oil trade. In the future, parallel to the increase of international trade volume of the Black Sea countries, connected with the Danube-Rhine and Danube-Main inland waterways, the number of companies using the TSSA will continue to increase (Usluer & Oğuzülgen, 2018). Given the fact that The Istanbul Strait is facing the risk of a major disaster at any moment due to the current traffic generated by tankers in the strait and its expected increase, the need for research to reduce oil pollution has been deemed inevitable.

The scope of work is to prepare an intervention procedure using synthetic adsorbents to control and then treat oil spills in order to ensure that the oil spill in the straits causes minimal damage to our ecosystem and protects water quality, considering the scenario of a possible oil spill accident that may occur during the traffic of oil tankers and ships passing through the Istanbul Strait, due to the risks posed by the geophysical nature of the region. Based on this idea, the aim is to develop an effective adsorbent against oil spills that may occur in The Istanbul Strait.

The first part has included examining the dimension of ship-borne oil pollution hazards and their causes in the Istanbul Strait. The second part consisted of obtaining composite materials by adding different additives such as maltodextrin and aerogel to polymeric structures such as Arabic gum which will be synthesized. In order to determine the structural, thermal, morphological, and surface-cross-sectional properties of these synthesized materials, FTIR, TGA, DSC, XRD, BET, and SEM analyses will be performed. During the third part, the synthesized materials will be added to petroleum-related pollutants that are expected to be found in seawaters and the results will be examined.

2. LITERATURE REVIEW

Maritime transportation has always been the dominant support of global trade, dating back to its humble beginnings as Egyptian coastal and river sail ships around 3,200 BCE. By 1,200 BCE, Egyptian ships had traded all the way to Sumatra, establishing one of the world's longest maritime routes at the time. Transport technologies such as the steamship had become ubiquitous and efficient enough to support a complex international trade system by the early twentieth century. The steamship, in particular, enabled economies of scale that were previously unattainable. However, the global regulatory framework did not open up enough to permit a more extensive kind of globalization until the middle of the 20th century (Rodrigue, 2020).

Marine transportation accounts for 80% of global trade (Pratson, 2023). Figure 2.1 shows that over 10 billion tons of solid and liquid bulk cargo containers are transported annually across the world's oceans (United Nations Conference on Trade and Development (UNCTAD), 2020).

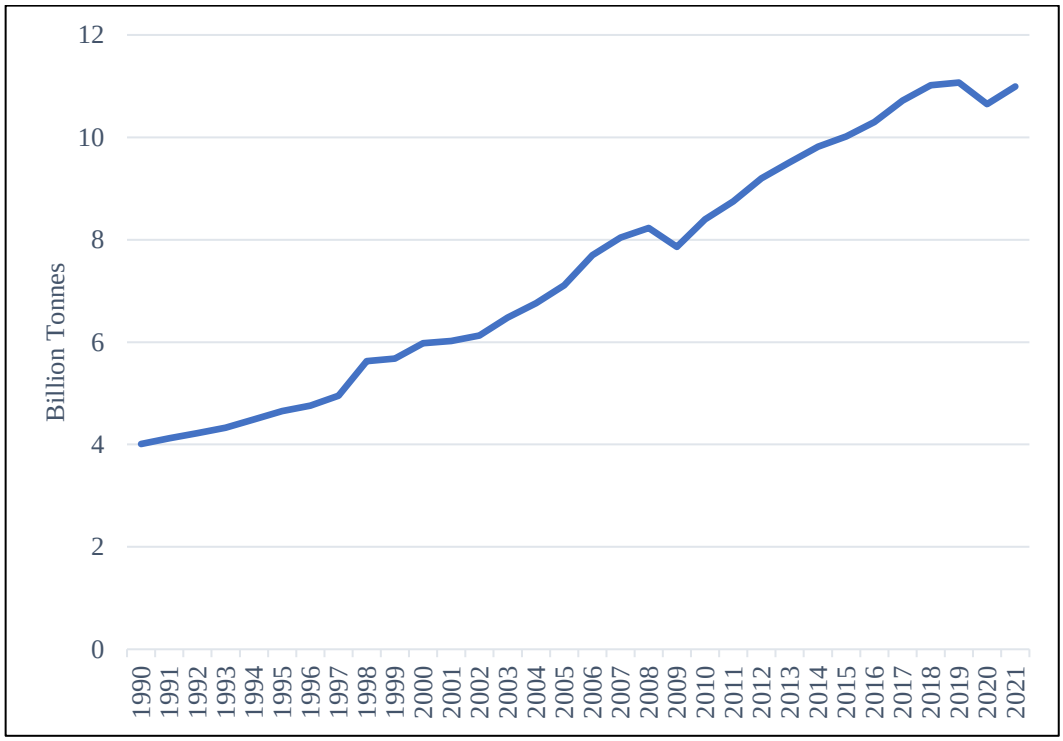

Figure 2.1: Transport volume of seaborne trade from 1990 to 2021 (UNCTAD, 2022).

Referring to Figure 2.1, the sector's continuous growth throughout the years can be observed and according to (UNCTAD, 2022) the maritime trade decreased during COVID-19, however, the maritime trade has recovered by 7 percentage points compared to 2020 and in 2021 the sector has boosted back again and it is expected to grow by 2.1% yearly in the period between 2023 and 2027.

Looking at Figure 2.2, the intensity of maritime routes around the world can be observed along with primary and secondary chokepoints. One of the primary chokepoints is The Strait of Istanbul (Bosphorus Strait) which is in Turkey.

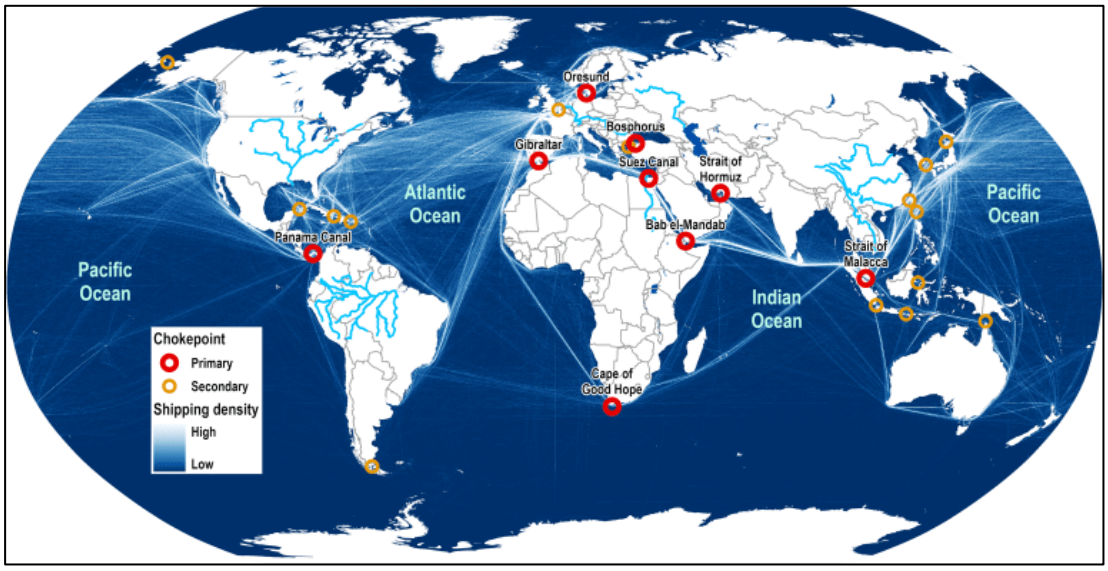

Figure 2.2: Marine transportation main routes and chokepoints (Rodrigue, 2020).

Among the 256 straits existing around the world, The Strait of Istanbul which connects The Black Sea and the Sea of Marmara is one of the most unique straits. Its waterway length is 32 kilometers with an average width of 1.5 kilometers. However, its narrowest width is 700 meters between Kandilli and Asiyan. Regarding the coastlines, the European side coastline is 55 kilometers long while the Asian side is 35 kilometers long which means that the coast of the European side is 36% longer and more concaved (Akten, 2003; İstikbal, 2020).

According to (Notes on The Turkish Straits, n.d) every day, more than 2.5 million people in Istanbul alone participate in maritime traffic via sea transportation and other activities. Not only has the frequency of passenger traffic increased in recent years, but so has the size of vessels and the type of goods. Besides that, the navigation is very congested as Romania, Bulgaria, Ukraine, and Georgia, four of the six riverain countries, have no other access to the global Ocean than the Black Sea. For that reason,

the Bosphorus Strait takes on added significance, and Turkish authorities look for reasons to keep it open at all times (Stefan, & Romanescu, 2010). For example, The Turkish Straits carry about 4% of the world's crude oil commerce (Ayasli et al., 2023). Indeed, the number of oil tankers and other risky cargo ships sailing through the Istanbul Strait has increased. As of 2017, the amount of hazardous cargo in million tons has reached 146.943 million tons which translates to 8832 tankers for the same year (Notes on The Turkish Straits, n.d). A navigational risk assessment of large vessels passing through the Bosphorus Strait has shown that due to the strait's narrow topography and sharp turns, the southern part of the Istanbul Strait is the most dangerous part in terms of movement (Aydogdu, 2022). As a result, the alarming traffic, the challenging topography, and the large amount of oil maritime transportation of The Bosphorus Strait make it one of the most dangerous straits in the world (Notes on The Turkish Straits, n.d).

2.1 Oil Spills

Oil spills take place when petroleum oil is spilled into the water due to an incident including vessel collisions, damage, or due to arising problems with oil platforms and drilling. They can have disastrous environmental effects, harming marine and coastal ecologies, and are difficult to remove. The movement of oil spills is affected by ocean tides, currents, and weather, making them unpredictable (Oil Spills, n.d.). Oil spills originate due to different reasons including collision, stranding, hull damage, equipment failure, fire, explosions, or unknown reasons (Chen et al., 2019). The figure below shows the 20 major oil spills worldwide, including their location and the amount of oil spilled.

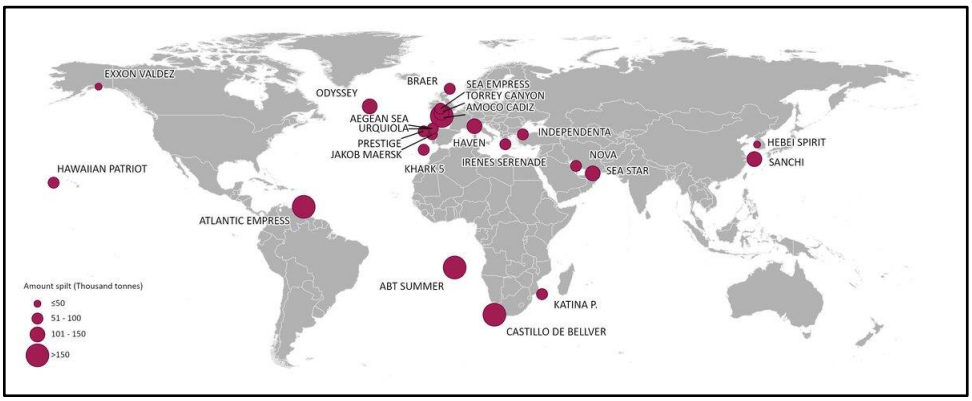

Figure 2.3: Top 20 oil spills around the world (ITOPF, 2023).

According to (ITOPF, 2022), when comparing the number of oil spill incidents between 1970 and 2010, oil spill incidents have reduced by 90% which amounts to 6 incidents per year. As of 2022, There were three major accidents (>700 tones) and four medium spills (7-700 tones). Two of the major breaches happened in Asia, and one occurred in Africa. Spills of middling size happened in North America, Asia, and Africa. This takes the decade average to nearly six leaks (over seven tones) per year. This is comparable to the 2010s norm.

Radar data is commonly used by satellites to identify oil spills, although it can be difficult to locate oil spills because hunting for relatively small patches of oil in enormous oceans is difficult. Identifying oil is extremely challenging because a dark spot on the ocean could be from the incident in question, a natural leak of oil, or a completely different substance. However, once a specific oil spill that has to be tracked is discovered, satellites can be effective in the observation of the source, plotting the extent, and following the leak's route (Oil Spills, n.d.). The table below demonstrates the different used oil spill identification methods.

Table 2.1: Oil spill identification methods (Fingas & Brown, 2017).

Oil Spill Identification Method	Sensing Type
Detection and Mapping of Oil on a Water Surface	Passive Means of Detection and Mapping Optical Techniques Visible Spectrum Infrared (IR) Near-Infrared (NIR) Ultraviolet (UV) Satellites Operating in the Optical Region Image Processing Passive Microwave Sensors
Use of Active Sensors for Oil Spill Detection and Mapping	Laser Fluorosensors Radar Satellites Radar System Radar Image Processing Ship-Borne Radar Oil Spill Detection
Slick Thickness Measurements	Passive Microwave Visual Appearance Infrared Brightness Acoustic Travel Time
Detection of Oil on the Sea Bottom	Ultrasonics Laser Fluorosensors Cameras Chemical Analysis

Not every oil spill is the same, different oils vary in terms of viscosity, volatility, and toxicity. The viscosity of an oil refers to its resistance to flow. The rate at which the

oil evaporates into the air is referred to as volatility. Toxicity describes how toxic, or harmful, oil is to humans or other species. For that reason, the oil spills are group ed based on the oil type that is spilled as shown in the table below (Oil Types, 2020):

Table 2.2: Oil spill types (Oil Types, 2020).

Group Number	Petroleum Type	Description
Group 1	Non-Persistent Light Oils (Gasoline, Condensate)	Highly volatile (should evaporate within 1-2 days). Do not leave a residue behind after evaporation. High concentrations of toxic (soluble) compounds. Localized, severe impacts to the water column and intertidal resources. Cleanup can be dangerous due to high flammability and toxic air hazard.
Group 2	Persistent Light Oils (Diesel, No. 2 Fuel Oil, Light Crudes)	It will leave a residue after a few days. (up to one-third of the spill quantity). The concentrations of toxic (soluble) chemicals are modest. Will "oil" intertidal resources, pose the risk of long-term pollution? Cleaning might be really useful.
Group 3	Medium Oils (Most Crude Oils, IFO 180)	One-third of the liquid will evaporate within 24 hours. Intertidal oil pollution can be severe and long-lasting. The effects of oil on waterfowl and fur-bearing animals can be severe. Cleaning is most effective when done promptly.
Group 4	Heavy Oils (Heavy Crude Oils, No. 6 Fuel Oil, Bunker C)	There is little to no evaporation or disintegration. Intertidal zones are likely to be heavily contaminated. Waterfowl and fur-bearing animals have suffered severe consequences. (coating and ingestion). Long-term sediment pollution is probable. Weather moves slowly. Shoreline cleaning is tough under any circumstances.
Group 5	Sinking Oils (Slurry Oils, Residual Oils)	will sink in the water Oil will behave similarly to Group 4 oil if spilled on the coastline. When oil is spilled over water, it generally sinks rapidly enough to avoid contaminating the coastline. When immersed, there is no evaporation or disintegration. Animals living in bottom sediments, such as mussels, face severe consequences. Long-term sediment pollution is probable. Dredging can be used to remove material from the bottom of a body of water.

2.2 Oil Types and Environmental Effects

As mentioned in the previous section, the oil spill nature is highly reliant on different factors. One of the main factors that contribute to the oil spill nature is the type of oil spilled. In this section, different oil types are demonstrated along with their properties and their environmental behavior.

2.2.1 Biodiesel oil

Biodiesel is a diesel substitute fuel that may be used in diesel engines. It is made from plant oils such as soybean oil, cottonseed oil, canola oil, and maize oil, as well as recycled culinary greases or oils such as yellow grease and animal fats, and different combinations of these feedstocks. Cooking oils are generally plant-based, although they may contain animal fats as well. Used cooking oils may be recycled and regenerated (Alleman et al., 2016). The kind and quantity of vegetable oils utilized as raw materials in biodiesel manufacturing are critical. Because the fatty acid kinds and amounts in the oil utilized indicate the fuel quality of the biodiesel generated (Aktaş et al., 2020). Biodiesels have a relatively low vapor pressure and hence pose less risk of fire. Biodiesels are also significantly lighter than water. (Specific gravity is 0.84-0.90) (Biodiesel Spills Factsheet, 2019).

Biodiesel is frequently referred to as a solvent due to its inherent polarity and high solubility with other oils. Because of its soluble nature, any aquatic fowl that comes into direct touch with recently spilled biodiesel may lose its water repellency due to the loss of its protective oil coating on its feathers. Any sea creature that comes into touch with a biodiesel slick may become covered as well. While it is definitely less harmful than diesel or oil, this coating will have a negative influence on the insulating characteristics of fur or feathers, putting the animals in danger of exposure. Foraging habits will be affected as well. The care of coated wildlife will be identical to that of an oil spill. A series of studies have taken place to investigate the toxicity of biodiesel spilled into surface water. (Of a pond). The concentration necessary to kill 50% of the fish population was 578 ppm, compared to diesel fuel's 27 ppm. The dosage necessary for larval invertebrates (shrimp) was 122 ppm for biodiesel against 2.9 ppm for diesel. Other research has validated biodiesel's decreased toxicity. Even though biodiesel is definitely less toxic than diesel fuel, traditional petroleum spill response and cleaning procedures are anticipated to be applied to control biodiesel spills. (Kass et al., 2021).

2.2.2 Denatured ethanol

Denatured ethanol is a combination of ethanol (grain alcohol) and 2-7% unleaded gasoline that has been combined to make it undrinkable (Denatured Ethanol Factsheet, 2019). Ethanol is a flammable, colorless liquid that is entirely miscible with water. It is heavier than air and has a larger flammable range than gasoline, ranging from 3.3% to 19% for the Lower Explosive Limit (LEL) to the Upper Explosive Limit (UEL).

Pure ethanol has a flash point of 13°C, but denatured ethanol has a substantially lower flash point (-20°C). With a flash point of 36°C, ethanol is nevertheless regarded a flammable liquid in concentrations as weak as 20%. The vapor pressure of ethanol is beyond the flammable range at cooler temperatures (below roughly 10°C). Denatured ethanol is labeled with a flammable liquids placard and the North American 1987 code (Massachusetts Department of Environmental Protection, 2011).

Because ethanol quickly combines with water and swiftly disperses throughout the water column, the effects of an ethanol spill may be large-scale. Ethanol is rapidly biodegraded in surface water bodies (e.g., lakes, ponds, streams, rivers), although biodegradation greatly reduces dissolved oxygen levels in receiving waters. Direct contact with high quantities of ethanol or decreased dissolved oxygen levels in the water caused by ethanol biodegradation can harm fish and other aquatic species. Ethanol introduced into a surface water body will have an influence on the recreational usage of the water body (e.g., fishing, swimming, boating) until the ethanol is destroyed or removed. Anaerobic biodegradation in groundwater can result in the emission of substantial amounts of methane and acetaldehyde, which can reach or surpass the lower flammable limits when combined with air, posing a secondary danger (Narin van Court et al., 2017).

2.2.3 Dielectric fluids

Dielectric fluids are made of mineral oils, silicone fluids, and synthetic esters. Mineral oils are petroleum distillates that include a complex combination of petroleum hydrocarbons (mainly aromatic and aliphatic hydrocarbons) that vary depending on the source of the oil and the distillation method. Naphthenic oil is one of the mineral oils used. These mineral oils are naphthene-rich distillates with saturated hydrocarbon components (C15-C50). They are intended to be chemically inert, stable, and have good thermal and dielectric characteristics (Bejarano et al., 2013; Dielectric Fluids Factsheet, 2019).

Smothering is the biggest risk that dielectric fluid leaks provide to biological resources. Dielectric fluids may result in hypothermia that kills birds due to matted feathers. Large gatherings might pose greater hazards to birds if they are close to the spill. Because of their low to extremely low water solubility (1 ppm), aquatic toxicity, and potential for bioaccumulation, mineral oils, silicone fluids, and ester-based fluids

provide little risk to aquatic resources (fish, invertebrates, and seaweed). Based on their chemical makeup, products made from light petroleum distillates will have certain physical and fate characteristics. The additives used in these items may be the main cause of the environmental risk. Highly biodegradable dielectric fluids may be at risk from the consequences of low dissolved oxygen content, especially if released into remote or shallow water bodies (Bejarano et al., 2013; Dielectric Fluids Factsheet, 2019).

2.2.4 Small diesel

Diesel fuel is a complicated combination created by fractionally distilling crude oil at temperatures between 200 and 350 degrees Celsius. 64% of the hydrocarbons are aliphatic (with carbon numbers primarily in the range of C9–C20), 35% are aromatic (including benzene and polycyclic aromatic hydrocarbons), and 1-2% are olefinic hydrocarbons. Its boiling point is between 163 and 357 °C. According to the type of engine they are used in, diesel fuels are categorized into groups starting with 1-D (high-speed, frequent load change engines) and ending with 4-D (low-speed engines) (Gad, 2014).

When a small diesel spill (500-5000 gallons) takes place, it will often evaporate and dissipate. This holds true even in cold water. As a result, there is rarely any oil on the surface for responders to retrieve. However, marine diesel is frequently a thicker intermediate fuel oil that will last longer if spilled. Diesel oil spreads swiftly on water, forming a thin film of rainbow and silver sheens, with the exception of marine diesel, which may generate a thicker coating of drab or dark hues (Small Diesel Spills Factsheet, 2006).

Diesel is one of the most hazardous forms of oil. Fish and invertebrates may be harmed if they come into close contact with diffused diesel in the water column. Small spills in open water, on the other hand, are so quickly diluted that fish deaths have never been documented. Small spills in restricted, shallow water and streams where weathering and mixing are minimized have resulted in fish fatalities. Small stream fish and invertebrates can be harmed for kilometers downstream of a diesel spill. Expect substantial animal and plant death where bigger volumes of diesel sink into marsh soils. Direct contact has an impact on marine birds. Ingestion while preening or hypothermia from matted feathers cause death. Because of the brief period the oil is

on the water's surface, few birds are directly damaged by small diesel spills. Small spills, on the other hand, might have major consequences for birds given the wrong conditions, such as a spill near a breeding colony (Small Diesel Spills Factsheet, 2020).

2.2.5 Diluted bitumen

Heating separates bitumen from the host rock or sand, reducing its viscosity and allowing it to flow to a collecting site. Once collected, it is combined with a diluent to reduce its viscosity to that of a transmission pipeline. Diluted bitumen refers to such mixes. The composition of diluted bitumen is determined by a number of factors, including the diluent or diluents used and the diluent-to-bitumen ratio. The same types of chemicals are found in diluted bitumen and other crude oils, although their relative abundances vary greatly. These variances are linked to significant disparities in physical and chemical characteristics. Standard studies classify substances into four categories: saturated hydrocarbons, aromatic hydrocarbons, resins, and asphaltenes. Light crude oils, which are the least thick and viscous, contain the most saturated hydrocarbons. Denser and more viscous crude oils have higher quantities of other components, such as resins and asphaltenes, which contain more polar molecules, frequently incorporating "heteroatoms" of nitrogen, sulfur, and oxygen, in addition to carbon and hydrogen (Medicine, Studies, Technology, & Environment, 2016).

Spilled oil in water has an immediate and/or chronic impact on organisms and ecosystems. Following the discharge of the oil, species along the beach may asphyxiate as a result of the floating oil, which impedes photosynthesis and reoxygenation activities. Oiling may cause birds and animals to lose their thermal insulation and buoyant capacities. Some of the substances in dilbit (metals, naphthenic acids, Polycyclic Aromatic Hydrocarbons, and so on) are known to be hazardous to fish (Zhong et al., 2022).

2.2.6 Heavy fuel oil

Heavy Fuel Oil (HFO) is one of the terminologies used to describe a wide variety of marine residual fuels and distillate fuels. Other words that are commonly used include bunker oil, bunker fuel oil, residual fuel, and heavy diesel oil. They all have one thing in common: they are all used aboard ships, and the nomenclature allows HFO to be distinguished from crude oils and other refined products (Fritt-Rasmussen et al., 2018).

HFO is created by blending residue (residual fuel) with cutter stock (distillate diluents, such as marine diesel oil or marine gas oil) to reach, for example, the necessary viscosity at a specified temperature (typically 50 °C, an earlier signal for storage). The physical and chemical features of the HFO will change based on the crude oil origin, the quality or attributes of the crude oil, differences in the distillate added to generate the requisite viscosity, and the various refining operations (Fritt-Rasmussen et al., 2018).

The specific gravity of an HFO can range from 0.95 to more than 1.03. Spilled oil can therefore float, be suspended in the water column, or sink. Small variations in water density can determine whether the oil sinks or floats (Heavy Fuel Oil Spills Factsheet, 2019). On top of that, Heavy fuel oils are among the most troublesome due to their high viscosity which only allows 5-10% of the spilled oil to evaporate. This situation is exacerbated in cold water and throughout the winter months. This implies that they do not naturally disperse or decay, making them extremely persistent. Spills of heavy fuel oils have the ability to travel long distances from the initial spill site, contaminating coasts, and sensitive resources (Heavy Fuel Oil Spills Factsheet, 2019; Ansell et al., 2001).

The most serious threat posed by heavy fuel oil spills to biological resources is suffocation. The primary negative impacts of floating HFO include the coating of animals on the water's surface, the suffocation of intertidal creatures, and long-term sediment pollution. For seabirds, ducks, and fur-bearing marine mammals, direct mortality rates can be substantial, especially when populations are concentrated in limited locations, such as during bird migrations or marine mammal haulouts. Shorebirds, which feed in intertidal settings where oil strands and remains, can be vulnerable to sublethal impacts from polluted or diminished prey numbers (Heavy Fuel Oil Spills Factsheet, 2019; Ansell et al., 2001).

2.2.7 Kerosene and jet fuels

Kerosene is a petroleum distillate mostly composed of C_{10}-C_{16} aliphatic hydrocarbons and aromatics such as benzene and naphthalene. It has a boiling point range of 175-325 ^{o}C. Kerosene can be made by either distilling crude oil (straight-run kerosene) or breaking heavier petroleum streams (cracked kerosene). Raw kerosene possesses qualities that allow it to be mixed with performance additives for use in a wide range

of commercial applications, including transportation fuel (Hodgson et al., 2015; Lam et al., 2012). Jet fuels based on kerosene are classified as non-persistent oil. Jet A-1 fuel contains the following general hydrocarbon compounds: volatile petroleum hydrocarbons (VPH) (C_6-C_{10}), light extractable petroleum hydrocarbons (LEPH) (C_{10}-C_{19}), petroleum hydrocarbon Fraction 1 (F1) (C_6-C_{10}), and PHC Fraction 2 (F2) (C_6-C_{16}) (Feldberg et al., 2013).

Because the components of Jet A-1 fuel are usually extremely volatile, comparatively insoluble, and less dense than water, most of them spread on the water's surface and volatilize fast after a spill. Some components would concentrate and settle into sediments in slower-flowing regions of surface water. Jet A-1 components may biodegrade moderately to rapidly. Plant absorption and bioaccumulation in the aquatic food chain are not thought to be key product fate mechanisms (Feldberg et al., 2013). When there is enough oxygen, kerosene-type fuels are degraded by naturally occurring bacteria in 12 months. Because spills to open water evaporate quickly, aquatic species are rarely exposed, and fish fatalities are rarely documented (Kerosene and Jet Fuel Spills Factsheet, 2019).

2.2.8 Non-Petroleum oil

Animal fats and vegetable oils are governed by 40 CFR 112, which applies to both petroleum and non-petroleum oils. Petroleum oils, vegetable oils, and animal fats all have comparable physical qualities and environmental implications (Vegetable Oils and Animal Fats, 2023; Fingas, 2014). The original rapeseed oil included higher erucic acid, a toxic and unwanted chemical. Canola oil has less than 2% erucic acid content. By weight, around 40% of the seed is oil, with only about 6% being unsaturated fat, the lowest of the vegetable oils. Canola is utilized in industrial lubricants in addition to being a culinary product. Canola oil is presently the most widely used and produced vegetable oil in Canada. It is ranked second in the United States. Soybean oil is another major vegetable oil. Corn oil is the third most significant commercial oil. Because of their unique qualities and applications, many different oils are utilized and delivered. The qualities and behavior of oils are determined by their fatty acid makeup also, it is important to mention that antioxidants are frequently added to the oils (Fingas, 2014).

Many vegetable oils are liquids, lighter than water with a specific gravity of 0.90-0.97, and will float and form slicks initially. Over time, their behavior can vary widely,

depending on oil type, volume, wave energy, temperature, presence of floating debris, etc. Some vegetable oils are solid at ambient temperatures and are heated during shipping; thus, they can solidify once spilled depending on ambient temperatures (Non-Petroleum Oil Spills Factsheet, 2019).

Many non-petroleum oils have comparable physical qualities to petroleum-based oils, such as restricted water solubility. They both cause slicks on the water's surface and generate emulsions and sludges. Furthermore, non-petroleum oils are long-lasting, persisting in the environment for extended periods of time. Non-petroleum oils, like petroleum-based oils, may have both immediate and long-term negative impacts on the environment and can be harmful or even fatal to wildlife. Non-petroleum oils, for example, can reduce the available oxygen required by aquatic species, pollute aquatic life, and coat the hair or feathers of wildlife. When non-petroleum oil is applied to a bird's plumage, the feathers lose their insulating characteristics, putting the bird at risk of freezing to death. Birds can potentially suffocate embryos by transferring oil from the parents' plumage to the eggs. Furthermore, birds and wildlife can absorb oil immediately and may continue to ingest the oil while they eat if their food supply includes non-petroleum oil-contaminated fish, shellfish, or plants. Other negative impacts of non-petroleum oil spills on birds and wildlife include drowning, predation mortality, dehydration, malnutrition, and/or asphyxia (Non-Petroleum Oil Spills Factsheet, 2019; Non-Petroleum Oils, 2022).

2.2.9 Light shale (tight) oil

Tight oil is discovered in the plays of shale formations. Tight oil is lightweight, sweet (low in sulfur concentration), and has properties comparable to standard oil. Hydraulic fracturing (fracking) is the most prevalent method for obtaining tight oil. Drilling downhill for up to 3048 meters to reach the sedimentary rock, then sideways or horizontally for 1.6 km or more, is the initial step. Following that, a high-pressure mixture of water, sand, and chemicals is forced into the wells to cause cracks in the rocks, allowing the trapped oil and gas in the tight layers of shale rock to flow through the drilled wells (Union of Concerned Scientists, 2016).

Light hydrocarbon concentrations can reach 7-8% dissolved gases ranging from methane to butane. If there is an ignition source, light shale oils will easily ignite. The viscosity of light shale oils is extremely low. When poured over water, they swiftly

spread in thin slicks and sheen and disperse throughout the water column. Light shale oils have a specific gravity of 0.7-0.8, compared to 1.00 for fresh water and 1.03 for seawater. These oils do not sink or settle on the bottom of a body of water as free oil. Although the amount of leftover oil is frequently a small percentage of the original spill volume, light shale oils behave similarly to light crude oil. Because of differences in the chemical makeup of the oil source, the aquatic toxicity of light shale oils varies greatly. Aquatic animals may be destroyed if they come into close contact with naturally diffused and entrained light shale oil in the water column. Small spills in open water, on the other hand, may not result in fish fatalities due to fast dilution and evaporation (Light Shale Oil Spills Factsheet, 2019).

2.2.10 Synthetic–Based drilling mud

High-pressure drilling fluids or muds are used to carry waste cuttings to the surface, maintain the well's stability, cool, lubricate, and support a portion of the weight of the drill bit and drill pipe. Water-based fluids (WBFs) and non-aqueous fluids (NAFs) are the two most common forms of drilling fluids. Non-aqueous drilling fluids are classified into three types based on the concentration of aromatics present: type I (High), type II (Medium), and type III (Low). Initially, NAF type I (diesel) was utilized as a foundation for drilling fluids. However, the long-term effects of diesel oil's high toxicity on the benthos within rather extensive areas and up to 6000 m from the platforms resulted in severe limits on the usage of such fluids. After that, NAF type II, which has a mineral or crude oil basis was used. NAF type III—synthetic-base fluids (paraffin, esters) have recently been proposed as a strategy to reduce the negative effects of NAFs. The fauna exhibited symptoms of recovery only after 3 years when fluid type II was employed, but for synthetic-based fluids, type III, the recovery ranged from 4 to more than 11 months (Netto et al., 2009).

The SBF base material typically accounts for 30 to 90 percent of the overall volume of the mud. All SBF systems include emulsifiers, wetting agents, thinners, weighting agents, and gelling agents. The relative amounts of the various elements fluctuate based on the SBF type as well as the chemistry, geology, and depth of the formation being drilled. The main components of all SBF systems are the same. Most SBF base materials (other than olefins) have a higher viscosity than diesel and mineral oils. To address drilling circumstances, the relative proportions of different constituents in the SBF are changed. Other than the base fluids themselves, emulsifiers and wetting agents

(detergents or surfactants) are the most environmentally hazardous of the primary constituents in SBFs. Commercial emulsifiers and wetting agents have unique formulations (Neff et al., 2000).

SBMs enter the maritime environment as a coating on drill cuttings released from drilling platforms, as well as unintentional leaks. Drill cuttings containing less than 5% SBM, do not clump when discharged to the ocean; they disperse and settle over a wide area, preventing the formation of a cuttings pile and hastening biodegradation. Water-soluble component concentrations are unlikely to surpass 1 mg/L at any moment during typical drill-cutting discharges. Because SBMs and their biodegradation products are not harmful to water-column species, there is no risk of direct toxicity from the settling material. Because SBM cuttings agglomerate and settle quickly, the effects of increased water-column turbidity are anticipated to be transient. However, slow-moving and sessile benthic animals inside the deposition zone's footprint are at risk of being suffocated by settling debris (Synthetic-Based Drilling Mud Spills Factsheet, 2019).

3. OIL CLEAN-UP TECHNIQUES

As demonstrated in the previous section, water pollution contributes to the destruction of biodiversity and the rest of the planet which has become a rising worry for various countries in recent years. Oil is a major cause of pollution in the oceans and navigable waterways. Crude oil-based hydrocarbons are responsible for the majority of global environmental pollution. Processing activities in the hydrocarbon oil business emit hazardous aromatic organic chemicals into the environment, including phenolic substances, polyaromatic hydrocarbons (PAHs), chlorophenols, and cresols poisons derived from hydrocarbons that are hardly degradable by nature. On the other side, crude oil leaks have exacerbated oil pollution issues during transportation and storage. As a result, spilled oil causes massive environmental concerns unless it is removed as soon as feasible. Besides that, water source preservation must be a prominent concern in our lives, and required efforts must be taken to eliminate these contaminants (Behnood et al., 2016; Sayed et al., 2021).

A major part of the efforts to remove oil contamination is done by scientists via developing, assessing, and improving various remediation methods and techniques to neutralize the impact of the oil spilled into our environment.

3.1 Biological

The oil spill is degraded using bioremediation technology. It entails the use of biological agents, which are biochemicals or microbes that allow the pace of natural biodegradation to be increased. These biochemicals or microbes are categorized according to the environmental setup they work in, such as those that consume sulfur, known as sulfate consumers, those that function in the presence of air, known as aerobic microbes, and those that work in the absence of oxygen, known as anaerobic microbes. This method is considered efficient from both economic and climate aspects. However, the major disadvantages lie in the fact that it’s time-consuming as well as the oil cannot be recovered by using this method (Hakami, 2020; Hoang et al., 2018; Sayed et al., 2021; Sharma et al., 2021).

3.1 Thermal

This oil spill clean-up technique which is referred to sometimes as in situ burning is a basic method that aims to burn the oil slick on top of the water. This method can mostly be utilized in cold weather conditions or when the slick is thick enough to maintain the combustion. The primary limitations of this technology can be summarized by the influence on human health and the environmental impact of charred by-products as well as the potential risk of resulting in additional flames. Besides that, even though this method's efficiency is estimated around 98%, this method is hard to apply and requires high cost and hard-to-install fire-resistant booms (Hakami, 2020; Hoang et al., 2018; Sayed et al., 2021).

3.2 Chemical

This oil spill clean-up is comprised of techniques like dispersants, solidifiers and demulsifiers that aim towards changing the physical and chemical properties of oil to mitigate the oil spill. These approaches were employed in conjunction with physical techniques to remediate oil spills. Dispersants are variety of surfactants that are used for oil spill management. Surfactants act as a catalyst or agents, settling at the tension interfaces between oil and water. Dispersants can assist to decrease oil from marines by reducing the coating of oil. Whereas solidifiers are the materials that made a physical link with the oil droplet. It is a chemical process in which the oil is converted into a viscous mass by a solidifier. Normally, oil is recovered oil by using boom technology after applying this method. However, it is important to mention that this procedure is mostly used for minor accidents or oil spills booms (Hakami, 2020; Hoang et al., 2018; Sharma et al., 2021). As for demulsifiers, they are organic particles that have two parts: a polar portion that attracts the water phase (hydrophilic) and a nonpolar portion that attracts the oil phase (hydrophobic). they are employed to separate water content in water-in-oil and oil-in-water emulsions at low concentrations. Demulsifiers are commonly classified into four types: nonionic, ionic, amphoteric, and polymer surfactant. Demulsifiers keep oil and water mixtures from forming. Some demulsifiers are polymers, whereas others have nonionic emulsifier structures (Raya et al., 2020). The advantages of chemical techniques can be summarized in the minimal need for manpower and the prevention of oil spills from getting into nearby habitats by breaking up the oil slick and this method provides about

90% cleanup efficiency. However, the downside of this method is that it poisons fish and other marine species as well as the gelatins formed by the demulsifiers expose the marine species to suffocation risks (Sayed et al., 2021).

3.3 Physical

This Technique can be simply described as an act of employing a physical barrier to restrict the spread of an oil spill. In this technique, the chemical and physical properties of the spilled oil remain the same. The methods that are used to control the oil spill include booms, skimmers, and absorbent barriers. The boom approach can either be a fence boom, curtain boom or fire boom. It is employed to prevent the spread of an oil spill. They are primarily determined by wind direction and current characteristics; additional criteria besides wind direction and currents include velocity and wave height. It is commonly used to limit the flow of oil. Whereas skimmers are mechanical devices used to skim oil off the surface of the water. Skimmers are classed based on where they are utilized, such as inshore, offshore, shallow water, or rivers, as well as the viscosity of the oil they are designed to retrieve, such as heavy or light oil (Hoang et al., 2018; Sharma et al., 2021). Skimmers come in a range of configurations, including standalone machines fitted into a vessel or confinement device, as well as units that may work in either a fixed or mobile (advancing) mode. Some skimmers contain storage capacity for collected oil, while some have equipment such as separators to process the recovered oil. Weather factors at a spill site have a significant impact on skimmer efficiency as skimmers work best in calm weather conditions with no ice or debris. After employing skimmers with a high capacity for adsorbing oil and repelling water, adsorbent materials were evaluated as an interest for recovering oil spills at the final cleanup phase (Fingas, 2021). The last type of physical technique is the use of adsorbent materials to turn liquids into semisolids in order to remove oil spills and oil slicks. Adsorbent materials are classified into three types: natural organic products (materials), inorganic sorbent materials, and synthetic materials. Organic adsorbents are derived from biomass such as wood, plants, animals, and naturally occurring materials. Organic adsorbents are chemical byproducts of several chemical industries. Synthetic adsorbents are also made from various sources that are adjusted chemically or physically (Hakami, 2020; Hoang et al., 2018; Sharma et al., 2021). Physical methods provide 90-95% cleanup efficiency and the main advantage of these

methods is that the oil can be recovered which prevents waste and more pollution. Regarding the disadvantages, in sorbents, they become heavier and sink which makes them hard to collect whereas the disadvantage of skimmers is due to their poor efficiency in rough sea conditions and their need for equipment operating on site (Sayed et al., 2021).

In general, studies advise the steps of the oil cleanup process as shown in figure 3.1.

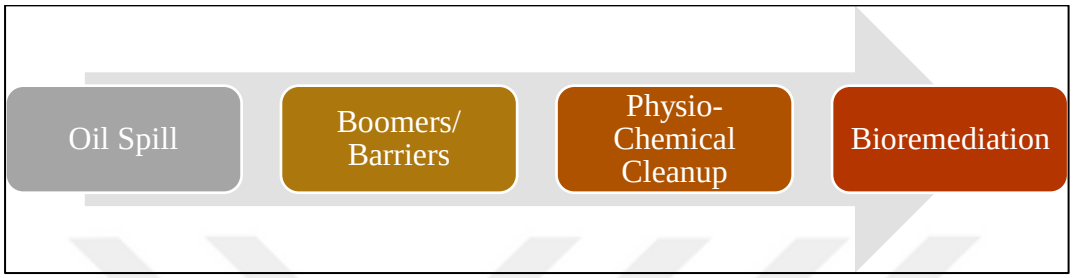

Figure 3.1: Proposed process of complete oil spill clean-up in seawater (Sayed et al., 2021).

3.4.1 Adsorption

The terms clean and recovery are used to describe the cleanup of an oil spill. In the context of an oil spill, clean can be defined as the return to a level of petroleum hydrocarbons that has no discernible influence on an ecosystem's function. The re-establishment of a biological community in which the plants and animal characteristics of that community are present and functioning properly characterizes ecosystem recovery. A sorbent is an insoluble substance or combination of materials used to recover liquids by absorption, adsorption, or both (Rengasamy & Das 2011; Abel et al., 2020). Adsorption is distinguished from absorption by its confinement to the sorbent's surface or interface; upon diffusion past the contact into the sorbent's bulk, absorption occurs. In this context, the discussion will be directed towards focusing on adsorption. In adsorption, the oil is preferentially drawn to the material's surface, whereas absorbents integrate the oil or other liquid to be recovered into the material's body as demonstrated in Figure 3.2. During the absorption phase, the oil is able to infiltrate pore spaces in the solid material body. The vast majority of oil spill response materials are adsorbents; just a handful are real absorbents (Aljammal, 2020).

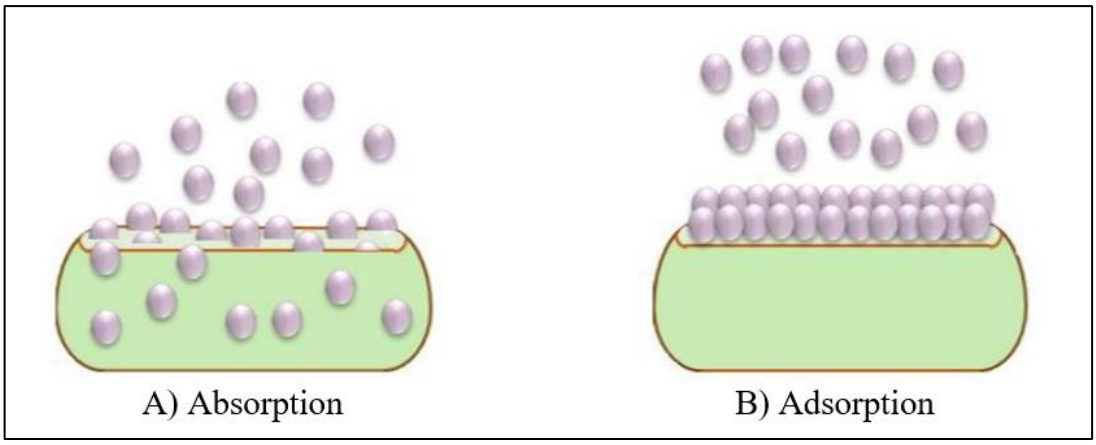

Figure 3.2: Absorption and adsorption demonstration (Aljammal, 2020).

The optimal sorbent material for oil spill cleanup should have the following properties: oleophilicity, durability, reusability, biodegradability, high oil absorption capacity, and high oil selectivity [58]. Sorbents are gaining an edge over other approaches because they are growing quicker, more selective, and have the higher adsorptive ability. This indicates that if these sorbents can be stored and deployed as needed at the size of a huge oil leak near the well site, they may be able to significantly lessen the long-term harm seen with major oil spill events (Patalano et al., 2019).

Adsorption is the physical process through which atoms, ions, or molecules of a liquid (adsorbate) get attached to the surface of a solid (adsorbent). Adsorption happens in three stages. First, the adsorbate diffuses from the main body of the stream to the adsorbent particles' exterior surface. Second, the adsorbate travels to the pores inside each adsorbent particle across a relatively tiny region of the outside surface. Because of the large surface area, the majority of adsorption occurs in these holes. Finally, the contaminating molecule adheres to the surface of the pore. Adsorption on a surface occurs as a result of the adsorbate's individual atoms, ions, or molecules attaching to the adsorbent's surface. Physical and chemical adsorption are the two types of adsorptions. When the molecules of adsorbate and adsorbent get bound together by the Van der Waals, London, or dipole-dipole force, physical adsorption occurs. This adsorption usually occurs at low temperatures, high adsorption rate, and low adsorption temperature, and is not selective. Due to the weak intermolecular attraction, the structure of the adsorbate molecules almost does not change at all, the adsorption energy is small, and the adsorbed substance is easily Decoupled again. Chemical adsorption is a process involving the formation and destruction of chemical bonds. The absorption or release of adsorption heat is greater, and the activation energy required

is also greater compared to physical adsorption. In other words, chemical adsorption occurs when the electron density (high polarity) between the adsorbate and the adsorbent's surface becomes considerable. In fact, physical adsorption and chemical adsorption cannot be considered separately from each other and often occur together (Hakami, 2020; Çöken, 2021). In Figure 3.3. chemical and physical adsorption is demonstrated.

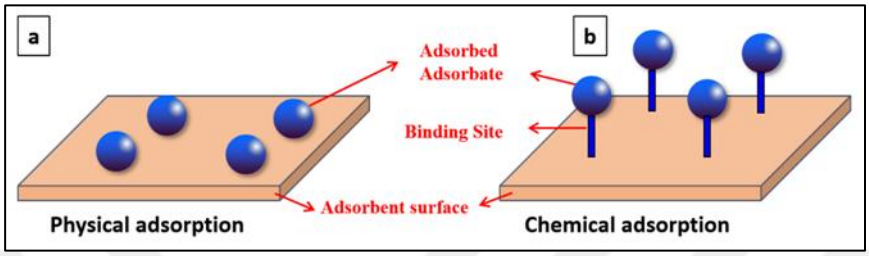

Figure 3.3: a) Physical adsorption and b) chemical adsorption illustration (Ho, 2022).

To wrap up the differences between chemical and physical adsorption with respect to parameters like bonding force types, adsorption heat, activation energy…etc. are shown in table 3.1.

Table 3.1: Chemical and physical adsorption comparison (Basuki et al., 2019).

Parameter	Chemical Adsorption	Physical Adsorption
Type of Bonding Forces	Similar to chemical bond	Van Der Waals
Adsorption Heat	20 – 400 kJ/mol	10 – 40 kJ/mol
Chemical Adsorptive Type	Surface compound formed	None
Reversibility	Irreversible	Reversible. Desorption of adsorbate happens when the activity of the adsorptive in the fluid around the surface decreases.
Activation Energy	High	Low (Near zero)
Temperature Effect	Positive effect to a certain extent	Negative
Specificity of Adsorbate-Adsorbent Interactions	High	Very Low
Multilayer Formation	No	Yes.

When deciding on which adsorbent to be used there are several factors that must be taken into account besides the factors mentioned earlier in this section. These factors are summarized in table 3.2.

Table 3.2: Adsorbent Selection (Aljammal, 2020; Razavi et al., 2014).

Factors Affecting Adsorbent's Selection	Description
Oil Type	even though oils that have higher viscosity get to the pores of the adsorbents at a lower rate (lower penetration velocity), the higher the viscosity of the oil spilled the better it adheres to the surface of the adsorbent.
Adsorption Rate	The absorption rate is directly affected by hydrocarbon type. The lighter the oil product is, the faster the rate of absorption is. Lighter hydrocarbons include gasoline and benzene.
Absorption Rate	The adsorption rate is inversely affected by how light the hydrocarbon is. In other words, the heavier the hydrocarbon the faster the adsorption takes place.
Applicability	Adsorbents are generally applied manually or mechanically and because most of the adsorbents are light materials (especially organic ones), it makes it challenging to apply in windy weather conditions.
Capacity of Adsorption	Adsorption capacity or oil recovery across a wide range of adsorbate concentrations (mass of pollutant adsorbed with respect to adsorbent's mass). This property is directly related to adsorbents with high porosity, homogeneous molecular-sized channels, and a large specific surface area.
Cost and Environmental Aspects	The adsorbent to be used must be feasible and not cause secondary environmental pollution when used to clean up oil spills.

Different adsorbents demonstrate different recyclability specifications. Some are single-use, however, recyclable adsorbents lead to more oil being collected and reduce waste. If recyclability is to be defined, it can be described as the number of times an adsorbent can be used before its capacity drops significantly or it physically dissolves. In light of that context, when an oil spill takes place, recyclable adsorbents mean easier purification and a drastic reduction in the total cost. On top of that, if the collected oil can be recovered at the site, it means a faster cleanup process besides the lower cost (Fingas, 2021). In the last 20 years, scientific research has shown a noticeable increase

in papers published in the area of oil spill cleanup. However, not all cleanup materials had the same share of the published research when looking at the data between 2000-2020. Figures 3.4 and 3.5 demonstrate the number of papers published between 2000-2020 on oil spill cleanup and oil sorbent fields.

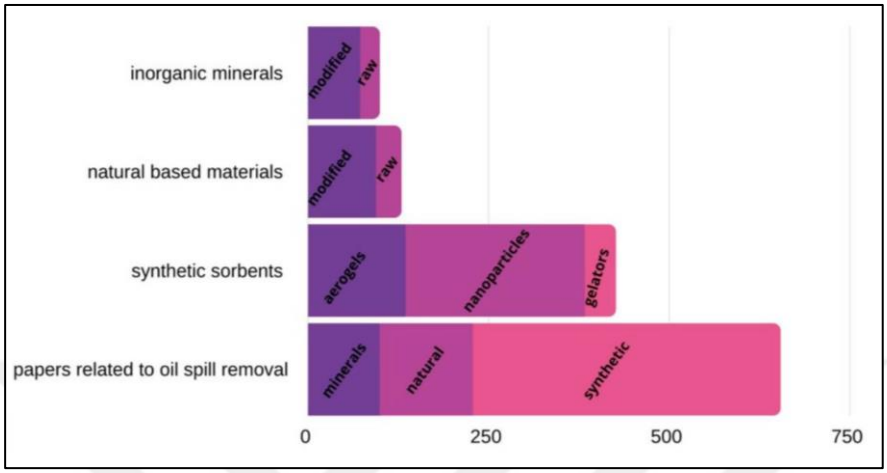

Figure 3.4: Oil spill removal and its related publications (Zamparas et al., 2020).

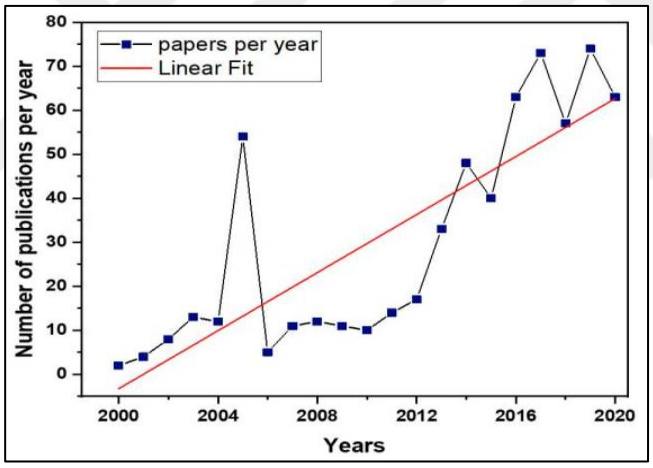

Figure 3.5: Oil spill-related publications/year between 2000-2020 (Zamparas et al., 2020).

Different adsorbent materials have different specifications and with that comes different advantages and disadvantages, the different types of materials with their advantages and disadvantages can be summarized as of below:

A. Organic: The main sources of organic adsorbents are plants and animals. These types of sorbents have increasing popularity due to their feasibility and effectiveness as they have demonstrated good oil adsorbing capacity as synthetic adsorbents. It is worth noting that organic adsorbents can be extracted from animals without causing any harm to the animal. There are various bio-adsorbents being researched at the

moment including Kapok fiber and cotton which have proven good adsorption capacity of low viscosity oil. However, organic adsorbents have their own limitations including a low adsorption rate for high-viscosity oil. Also, when considering an oil spill in an ocean or high-wave environmental setup, it is challenging for organic adsorbents to resist such rough conditions. Finally, organic adsorbents by nature have relatively high hydrophilicity which inhibits their buoyancy (Wolok et al., 2020; Rengasamy & Das, 2011; Bandura et al., 2017).

B. Inorganic minerals: Mineral Adsorbents sometimes referred to as sinking sorbents, are minerals resulting from finely grained highly dense materials that include a large set of different materials such as clay, silica, and zeolites. The use of inorganic minerals for oil spill cleanup has grown popular due to their several advantages like their low cost, chemical inertness, and their availability. Inorganic minerals sink floating oil and their petroleum products' sorption capacity covers a range of 0.2 to 0.5 g/g. However, inorganic minerals have their own disadvantages such as dust formation risk which implies using protective equipment when being applied. Besides that, inorganic minerals function best on land, and they're not preferred as an oil spill cleanup material in water due to their low buoyancy (Bandura et al., 2017).

C. Synthetic: Synthetic sorbents have grown more popular in research over the past 20 years (refer to figure 3.4) as they demonstrated the ability to absorb 70 times their weight. include a wide range of materials such as plastic-like manmade synthetic sorbents including polyurethane, polyethylene, polypropylene, and nylon fibers (Aboul-Gheit et al., 2006). Synthetic sorbents can either be the result of the synthesis of unstructured chemical precursors or from utilizing the porosity of existing materials to form a new sorbent. The synthesis of biomaterials has been showing clear signs of success. Also, the use of aerogel formation to dense biomaterials after applying drying techniques resulted in a more porous material. The main concern regarding the use of synthetic sorbents is the challenges associated with their cleaning process and slow degradability (Raya et al., 2020; Fingas, 2021).

3.4.1.1 Adsorption isotherm

The adsorption isotherm represents the amount of adsorbate that has been absorbed on the adsorbent surface and the pressure when the temperature is constant. Various isotherm models have been made in order to provide information about the adsorption

process, such as the maximum adsorption capacity, surface heterogeneity, and adsorption energetics. The data obtained from experiments are fitted into isotherm models to obtain the optimal fit so as to extract the relevant parameters for a given adsorption system (Salih, 2022). The most commonly used adsorption isotherms are:

Langmuir isotherm: This adsorption isotherm model was originally developed for the identification of gas adsorption in a solid adsorbent such as activated carbon. According to Langmuir's theory, the process of adsorption to a solid surface is based on a kinetic principle that assumes that the adsorption and desorption rates are equal. The Langmuir isotherm model assumes that the adsorption has constant adsorption energy, and constant enthalpies and is homogeneous for each homogeneous molecule. All regions should have an equal affinity for the adsorbate, as well as the adsorbate transition in the surface plane. The nonlinear mathematical expression of the Langmuir isotherm model often expressed as in equation 3.1 (Çöken, 2021; Salih, 2022)

$$q_e = \frac{q_m K_L C_e}{1 + K_L C_e} \tag{3.1}$$

Where q_e is the amount adsorbed onto the unit adsorbent in the equilibrium state mg/g; K_L is the free adsorption energy constant; q_m is the maximum monolayer adsorption capacity mg/g and C_e is the solution concentration in the equilibrium state mg/L (Çöken, 2021). Equation one is rewritten in a linear form as shown in equation 3.2.

$$\frac{1}{q_e} = \frac{1}{q_m} + \frac{1}{q_m K_L C_e} \tag{3.2}$$

Weber and Chakravorti defined a dimensionless constant called separation factor (R_L) that is used to determine the suitability of adsorption to the Langmuir isotherm as in equation 3.3.

$$R_L = \frac{1}{1 + K_L C_o} \tag{3.3}$$

Where C_o represents the initial concentration in mg/L.

By looking at the value ranges of R_L in table 3.3 it is determined whether the adsorption is suitable for the Langmuir isotherm or not.

Table 3.3. R_L values and Langmuir isotherm feasibility.

R_L	Feasibility
$R_L > 1$	Not feasible
$R_L = 1$	Linear
$0 < R_L < 1$	Feasible
$R_L = 0$	Irreversible

Freundlich isotherm: The Freundlich isotherm model is an empirical equation that describes the reversible and non-ideal adsorption process. In contrast to the Langmuir isotherm model, it shows that adsorption is not limited to monolayer adsorption, but multilayer adsorption is also possible with this model. According to this model, in the adsorption process, firstly, the adsorbate occupies stronger binding sites, and then an exponential decrease in the adsorption energy occurs upon completion of the adsorption process. For this reason, the Freundlich isotherm model describes the heterogeneity of the surface and shows that the active regions and the active region energies also have an exponential distribution (Çöken, 2021; Salih, 2022; Majd et al., 2022). The Freundlich isotherm equation is as shown in equation 3.4 (Çöken, 2021):

$$q_e = K_F . C_e^{\frac{1}{n}} \tag{3.4}$$

Where C_e is the solution concentration at equilibrium (mg/L); q_e is the amount adsorbed on the unit adsorbent at equilibrium (mg/g); K_F is the constant expressing the relative adsorption capacity (L/g); 1/n is the heterogeneity factor of the surface (Çöken, 2021). The equation 3.4 is rewritten in the linear form as represented in equation 3.5.

$$\log q_e = \log K_F + \frac{1}{n} \log C_e \tag{3.5}$$

The value of 1/n indicates the intensity of adsorption or surface heterogeneity. By looking at the value ranges of 1/n in table 3.4 the adsorption feasibility of this isotherm model can be determined (Çöken, 2021).

Table 3.4. 1/n values and Freundlich isotherm feasibility (Çöken, 2021).

1/n Values	Feasibility
$1/n > 1$	Not feasible
$1/n = 1$	Irreversible
$0 < 1/n < 1$	Feasible

The irreversibility of the isotherm can be attributed to the fact that the pressure or concentration drops to an extremely low value before the desorption of adsorbate molecules from the surface (Çöken, 2021).

Timken isotherm: This model, which assumes a multilayer adsorption process, overlooks extremely low and extremely high concentration values and only takes into account the adsorbent and the adsorbate interactions. The nonlinearized Temkin isotherm is represented by equation 3.6 (Kalam et al.,2021; Dada et al., 2012).

$$q_e = \frac{RT}{b_T} \ln A_T\, C_e \tag{3.6}$$

The linearized form of equation 3.6 is represented in equation 3.7 (Kalam et al.,2021; Dada et al., 2012).

$$q_e = \frac{RT}{b_T} \ln A_T + \frac{RT}{b_T} \ln C_e \tag{3.7}$$

$$B = \frac{RT}{b_T} \tag{3.8}$$

Where A_T, b_T, R,T and B is Temkin isotherm equilibrium binding constant (L/g), Temkin isotherm constant, universal gas constant (8.314J/mol/K), temperature at 298K and constant related to heat of sorption(J/mol) respectively (Kalam et al.,2021; Dada et al., 2012).

Dubinin–Radushkevich: This isotherm model is an empirical adsorption model usually obtained by applying the adsorption mechanism with Gaussian energy distribution to heterogeneous surfaces. With this model, the adsorption phenomenon is described by the pore filling mechanism and is a semi-experimental equation. It assumes a multilayer adsorption involving Van Der Waals forces applicable to physical adsorption processes and is a basic equation that qualitatively describes the adsorption of gases and vapors to microporous adsorbents (Dada et al., 2012; Çöken, 2021; Inyinbor et al., 2016).

$$q_e = Q_e^{(-\beta\varepsilon^2)} \tag{3.9}$$

$$\varepsilon = RT \ln(1 + \tfrac{1}{C_e}) \tag{3.10}$$

$$E = \frac{1}{\sqrt{2\beta}} \tag{3.11}$$

The linearized form of this isotherm model is shown in the equation below (Dada et al., 2012; Çöken, 2021; Inyinbor et al., 2016).

$$\ln q_e = \ln Q - \beta\varepsilon^2 \quad (3.12)$$

Where C_e refers to the solution concentration in the equilibrium state (mg/L); q_e refers to the amount of adsorbed on the unit adsorbent in the equilibrium state (mg/g); Q refers to the maximum amount of adsorbate per unit mass of the adsorbent (mol/g); E refers to the average free energy value (kJ/mol); Ɛ refers to the Dubinin-Radushkevich constant; T refers to the temperature (K); R: the ideal gas constant (Dada et al., 2012; Çöken, 2021; Inyinbor et al., 2016).

One of the distinctive features of this isotherm model is that it depends on the temperature; therefore, when the adsorption data at different temperatures are plotted as a function of the logarithm of the amount adsorbed against the square of its potential energy, all the appropriate data can be obtained (Dada et al., 2012; Çöken, 2021; Inyinbor et al., 2016).

3.4.1.2 Adsorption kinetics

Adsorption kinetics is the study of chemical processes to understand their speed and the factors affecting that speed. In other words, by applying adsorption kinetics models the rate at which the adsorbate accumulates on the adsorbent surface can be determined. The study of chemical kinetics involves the careful monitoring of experimental conditions that affect the speed of a chemical reaction and therefore help to achieve equilibrium in a reasonable time. Such studies provide information about the possible adsorption mechanism and different transition states leading to the formation of the final adsorbate adsorbent complex and help in the development of appropriate mathematical models to explain the interactions. Once the reaction rates and dependent factors are clearly known, adsorbent materials can be developed for use in industrial applications and the complex dynamics of the adsorption process can be easily understood. The most commonly used models are (Çöken, 2021; Qui et al., 2009):

Pseudo-first-order rate equation: This equation has been developed by Lagergren in 1898. It is said to be the first model referring to the adsorption rate based on adsorption capacity. This model estimates the rate of change in adsorbate uptake at a specific reaction time to be directly proportional to the difference in adsorbate concentration

and rate of removal with time. The developed mathematical representation is shown in equation below (Çöken, 2021; Qui et al., 2009; Musah et al., 2022):

$$\frac{dq_t}{dt} = k_{p1}(q_e - q_t) \tag{3.13}$$

Where q_e is the adsorption capacity at equilibrium in mg/g, q_t is the adsorption capacity at a given time t in mg/g and k_{p1} is the pseudo-first-order rate constant for the kinetic model in min^{-1}. Integrating equation 4 with the boundary conditions as q_t=0 at t=0 and q_t=q_t at t=t results in equation 3.14 (Qui et al., 2009):

$$\ln(\frac{q_e}{q_e - q_t}) = k_{p1}t \tag{3.14}$$

This model is generally applied to the adsorption of pollutants from wastewater. However, it has been found that this model gives reliable results during the first 20-30 min of the adsorption process only given that as the concentration increases the adsorption decreases (Çöken, 2021; Qui et al., 2009).

Pseudo-second-order rate equation: This model has been based on the premise that chemical sorption is the rate-limiting step and predicts behavior over the whole adsorption range. In this case, the adsorption rate is determined by adsorption capacity rather than adsorbate concentration. One significant benefit of this model over first order is that the equilibrium adsorption capacity can be determined from the model; hence, there is no need to assess adsorption equilibrium capacity from experimentation. The mathematical representation of this model is shown in equation 3.15 (Sahoo & Prelot, 2020):

$$\frac{dq_t}{dt} = k_2(q_e - q_t)^2 \tag{3.15}$$

Where q_e and q_t are the amounts of adsorbed per unit adsorbent in mg/g at equilibrium and at any time t, respectively; k_2 is a pseudo-quadratic kinetic model velocity constant. The separation of the variables and then the integration and application of the boundary conditions of q_t = 0 at t = 0 and q_t = q_t at t = t gives the linear expression shown in equation 3.16 (Çöken, 2021; Sahoo & Prelot, 2020):

$$\frac{t}{q_t} = \frac{1}{k_2 q_e^2} + \frac{1}{q_e}t \tag{3.16}$$

K_2 usually depends on the applied operating conditions, 3.16)like the initial adsorbate concentration, the pH of the solution, the temperature and the agitation speed. With this equation, the parameters of the equation are calculated by passing t/q_t against time to the graph (Çöken, 2021).

Both models' rate expressions have been and continue to be widely used in the study of pollutant adsorption from aqueous solutions. The chemisorption process is preferable in the pseudo-second-order model to the pseudo-first-order model because it considers the interaction of adsorbent and adsorbate via their valency forces. The most well-known model for the adsorption of contaminants from aqueous solutions is the pseudo-second-order kinetic model (Ebelegi et al., 2020).

Elovich kinetic model: This model assumes that solid surfaces are energetically heterogeneous and that desorption cannot significantly affect adsorption kinetics at a low surface area. The second assumption is that as the adsorption time increases, the activation energy also increases. The Elovich equation is demonstrated in the equation below (Wang & Guo, 2020; Tan & Hameed, 2017):

$$\frac{dq_t}{dt} = \alpha e^{(-\beta q_t)} \tag{3.17}$$

By integrating the equation above where $q_o = 0$ the following equation will be obtained.

$$q_t = \frac{1}{\beta}\ln(1 + \alpha\beta t) \tag{3.18}$$

The equation above is nonlinear, and it may be solved using either the nonlinear least square regression approach (plot q_t vs t) or the linear method by plotting q_t against $\ln t$. The nonlinear technique, on the other hand, is more complicated than the linear method. The linearized equation is shown below where α represents the initial adsorption rate in mg/g.min and β is the adsorption constant in g/mg (Wang & Guo, 2020; Tan & Hameed, 2017).

$$q_t = \frac{1}{\beta}\ln(\alpha\beta) + \frac{1}{\beta}\ln t \tag{3.19}$$

This model have been used to demonstrate solid-liquid adsorption system. However, the equation above is based on the assumption that $\alpha\beta t >> 1$, which may decrease the accuracy of the Elovich model. with a longer adsorption time (e.g. $t \rightarrow \infty$) The Elovich

equation can be observed to exhibit non-physical behavior caused by neglecting the desorption rate that occurs simultaneously. Therefore, in practice, the applicability of the Elovich equation is limited to the first part of the adsorbate interaction process when the system is relatively far from equilibrium, that is, the adsorbate (Wang & Guo, 2020; Tan & Hameed, 2017).

Weber-Morris particle diffusion model: Adsorption may be divided into three phases in general. First, film diffusion that takes place due to mass transfer of adsorbate from the fluid phase to the adsorbent surface. Second, adsorbate diffuses to adsorption sites via pore or intraparticle diffusion. Lastly, the adsorbate interacts with the adsorption site quickly enough to be ignored when determining the rate-limiting phase during adsorption. The adsorption rate of an adsorbate in intraparticular diffusion is expressed by (Qian et al., 2018):

$$\frac{q_t}{q_e} = 1 - \left(\frac{6}{\pi^2}\right)\sum\left(\frac{1}{n^2}\right)e^{\left(\frac{-n^2\pi^2 D_c t}{r^2}\right)} \tag{3.20}$$

Where, q_t/q_e is the ratio that gives a fractional approach to equilibrium; D_c represents the intra-crystalline diffusivity; r is the particle radius; and t represents the reaction time. Solving the equation above from n = 1 to n = α yields the equations below (Çöken, 2021).

$$1 - \frac{q_t}{q_e} = \left(\frac{6}{\pi^2}\right)e^{\left(\frac{-\pi^2 D_c}{r^2}\right)t} \tag{3.20}$$

The above equation can be rearranged in the form below (Quit et al., 2009).

$$\ln(1 - \frac{q_t}{q_e}) = \left(\frac{-\pi^2 D_c}{r^2}\right)t + \ln\left(\frac{6}{\pi^2}\right) \tag{3.21}$$

Thus, by graphing ln $(1 - \frac{q_t}{q_e})$ against t, the total velocity constant $\left(\frac{-\pi^2 D_c}{r^2}\right)$ can be calculated from the slope (Quit et al., 2009).

The total velocity constant is inversely proportional to the square of the particle radius. Weber and Morris developed a simpler expression to obtain the diffusion rate constant k_i (Quit et al., 2009).

$$q_t = k_{id}t^{0.5} + C \tag{3.22}$$

In this equation $t^{0.5}$ is plotted against q_t and the velocity coefficient k_{id} ($mg.g^{-1}.min^{-0.5}$) is calculated from the slope of the graph (Çöken, 2021).

The Weber and Morris intra-particle diffusion model represents pore diffusion kinetics with a simple approach without taking into account the possible effects of pore sizes. The literature contains shortcomings in these aspects, and there are very few detailed studies of the effect of pore diffusion processes on the removal of pollutants, especially the effects of pore radius and pore size on sorption kinetics (Çöken, 2021).

3.4.1.3 Adsorption thermodynamics

Adsorption may be thought of as a heterogeneous chemical equilibrium. Although this term is not necessarily valid in many circumstances, it is accepted by the adsorption community. As a result, the chemical equilibrium between the adsorption (→) and desorption (←) processes of adsorbate by adsorbent may be described broadly as equation 8 (Tran, 2022).

$$Adsorbent_{(solid)} + Adsorbate_{(liquid)} \rightleftharpoons Adsorbent - Adsorbate_{(solid)}$$

Because adsorption is a temperature-dependent process, the thermodynamic characteristics of adsorption processes are easily assessed. Adsorption experiments involve thermodynamic considerations to determine the spontaneity and feasibility of such processes. As a result, thermodynamic parameters such as Gibbs free energy change (ΔG^o), change in enthalpy (ΔH^o), change in entropy (ΔS^o) and adsorption potential (A) are determined using experimental data obtained from adsorption procedures (Ebelegi et al., 2020).

Gibbs Free Energy of Change (ΔG^o): To assess the spontaneity and practicality of adsorption processes, the Gibbs free energy of change is utilized. Equation 3.23 calculates the changes in the equilibrium constant as the temperature varies (Ebelegi et al., 2020).

$$\Delta G^o = RT \ln K_C \qquad (3.23)$$

where R, T and K_C represent universal gas constant in $Jmol^{-1}\cdot Kg^{-1}\cdot K^{-1}$, Temperature in K and equilibrium constant respectively (Ebelegi et al., 2020).

Entropy Change (ΔS^o): An entropy change while an adsorption process takes place can be calculated using the Vant' Hoff equation, where a positive ΔS^o indicates the adsorbent's affinity for the adsorbate, as well as increased randomness at the

solid/liquid interface and structural changes in the adsorbent and adsorbate (Ebelegi et al., 2020).

Enthalpy Change (ΔH^o): In adsorption research, enthalpy change provides insight about the nature and mechanism of adsorption processes and is often calculated using the Van't Hoff equation. The energy provided as heat at constant pressure while the system accomplishes no extra work is referred to as the change in enthalpy. A calorimeter is primarily used to detect enthalpy change by measuring the temperature change that occurs under constant pressure (Ebelegi et al., 2020).

$$\log K_C = \frac{\Delta S^o}{2.303R} + \frac{\Delta H}{2.303RT} \tag{3.24}$$

Where R, T, K_C are universal gas constant in $Jmol^{-1}\cdot K^{-1}$, temperature in K and distribution coefficient which is C_a/C_e respectively. Where C_a is the amount of adsorbate adsorbed at equilibrium in $mg\cdot L^{-1}$ and C_e is the equilibrium concentration of adsorbate in solution $mg\cdot L^{-1}$(Ebelegi et al., 2020).

Adsorption Potential (A): Adsorption potential is the chemical potential that happens during an adsorption process when an adsorbate molecule travels from solution to the surface of an adsorbent. This parameter may be used to calculate an adsorbent's capacity to adsorb the adsorbate molecules at a certain temperature. Equation 11 can be used to calculate adsorption potential A (Ebelegi et al., 2020).

$$A = -RT \ln \frac{C_o}{C_e} \tag{3.25}$$

Where R represents the universal gas constant in $Jmol^{-1}\cdot K^{-1}$, T is the absolute temperature when the sorption happens, C_o and C_e are initial and final concentration of the adsorbate solution in $mol\cdot mg^{-1}$ (Ebelegi et al., 2020).

3.5 Characterization Analysis of Synthesized Adsorbent

3.5.1 Fourier transform infrared spectroscopy (FTIR)

FTIR stands for Fourier Transform Infrared spectroscopy. It is an analytical technique used to identify organic or inorganic compounds. The IR spectrum can be viewed as a fingerprint of substances where absorption peaks corresponding to the frequencies formed by the vibration of the bonds between the atoms that make up the substance.

Every substance has its own spectrum. The only exception to this is optical isomers (Buyuksirt & Kuleaşan, 2014).

A spectrophotometer is a device used to determine a compound's absorbance spectrum. The IR spectrum is provided by the Fourier transform spectrophotometer faster than ordinary spectrophotometers. It generates an infrared radiation beam from a blazing black-body source, which is subsequently processed by an interferometer for spectral encoding. The interferometer combines beams with varied path lengths to produce an interferogram, which is composed of constructive and destructive interference (Mohamed et al., 2017).

The beam next enters the sample compartment, where the sample absorbs certain frequencies of energy that are unique to itself, as depicted in the interferogram. The detector measures the special interferogram signal for all frequencies at the same time. A reference beam is also placed to act as a backdrop for the instrument's functioning (Mohamed et al., 2017).

Using Fourier transformation computer software, the required spectrum is generated by automatically removing the background spectrum from the sample spectrum. The FTIR spectrometer produces an IR spectrum that is generally in the mid-IR range, spanning from 4000 to 400 cm^{-1}. Transition energies related to changes in vibrational energy state for distinct functional groups are found in this area. The existence of particular functional groups inside the molecule can be determined by studying absorbance bands in this area. FTIR can typically evaluate four bond-type areas. Single bond, double bond, triple bond, and fingerprint area are seen between the wavelengths of 2500-4000 cm^{-1}, 1500-2000 cm^{-1}, 2000-2500 cm^{-1} and 650-1500 cm^{-1} respectively (Mohamed et al., 2017).

Infrared spectra are used to answer questions about diverse substances. The identification of molecules contained in a particular sample, also known as unknown analysis, is a frequently asked question. Peak positions in an infrared spectrum correspond to molecular structure, making infrared spectroscopy useful. A large number of infrared spectra have been collected throughout the last century, allowing the use of peak locations from known compounds to identify chemicals in unknown samples (Smith, 2011).

The goal of a spectral comparison, also known as identification testing, is to identify whether two samples are the same. The unknown spectrum is compared to a reference spectrum, and the similarities in peak locations, heights, and widths between the two spectra are observed. Comparing spectra is less difficult than understanding an unknown spectrum, but it still requires appropriate execution. The estimation of molecule quantities in a sample is another question that an infrared spectrum can answer. To do this, the spectra of samples with known concentrations must be measured and Beer's Law used to build a calibration line that connects absorbance to concentration. Once created and confirmed, the calibration may be used to determine the amounts of molecules in unknown samples (Smith, 2011).

3.5.2 Thermogravimetric analysis (TGA)

TGA is a method used in materials science and analytical chemistry to investigate a sample's thermal behavior. It entails weighing a sample while subjecting it to controlled temperature fluctuations in a controlled setting (Jing et al, 2002; Ebnesajjad, 2011).

A tiny sample of the material is put on a sensitive balance inside a furnace in a typical TGA experiment. The temperature is then progressively raised or lowered while the sample weight is constantly checked. Weight changes are recorded and plotted against time or temperature (Saadatkhah et al., 2020; Ebnesajjad, 2011).

TGA gives vital information on different thermal processes such as breakdown, desorption, oxidation, and other chemical reactions by assessing the weight loss or gain of the sample as a function of temperature. It may be used to calculate parameters such as reaction start and completion temperatures, reaction kinetics, and sample composition (Jing et al., 2002).

TGA is frequently used to examine heat stability, degradation, and material composition in domains such as polymers, medicines, catalysts, and materials science. It aids researchers in understanding the behavior of materials at various temperatures and gives insights into their qualities and performance.

3.5.3 Scanning electron microscopy (SEM)

The Scanning Electron Microscope (SEM) is a flexible and sophisticated equipment used to study surface phenomena in a variety of materials. SEM exposes materials to

high-energy electrons, and the released electrons and X-rays are examined. These emissions reveal information on the topography, morphology, composition, grain orientation, and crystallographic structure of the material. The scanning electron microscope (SEM) is a sophisticated equipment that can provide very detailed visual pictures with spatial resolution as fine as 1 nanometer and magnifications of up to 300,000 times (Akhtar et al., 2018).

SEM has great usefulness for evaluating sample qualities including crystallography, magnetism, and electrical features despite its concentration on surface viewing. Additionally, it may spot morphological alterations brought on by surface adjustments to the material. SEM provides qualitative data on the topography, morphology, composition, and crystallography of a material. It explores particle size, shape, arrangement, and texture as well as surface characteristics. Additionally, SEM can identify the ratios and atomic arrangements of the elements and compounds present in the sample, even how a scanning electron microscope (SEM) works (Akhtar et al., 2018).

The SEM uses an electron cannon to create an electron beam that is focused using orifices and lenses and aimed towards the object being studied. In order to assist scatter products, the ray scans the instance's face and creates a picture similar to what would appear on a television screen inside of a vacuum. When electrons strike the instance, vibrant signals are created, some of which may be used for compositional analysis and others for imaging. Due to their low energy, secondary electrons (SEs) disclose face geomorphology, but backscattered electrons (BSEs) exhibit compositional disparity based on infinitesimal number. Despite showing relative differences, BSE pictures are brilliant where tiny figures are high and black where they are low (Frahm, 2014; Mohammed, & Abdullah, 2018).

Emission of X-rays when an electron collides with anything allows for element identification. EDS instruments measure these X-rays to ascertain their chemical makeup. EDS systems, sometimes referred to as EDX or EDXA, are typically used in SEMs and are used to analyze distinguishing X-rays at precise strengths matching to rudiments. Some trace rudiments generate weak signals, and some EDS gamuts can have coincident peaks. Small areas are the focus of SEM-EDS for crucial analysis, producing focused data and allowing the examination of millisecond samples or facial alterations. It may be used for fusions, element distribution mapping, and picture

construction using X-ray measurements (Frahm, 2014; Mohammed, & Abdullah, 2018).

3.5.4 X-ray diffraction (XRD) analysis

A nondestructive method for examining the chemical make-up, physical characteristics, and crystallographic structure of materials is called X-ray diffraction analysis (XRD). It is dependent on X-ray interference with a crystalline sample. Charged particles are accelerated and directed towards the material to produce X-rays, which are then detected and analyzed. Each material's chemistry and organization determine the specific diffraction pattern that results from the intensity at various angles. The pattern is impacted by flaws in the sample, including compositional differences and crystal imperfections. For phase identification, XRD patterns are compared to databases like ICDD. Sharp peaks imply bigger crystallites, whereas wide ones suggest smaller ones, and peak features, including peak breadth, disclose nanoparticle qualities (Ali et al., 2022; Raja et al., 2022).

3.5.5 Differential scanning calorimetry (DSC)

Differential surveying calorimetry (DSC) is a thermal analysis technique used to acquire data on the thermal history of items. It operates in a variety of disciplines, including polymers, medicinals, ceramics, and biomaterials. In a controlled environment, DSC monitors heat influx linked to structural changes (unformed or liquid transitions) in materials as temperature and time vary. When the sample undergoes transitions, heat is exchanged with the sample pan to maintain temperature (Raju et al., 2022; Fatahi et al., 2022).

The DSC instrument comprises several components (Raju et al., 2022; Fatahi et al., 2022):

A. Heat Source: Provides constant heating rate to the sample.

B. Sample Holder: Consists of two pans – one for the sample and the other as a reference.

C. Chamber: Operates under vacuum or nitrogen gas to control the sample's environment.

DSC provides quantitative and qualitative insight into a variety of physical and chemical changes, including endothermic or exothermic processes and alterations in the heat capacity of materials. Temperature or time variations are used to detect differences in heat influx between a sample and a reference material. Throughout the dimension, the sample and the reference are kept at the same temperature, and the energy needed to keep this temperature balance is noted. DSC analysis provides valuable information about the thermal stability, phase transitions, and reaction kinetics of materials (Raju et al., 2022; Fatahi et al., 2022).

3.5.6 Brunauer-Emmett-Teller (BET)

The Brunauer-Emmett-Teller (BET) theory seeks to explain how gas molecules physically adhere to a solid surface. It serves as the essential underpinning for an important analytical method that is employed to ascertain the precise surface area of materials. Non-reactive gases are frequently used as probing agents in the BET theory to measure the material's specific surface area. This theory is applicable to systems that include the adsorption of many layers. Nitrogen is the gas that BET techniques most typically employ for surface probing. As a result, the normal BET analysis is usually carried out at nitrogen's boiling point. Surface area may also be measured at different temperatures and scales by using additional probing agents such argon, carbon dioxide, and water. There isn't a single, objectively correct figure for the particular surface area because it depends on the scale of measurement. Consequently, the adsorbate molecule selected, and its adsorption cross section may affect the specific surface area calculations based on the BET theory (Nasrollahzadeh et al., 2019)

4. MATERIALS AND METHOD

4.1 Materials

In this thesis, Arabic gum, Maltodextrin and Aerogel have been used to synthesize an adsorbent that adsorbs oil that is spilled in water. In the subsections 4.1.1, 4.1.2, 4.1,3 and 4.1.4. the specification of the aforementioned materials will be demonstrated.

4.1.1 Aerogel

Aerogel properties vary depending on the specific composition and manufacturing process used. Different types of aerogels, such as silica, carbon, or polymer-based aerogels, may exhibit variations in properties and applications (Moheman et al., 2021). The aerogel used during the course of work was prepared by using the sol-gel method where raw sodium silicate was diluted with distilled water at a molar ratio of 0.4:1.0 (v/v); 1 Macetic acid solution was then added dropwise until gelation occurred. To reinforce the gel structure, the gelling aerogels were aged at 40°C for 1 hour. Following the aging process, the gels were subjected to solvent exchange by immersing the produced gel in an ethanol/n-hexane solution (v/v:1/1) at room temperature. The gels were silylated in hexane for 24 hours at room temperature with a 6% silylating agent. The silylated gel was dried at 50°C for 1 hour and at 225°C for 1 hour. The aerogel production yield was estimated by gravimetric analysis under the synthesis condition. The synthesized aerogel formation yield was estimated to be between 42% to 81% (Ozcan et al., 2022).

The synthesized aerogel has a specific surface area of 875.6 m^2g^{-1} and contained big open pores and small pores with widths ranging from 100 to 150 μm and 0.5 to 10 μm respectively. Furthermore, it was noticed that the huge number of 0.5 - 0.1 μm-sized subnetworks grow in the pores, covering the whole surface contributes to providing a homogeneous area. Regarding thermal stability, the synthesized aerogel have shown high thermal stability till 800 ^oC (Ozcan et al., 2022).

4.1.2 Maltodextrin

Maltodextrin is a common food additive and carbohydrate often used as a thickener, filler, or preservative in a wide range of food and beverage products. Its specifications may vary depending on the intended application and the manufacturer. The maltodextrin that has been used in this thesis has been bought from Sigma-Aldrich company with dextrose equivalent of 8.0-15.0 with CAS number of 9050-36-6. With a chemical structure shown in figure 4.1.

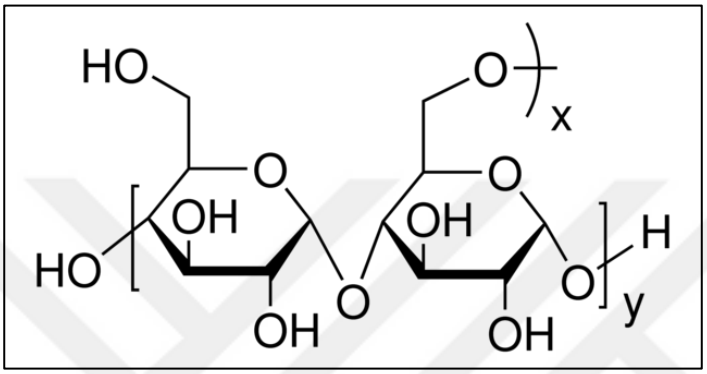

Figure 4.1: Chemical structure of Maltodextrin.

The physical and chemical specifications of the maltodextrin used are shown in the table 4.1.

Table 4.1: Maltodextrin specifications.

Test	Result	Specification
Color	Colorless or white	White
Form	Powder	Powder
Loss on Drying	≤ 7.5 %	4.6 %
Sulfated ash	≤ 0.5 %	0.3 %
IR Spectrum	Conforms to Structure	Conforms
Viscosity (Rotation)	10 - 20 MPAS	17 MPAS
Viscosity (Conditions)	-	50% IN H2O AT 20 C, DIN 45, 100 S- -1
Miscellaneous Tests	Reducing matter (as glucose, Calc. On dried substance): 8.0 - 15.0%	Reducing matter (as glucose, calc. On dried substance): 13.2%

4.1.3 Arabic gum

This material (E414) bought from Tito having CAS number of 9000-01-5, often known as gum arabic, acacia gum, gum arabic, or gum arabic, is a natural polysaccharide derived from the tropical African plants Acacia senegal and Acacia seyal. When the tree's bark is sliced, it makes gum to fill the spaces, and this process (gummosis) takes around 38 weeks. Arabic gum is a carbohydrate polymer that is partly digested in the large intestine. The energy content of arabic gum is less than half that of starch and maltodextrin. Arabic gum is a complex combination of arabinogalactan oligosaccharides, polysaccharides, and glycoproteins. Sugar content after hydrolysis. The Arabic gum used is a brown powder that has no smell with a particle size of 160 μm. A 40 g of Arabic gum dissolves in a 100 ml of water. It contains: Galactose 35%-45%, Arabinosis 25%-45%, Rhamnosis % 4-13 and Glucuronic Acid 6%-15%. The average molecular weight is 350000, the pH of the 25% solution is 4.4, intrinsic viscosity 12 ml/g and a total ash (Potassium, Calcium & Sodium salts) of 3%-4%.

4.1.4 Diesel oil

The diesel oil used in this thesis is bought from Castroll company with technical specifications shown as of below.

Table 4.2: Diesel specifications.

Name	Method	Units	Castrol MAGNATEC Diesel 10W-40 B4
Density @ 15C, Relative	ASTM D4052	g/ml	0.869
Viscosity, Kinematic 100C	ASTM D445	mm^2/s	14.4
Viscosity, CCS - 25C (10W)	ASTM D5293	mPa.s (cP)	6396
Viscosity, Kinematic 40C	ASTM D445	mm^2/s	98
Viscosity Index	ASTM D2270	None	152
Pour Point	ASTM D97	°C	-36
Flash Point, PMCC	ASTM D93	°C	203
Ash, Sulphated	ASTM D874	wt%	1.1

4.2 Methods

The first part consisted of synthesizing material composed of aerogel, Arabic gum and maltodextrin. Using the mentioned materials, three samples were made based on different mixing percentages in order to assess which one will provide better adsorption percentage. The percentages of the samples prepared are shown in table 4.3.

Table 4.3: Sample preparation and coding.

Sample No.	Mixture	Code
1	10% Arabic gum, 10% Maltodextrin, 80% distilled water, 2% aerogel.	S1
2	20% Arabic gum, 10% Maltodextrin, 70% distilled water, 2% aerogel.	S2
3	30% Arabic gum, 10% Maltodextrin, 60% distilled water, 2% aerogel.	S3

After the samples were prepared, they were put on Velp Scientifica Arex-6 Digital Pro magnetic stirrer for 24 hours to mix thoroughly. Then they were placed in Binder laboratory oven (etuve) under 150 ^{o}C for 24 hours. Before the prepared samples being tested in oil in order to investigate adsorption process, Fourier Transform Infrared (FTIR), Thermogravimetric Analysis (TGA), Differential Scanning Calorimetry (DSC), X-ray Diffraction (XRD) Analysis, Scanning Electron Microscopy (SEM), and Brunauer-Emmett-Teller (BET) were examined.

FT-IR spectra of all samples were acquired using a Jasco 4700 spectrometer with a diamond crystal ATR. With 64 accumulations and a spectral resolution of 4 cm^{-1}, all of the spectra were obtained between 4000 and 600 cm^{-1}.

The thermal stabilities of the samples were investigated using TA Instruments TGA 55 thermogravimetric analyzers in an inert nitrogen environment at a heating rate of 10 °C/min. Thermal behavior was determined using TA Instruments Q2000 DSC. Measurements were carried out in an inert nitrogen environment at a flowrate of 50 ml/min and a heating rate of 10 ^{o}C/min between 20 and 160 ^{o}C.

The morphologies of the materials were examined using a 300 kV scanning electron microscope (SEM).

The apparent density of the samples was determined using the graduated cylinder method, and the surface area and pore volume distribution were determined using nitrogen adsorption measurements using the BET and BJH methods, respectively, using the Quantachrome-Autosorb iQ Station.

After that, a 0.25 g, 0.5 g and 1.0 g of samples S1, S2 and S3 have been weighed and placed in 10 ml of water containing oil spill with different concentrations for 1h, 2h,3h, and 24h in an Edmund Buehler SM2 shaker. From now on the samples are labeled with their code next to their weight for easier arrangement of the further obtained data as of S1-0.25, S1-0.5, S1-1.0, S2-0.25, S2-0.5, S2-1.0, S3-0.25, S3-0.5 and S3-1.0. The weight of the sample has been measured at the forementioned intervals to calculate the weight increase at each interval then the obtained data were used for isotherm and kinetics calculations.

Thermodynamic properties of the adsorption process were determined by adsorption studies at different temperatures. For this purpose, ΔG^o, ΔS^o, and ΔH^o values were determined by adsorption studies at 25 ^oC, 45 ^oC and 60 ^oC.

5. RESULTS

5.1 Characterization

5.1.1 Fourier transform infrared spectroscopy results

In the present thesis FTIR spectroscopy is used to find the extent of interactions between polymers such as maltodextrin and gum arabic and their chemical stability during adsorbent synthesis by determining any change in their original structure. The spectra of the samples synthesized by aerogel, maltodextrin and gum arabic samples were shown in Fig. 5.1.

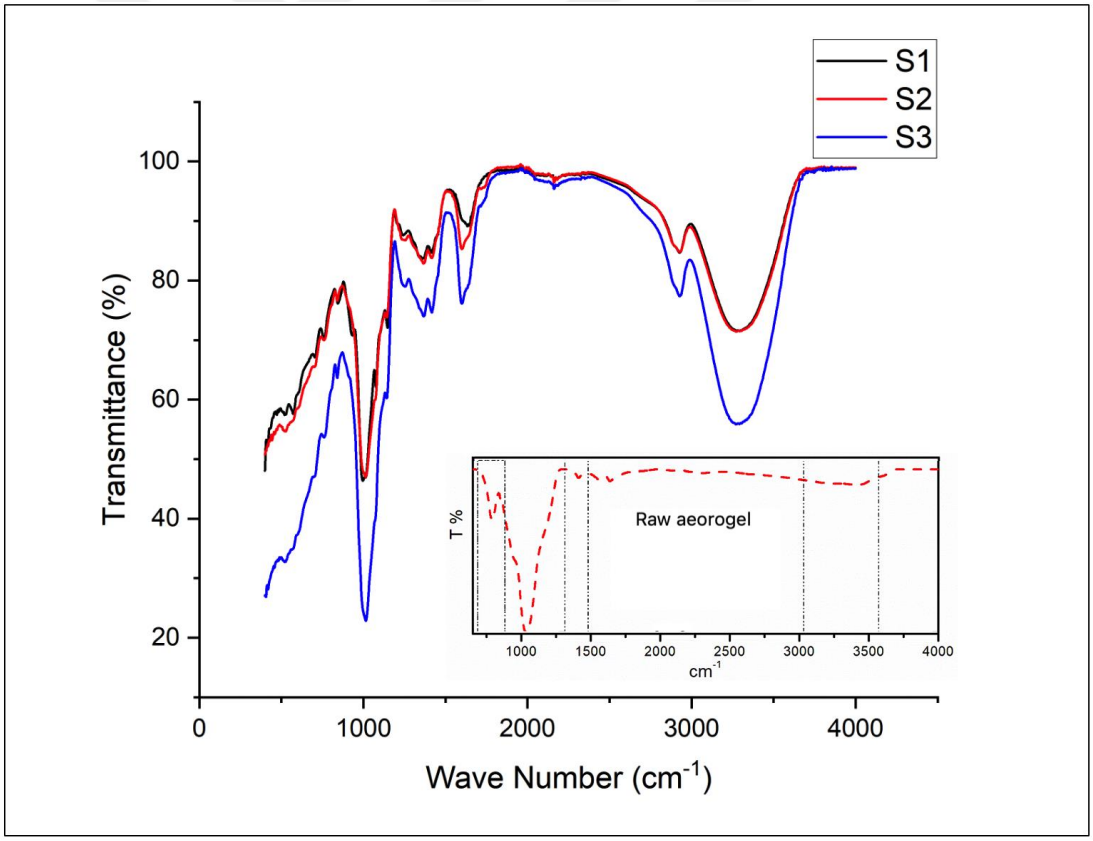

Figure 5.1: FTIR results for S1, S2 and S3.

Firstly, when the FTIR spectrum was examined for the characterization of the synthesized silica aerogel, it was found that it contained all the characteristic peaks. In this spectrum, adsorption peak showing Si-O-Si symmetrical stretching vibration and stretching vibration peaks belonging to Si-OH groups were observed. Silica aerogel,

the adsorption bond near 800 cm^{-1} shows symmetrical stretching vibrations of Si-O-Si bonds, the peak near 1022 cm^{-1} shows stretching vibration of free Si-OH groups. Peaks at 1647 cm^{-1} and 1392 cm^{-1} correspond to O-H and Si-OH, respectively. For aerogel in the samples, the broad absorption peak centered at 3450 cm^{-1} illustrates the O-H stretching band of hydrogen-bonded water molecules.

In the spectrum obtained for gum arabic, a broad absorption band was observed around 3000 - 3600 cm^{-1} representing the characteristics of the glucosidic ring and for -OH stretching (Dai et al., 2018), 3000 - 2800 cm^{-1} for –CH stretching of methyl groups, 1613 cm^{-1} for –C=O stretching and -NH bending, and 1100 - 1050 cm^{-1} for -C-O-C stretching, vibrations. The results were supported by previous studies (Williams et al., 2006; Kang et al., 2019). The absorption at wave number 880 cm^{-1} and 900 cm^{-1} corresponds to the β-D-manopyranose units.

For maltodextrin, the band around 3330 cm-1 corresponds to O-H stretching vibration, 2900 and 2850 cm^{-1} corresponds to asymmetric and symmetric lipid C-H stretching vibration respectively. The area between 800 and 1200 cm^{-1} is called fingerprint region for carbohydrates. The main infrared regions of maltodextrin are below 1000 cm-1 and characterize the stretching vibrations of anhydroglucose ring. Concurrent peaks were found in the spectra of adsorbents at different concentration levels of gum arabic and maltodextrin without any significant deviation. This observation was supported by the similar results obtained by Rezvankhak et al. (2020).

The specific peaks of maltodextrin, arabic gum and aeorogel in the adsorbents overlapped. In addition, it is clearly seen from the FTIR spectrum that the spectrum curves of samples S1 and S2 coincide with each other. Sample S3 was revealed at different transmittence values than S1 and S2. This may be due to the change in the amount of gum arabic in the sample.

5.1.2 Thermogravimetric analysis results

The thermogravimetric analysis was performed on the three samples S1, S2, and S3 (Fig. 5.2 and Fig. 5.3).

TGA is widely used as useful and accurate technique to examine decomposition temperature and the lifetime behavior of adsorbents (Blanco & Siracusa, 2021) Derivative thermogravimetric (DTG) resulting from the first derivative TGA, can examine the relative rates of polymer thermal decomposition process. The maximum

rate of mass loss can directly obtain from the peak in the DTG curve and the peak in a particular temperature range represents a separate event.

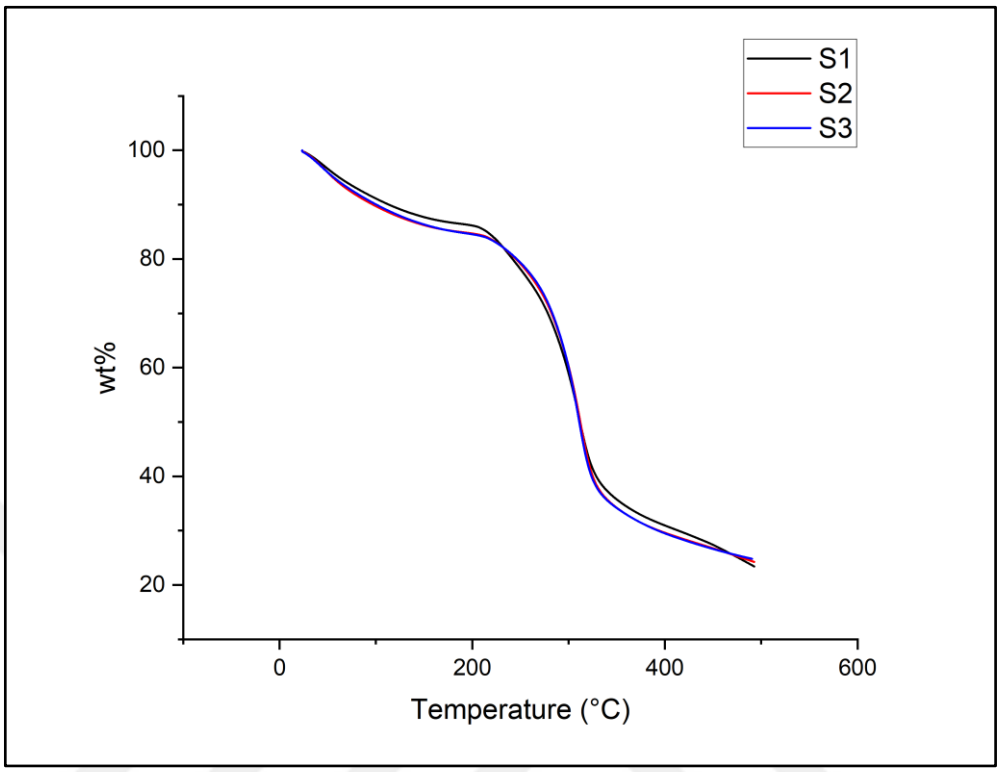

Figure 5.2: TGA graph of S1, S2, and S3**.**

Fig. 5.2. and 5.3 represented the TG and DTG profiles of S1, S2, and S3 samples. The thermal degradation behaviors of the samples were compared using the 20% weight loss and the maximum rate of mass loss temperatures. Some differences in terms of the residual mass, 20% weight loss, the maximum rate of mass loss temperatures, and the number of decomposition stages of the samples can be seen clearly.

As it was clearly visible in Fig. 5.2., all samples showed typical small mass loss signal at temperature below 200°C, corresponding to the initial mass loss of 20%. It can be related with the release of physically absorbed water and there was no connection with the decomposition step of the maltodextrin, gum arabic, and aerogel. Whereafter, the main decomposition stage of S1, S2, and S3 were visible as a large signal on the DTG curve from 200 °C to 380 °C and it was associated with nearly 65% mass loss. At temperatures above 400 °C, a further slow mass losses were observed on TG curves as the temperature was increased. The residual mass values were determined to be nearly 20% for all samples at 500°C.

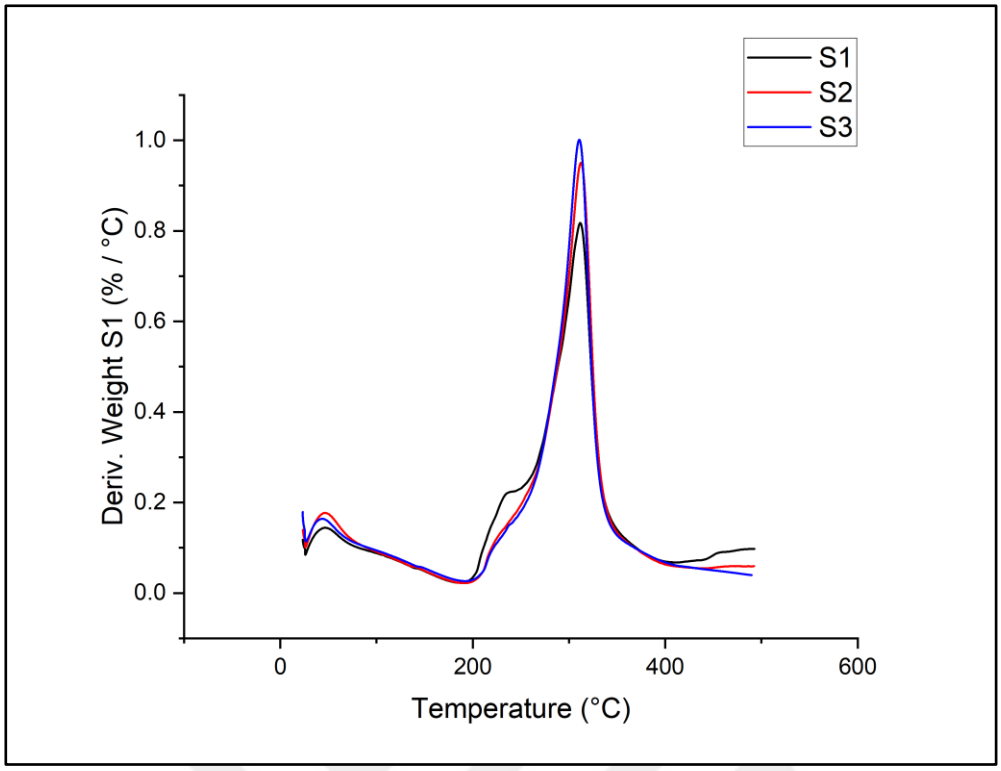

Figure 5.3: DTG graph of S1, S2 and S3.

When the DTG curves of S1, S2, and S3 samples were analyzed, the difference in degradation rates can be clearly seen. While the lowest degradation rate was observed in S1, the highest degradation rate was determined in S3. This is due to the fact that the degradation rate of gum arabic, which was found more in the structure of S3, was higher than the other samples.

5.1.3 DSC analysis results

DSC thermograms for raw aerogel, S1, S2, S3, and maltodextrin samples, obtained over a temperature range from -20°C to 120°C, at a heating rate of 10°C/min, are depicted in Fig. 5.4. Raw maltodextrin showed a low- intensity broad peak at -20–120°C that decreased in treated maltodextrin thermogram. This peak was mostly due to evaporation of loosely bound water. This may be attributed to elution of strongly bound water in the structure of conditioned maltodextrin that required more heat for liberation.

This peak may also be due to changes in the internal structure of maltodextrin. As shown in Fig. 5.4, raw aerogel has an endothermic peak at nearly 60°C.

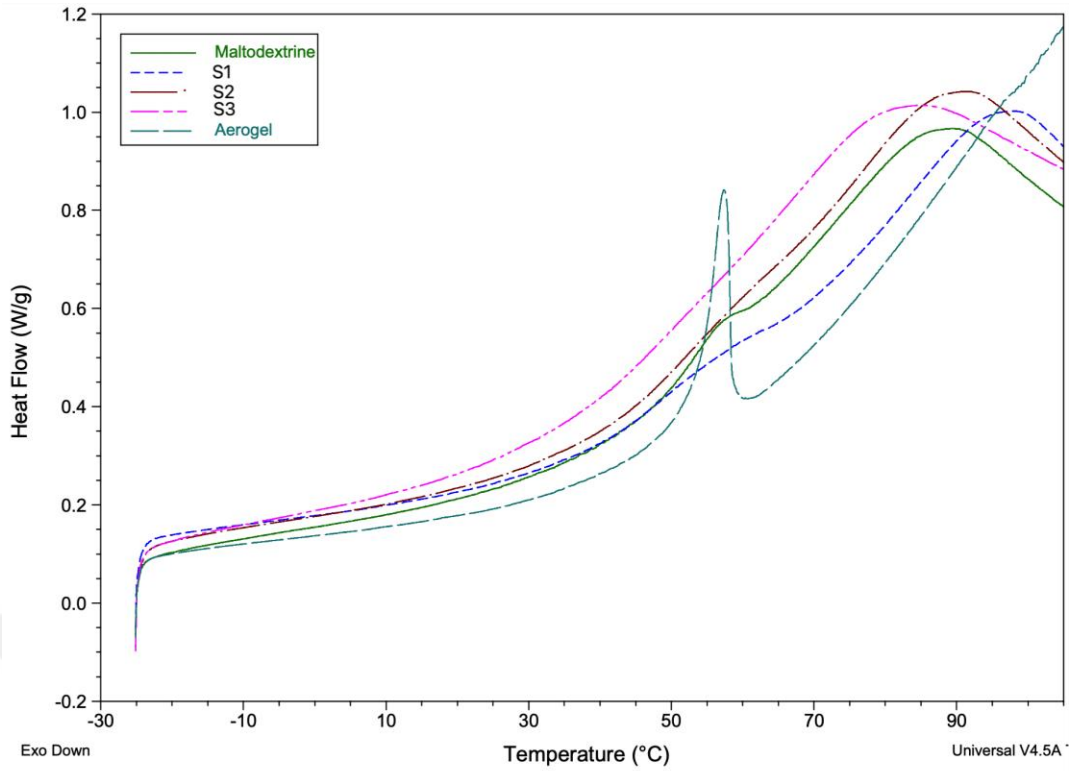

Figure 5.4: DSC Thermogram of aerogel, S1, S2, S3, and maltodextrin.

However, no thermal transition was observed in the range of -20-120 ^{o}C in samples S1, S2, and S3 and DSC graphs of the samples are closely similar due to low add-on of silica aerogel and gum arabic in the maltodextrin structure. These results indicated that incorporation of silica aerogel and gum arabic did not change the thermal characteristic of adsorbents.

5.1.4 X-Ray diffraction analysis results

Figure 4 shows the XRD patterns of aerogel, S1, S2, and S2 samples. S1, S2, and S3 samples had a completely amorphous surface, as could be shown by the presence of broad peaks and large amounts of noise. All adsorbent samples showed an amorphous profile with no crystallinity. In addition, all samples showed some small peaks not well defined and many noises between 10º to 25°.

X-ray diffraction pattern of raw aerogel reveals the amorphous nature of silica aerogel. In Figs. 11, a hump was observed for the amorphous matrix of SiO_2 at around 2θ=22 and 23 °C for silica aerogel. X-ray diffraction pattern of raw aerogel reveals the amorphous nature of silica aerogel.

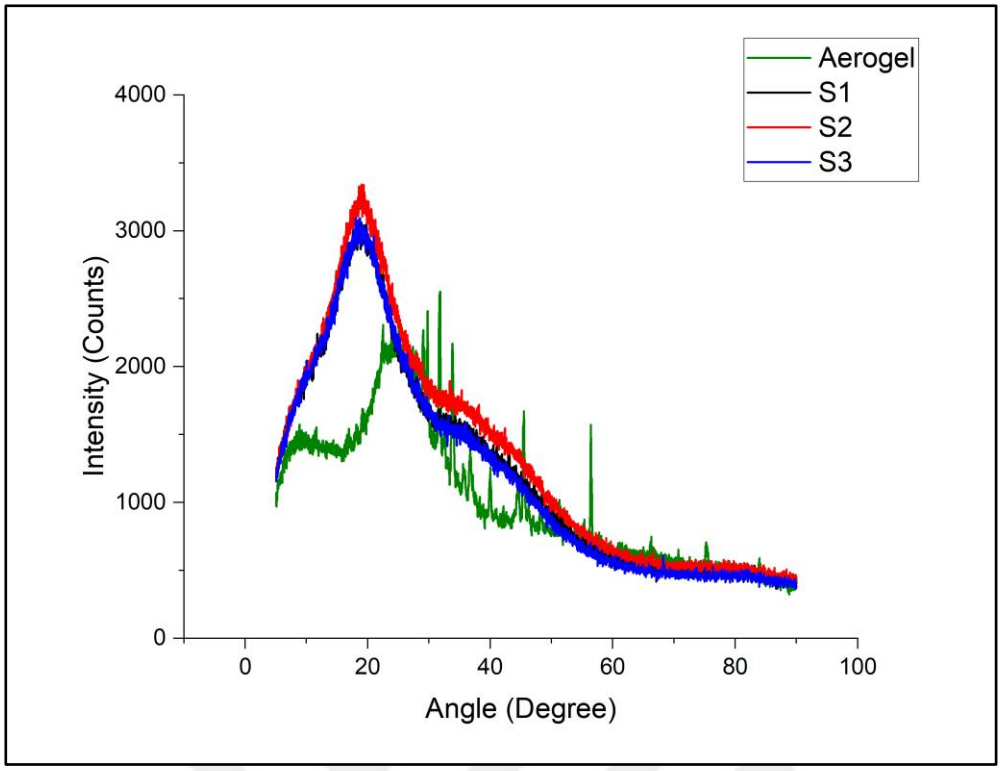

Figure 5.5: XRD pattern of raw aerogel, S1, S2, and S3.

In Fig. 5.5, a hump was observed for the amorphous matrix of SiO_2 at around 2θ=22 and 23º for silica aerogel. Also, some Si-O peaks can be seen on the XRD pattern of the raw aerogel between 25 and 60º (Taufik et al., 2020; Ahmed., 2023). In addition, due to the very low content of raw aerogel in the adsorbents, it is normal that no peak belonging to the crystalline phase is observed in the XRD pattern of samples S1, S2 and S3.

5.1.5 SEM

SEM images of raw aerogel, S2, and S3 samples are shown in Fig. 5.6. The raw aerogel had large open pores with sizes ca. 5.0-10 μm with small pores ranging from 0.5 μm upon 2 μm. In addition, there is the formation of a large number of 0.5-0.1 μm sized subnetworks in the pores that cover the entire surface and provide a uniform area. There were numerous long barred structures (ca. 10–100 μm) on the surface of raw aerogel. These structures can be described as micro-connections on the surface of the aerogel rather than pores.

When we investigate at the surfaces of S2 and S3, completely different and uniform structure were obtained. The smooth and homogenous structure is completely due to the maltodextrin and gum arabic structure. A smooth and homogenous surface was

obtained due to the perfect mixture applied in adsorbent synthesis. When the surface is examined at high magnification, the point-like appearance of aerogels is also a proof of the synthesis.

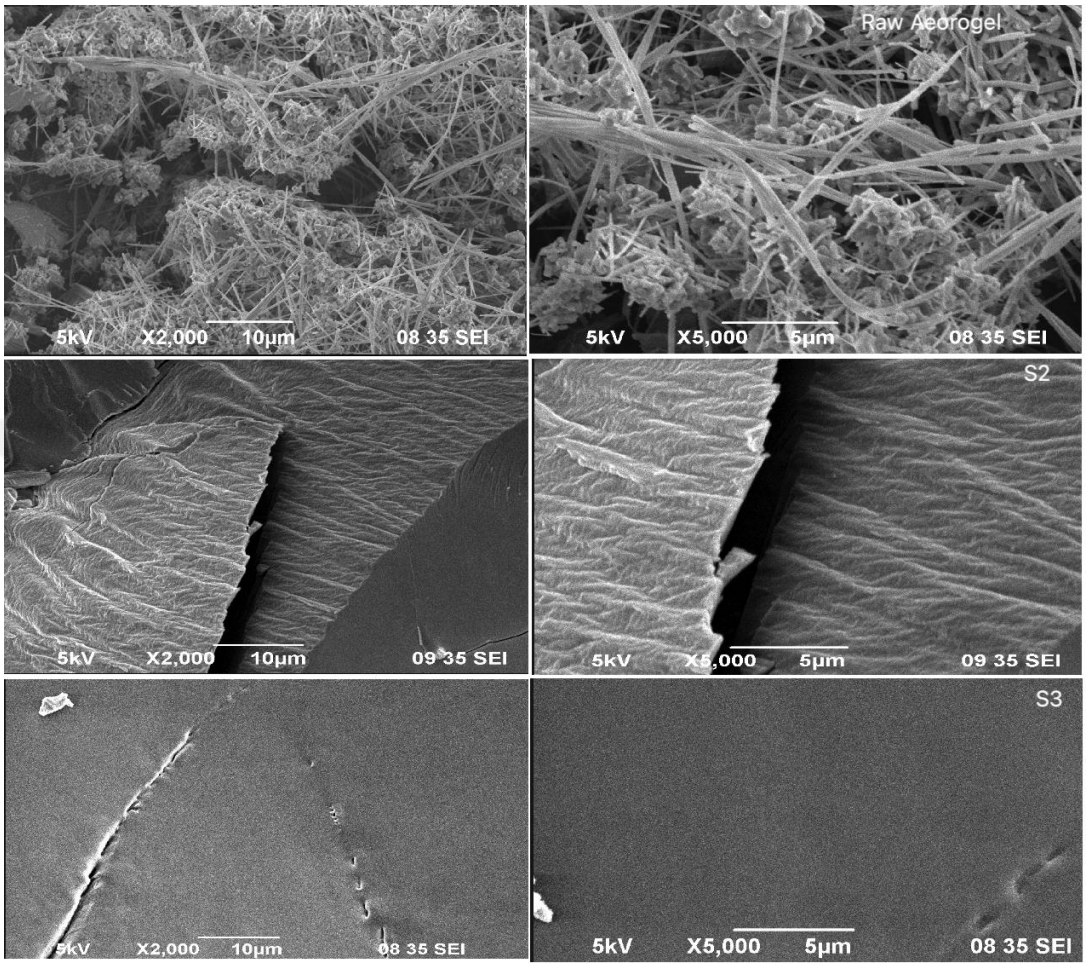

Figure 5.6: SEM results of aeorogel, S2, and S3 samples.

These results may be considered evidence of the successful introduction of both aerogel and gum arabic into maltodextrin. The large surface area of S2 and S3 where all potential binding sites are at receptive position were determined to contribute to a significant increase in the adsorption of oil spill.

5.1.6 BET

By the BET surface area analysis, the surface area and pore size are measured using mass of aerogel, S1, S2, and S3 samples is calculated. The N_2 adsorption-desorption isotherm plot of all samples are shown in Figure 5.7 and Table 5.1.

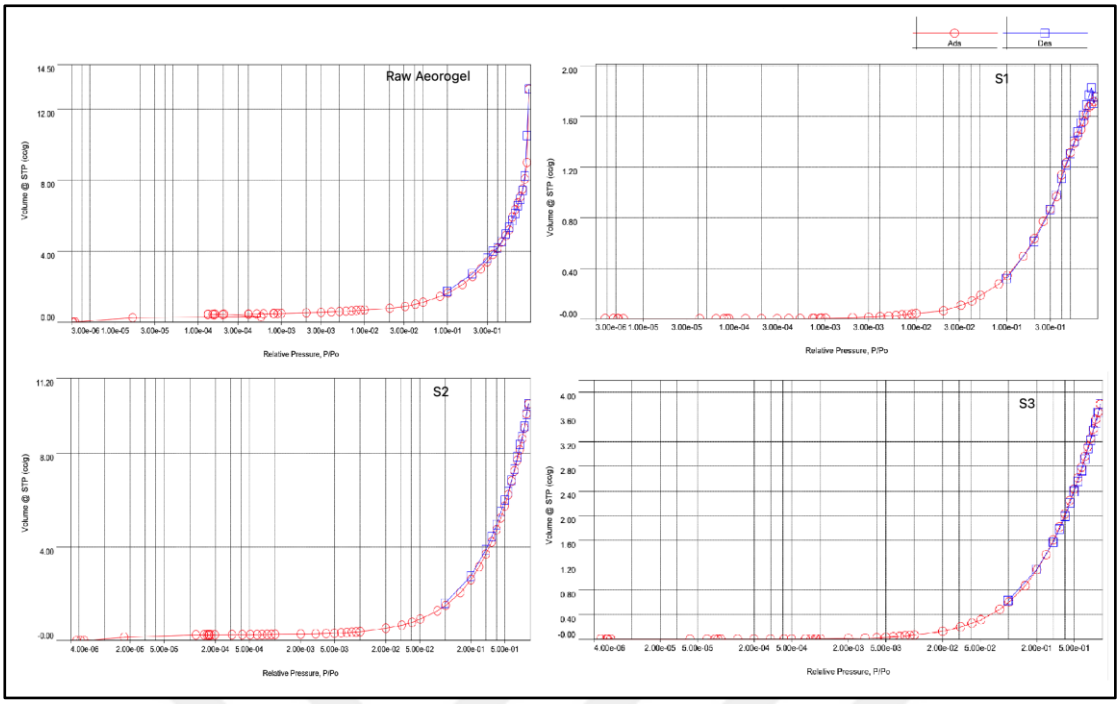

Figure 5.7: BET surface area analysis.

Table 5.1: N_2 adsorption-desorption isotherm of all samples.

	BET surface area (m^2g^{-1})	Pore size (nm)
Raw aerogel	12.190	78.13
S1	4.845	60.91
S2	5.278	15.127
S3	8.631	55.3

The specific surface areas of raw aerogel, S1, S2, and S3 samples were 12.19, 4.845, 5.278, and 8.631 m^2g^{-1}, respectively. However, S1 exhibited the least specific surface area while aerogel has the highest one, and S3 resulted in a larger surface area than S1 after introducing aerogel and gum arabic. The specific surface area was in the order of aerogel > S3> S2 > S1. In addition, total pore volumes were increased with introducing both aerogel and gum arabic into maltodextrin. Aerogel showed larger pore size, indicating the larger pores in maltodextrin and gum arabic. One may suggest that improvement of the surface properties of maltodextrin occurred by using both aerogel and gum arabic as a supporting material.

Surface area and pore size of the samples are sufficiently high. Small pore size and pore volume also prove that they can be utilized as other porous materials, and their surface area can be used in proper situation. The pore distribution and surface area of adsorbent are as the main factors that should be considered in adsorption. Micro- and

mesoporous adsorbents have larger surface area, and thus a higher use in the adsorption process (Mohammadi & Moghaddas, 2015). The porous structure results in high pore volume, leading to enhanced adsorptive capacity and increased ability of the adsorbate to find its way into pores.

5.2 Adsorption Test Results

The readings obtained from noting down the weight change at different time intervals namely, 1, 3, 5, 8 and 24 hours for raw aerogel and the three samples S1, S2 and S3 for the three different starting weight of all the forementioned samples have been used to calculate the removal percentage using the equation 5.1

$$removal\ \% = \frac{w_f - w_i}{w_i} \times 100\% \tag{5.1}$$

Where w_i is the initial weight and w_f is the final weight at a specified time.

The figure 5.8. represents the removal percentage calculated at the forementioned time intervals.

It can be observed from the graph that S1 – 0.25 had an increasing removal percentage up to 3h and then started decreasing till it significantly dropped at 24h, whereas for S1- 0.5 and S1- 1.0 the removal percentage where about the same throughout the 24 hours span with slight increase around 5 and 24 hours.

Regarding S2 samples, S2- 0.25 had shown similar behavior as S1- 0.25 while S2-0.5 and S2-1.0 remained relatively stable during the 24 hours and had their peak removal percentage around 8 hours.

As for S3 samples, S3-0.25 had its peak at 3h reading and it remained somewhat stable for the rest of timespan. While S3-0.5 have shown stable results between 3 and 8 hours and peaked at 24 hours. Finally, S3-1.0 have shown similar readings at 3, 5 and 24 hours.

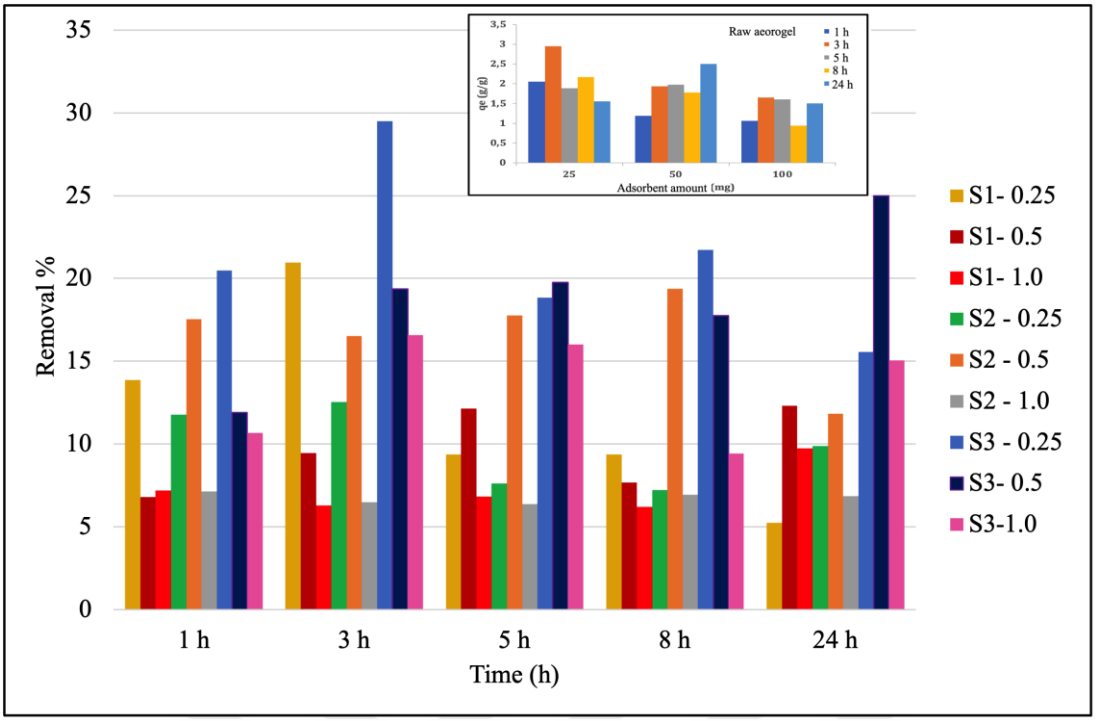

Figure 5.8: Removal percentage versus time for all the samples.

In order to determine the relationship between time and the adsorption of oil by S1, S2 and S3, the amount of q_e (g/g) adsorbed onto the unit adsorbent in the equilibrium state against time was graphed in figure 5.9, 5.10 and 5.11 for the concentrations 25 g/L, 50 g/L and 100 g/L respectively.

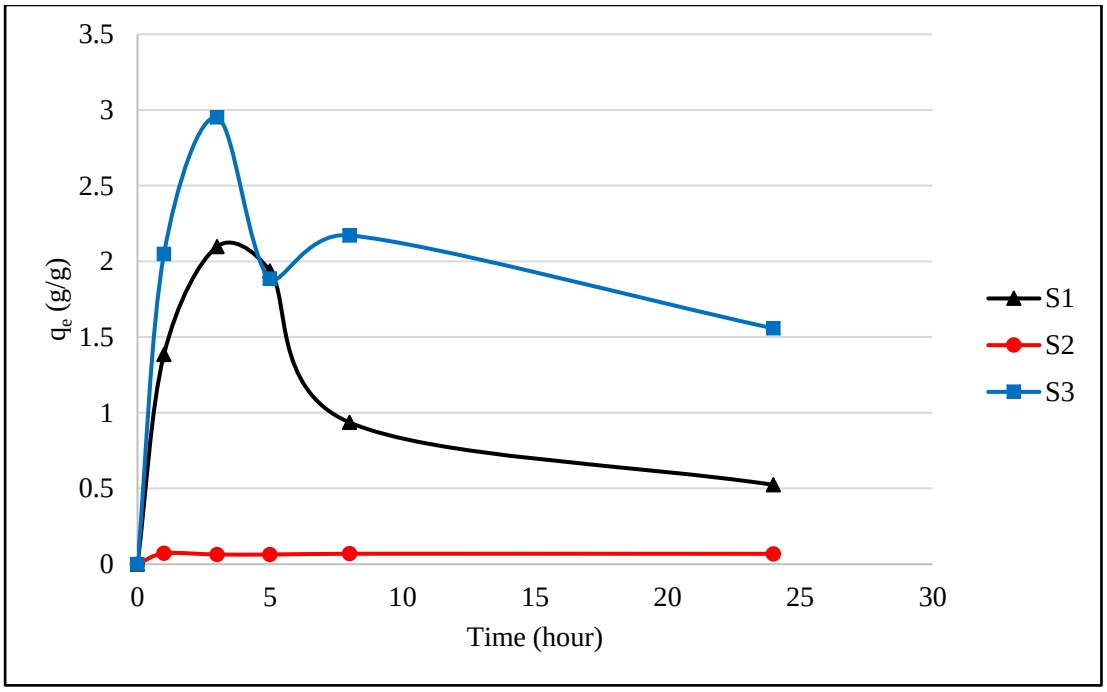

Figure 5.9: Adsorbent capacity in equilibrium state against time at 25 g/L concentration.

At 25 g/L C_e it is noticed that even though S2 have reached equilibrium state the fastest (after 5 hour) it has the lowest removal percentage of about 7.6% whereas S1 and S3 have 9.5% and 21.7% respectively at equilibrium state that is reached after 8 hours.

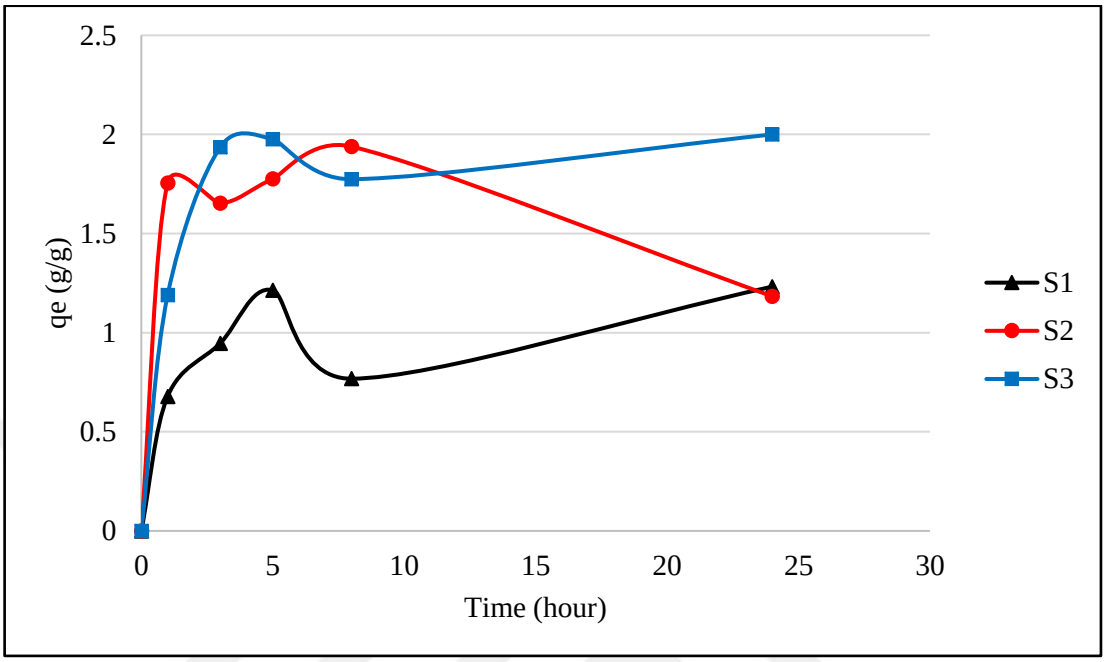

Figure 5.10: Adsorbent capacity in equilibrium state against time at 50 g/L concentration.

At 50 g/L C_e it is noticed that the equilibrium state was reached at 8 hours for all three samples where S, S2 and S3 showed around 7.7%, 19.4% and 17.7% respectively.

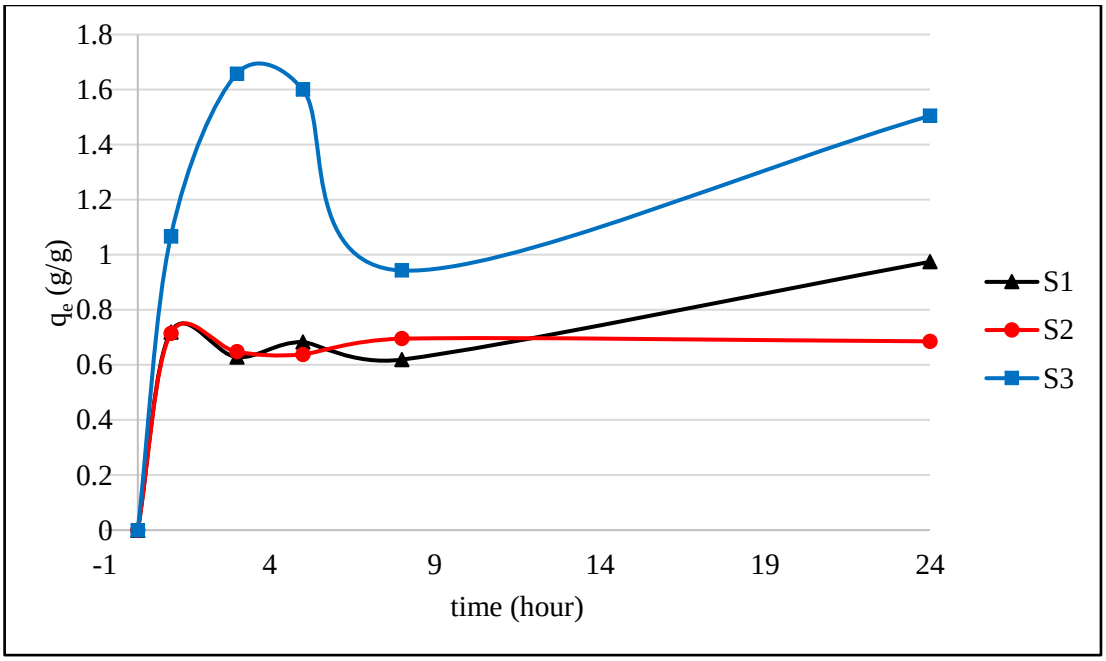

Figure 5.11: Adsorbent capacity in equilibrium state against time at 100 g/L concentration.

Referring to Figure 5.7, S1 and S2 reach equilibrium around the third hour with removal percentage of 6.3% and 6.5% respectively. Whereas S3 takes 8 hours to reach equilibrium with removal percentage of 9.4%. with reference to figure 5.11., 5.10. and 5.11. it has been deemed reasonable to calculate the isotherm models at equilibrium state of 8 hours.

5.2.1 Adsorption isotherm

Adsorption isotherms plays an important role in determining the how the adsorbent interact with the adsorbate so that the adsorbent use can be optimized. For that reason, choosing the right correlation is crucial for determining the equilibrium parameters so that the needed information for an adsorption system for oil removal can be obtained. The Langmuir, Freundlich, Temkin and Dubinin-Radushkevich (D-R) adsorption isotherms were used in this study.

In the first part of the adsorption studies, the preliminary experiments were carried out with raw silica aerogel. According to the isotherm studies carried out to understand the adsorption mechanism in the adsorption of oil of ship origin with raw silica aerogel, Freundlich, Temkin and D-R models were found to explain the adsorption of petroleum derivatives well. According to these results, it was concluded that adsorption occurs on a multilayer heterogeneous surface and has a homogeneous binding energy. According to the results of the kinetic study on the adsorption of oil on silica aerogel, it was determined that the most compatible model was the pseudo-second order kinetic model. Thus, it can be said that the rate determining step of adsorption of petroleum derivatives is chemical reaction.

Referring to the forementioned Equation 3.2 which is the linearized version of the Langmuir adsorption isotherm, $1/Q_e$ against $1/C_e$ was calculated and plotted as in figure 5.12 and Langmuir parameters were calculated.

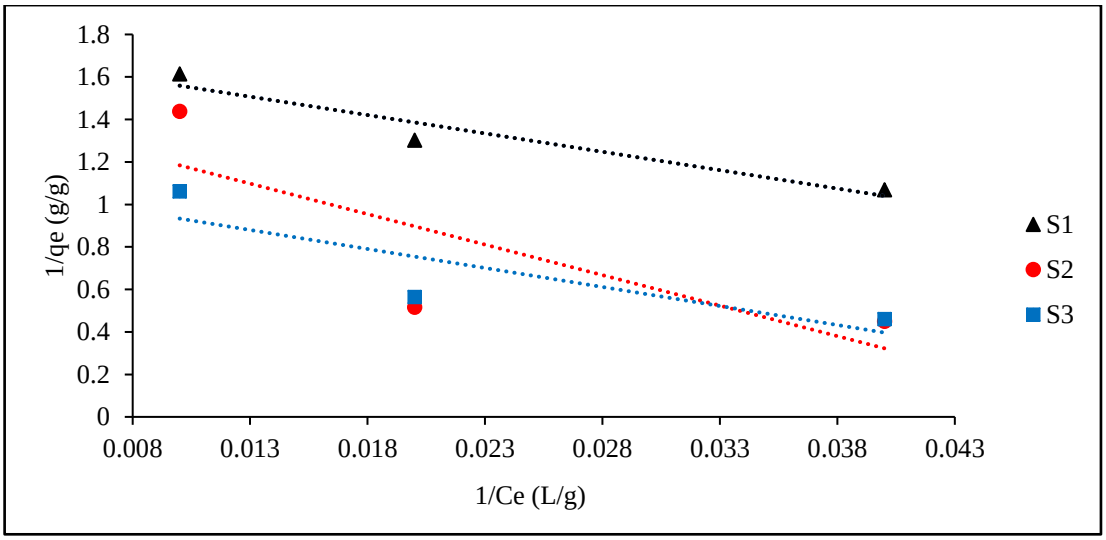

Figure 5.12: Langmuir isotherm for S1, S2 and S3.

The Langmuir isotherm parameters for all the samples were studied using the slope lines obtained from Figure 5.12. where the slope represents ($1/q_m.K_L$) and the line offset is $1/ q_m$ where K_L is the free adsorption energy constant and q_m is the maximum monolayer adsorption capacity in g/g. In addition, the separation factor R_L, which is a measure of the suitability of the Langmuir isotherm model is determined by using the 3.3 equation. The calculated Langmuir model parameters are shown in Table 5.2.

To obtain the Freundlich isotherm model parameters, $\log(C_e)$ versus $\log(q_e)$ was plotted using equation 3.5. The Freundlich isotherm model is shown in Figure 5.13.

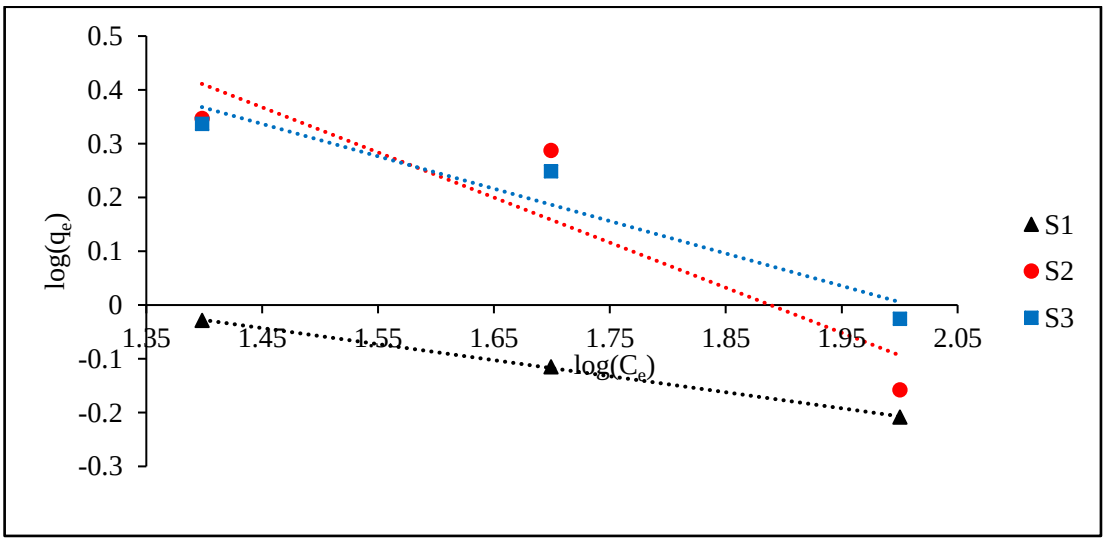

Figure 5.13: Freundlich isotherm model for S1, S2 and S3.

In Freundlich isotherm model parameters, K_F which is calculated from the offset of the line and refers to adsorption capacity while 1/n which represents the heterogeneity

factor is calculated from the slope. The experimental data of S1, S2 and S3 were applied to the Temkin isotherm model by plotting q_e against $\ln(C_e)$ and is shown in Figure 5.14.

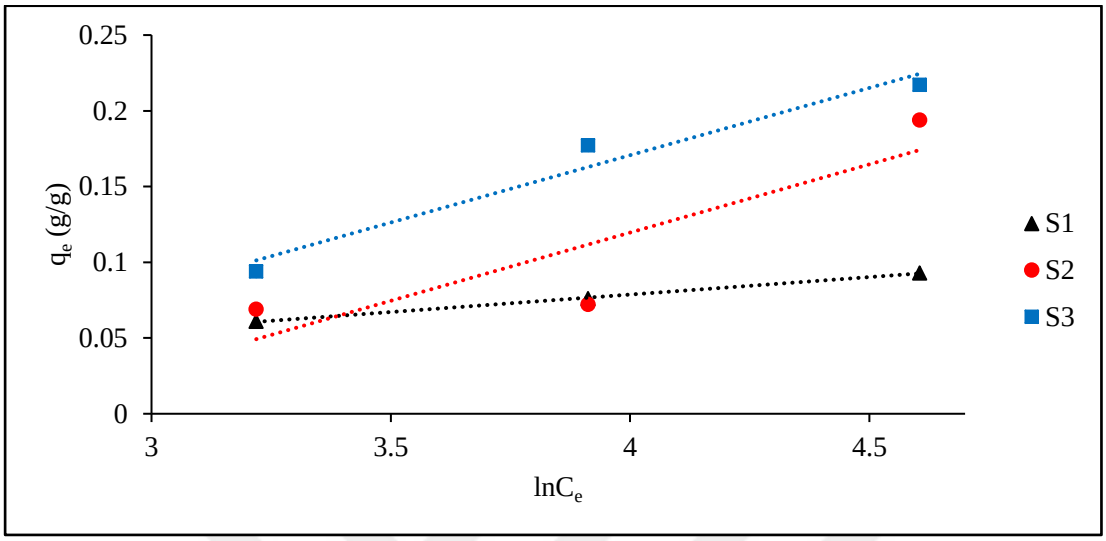

Figure 5.14: Temkin isotherm model for S1, S2 and S3.

The isotherm parameters of Temkin for S1, S2 and S3 were studied using the trendlines obtained in Figure 5.14. Where A_T which is Temkin isotherm equilibrium binding constant (L/g) is calculated from the solve of the trendline and B which is the constant related to heat of sorption(J/mol) is obtained from the offset.

In order to evaluate the Dubinin-Radushkevich isotherm model, $\ln(q_e)$ was graphed against ε^2 and is shown in Figure 5.15.

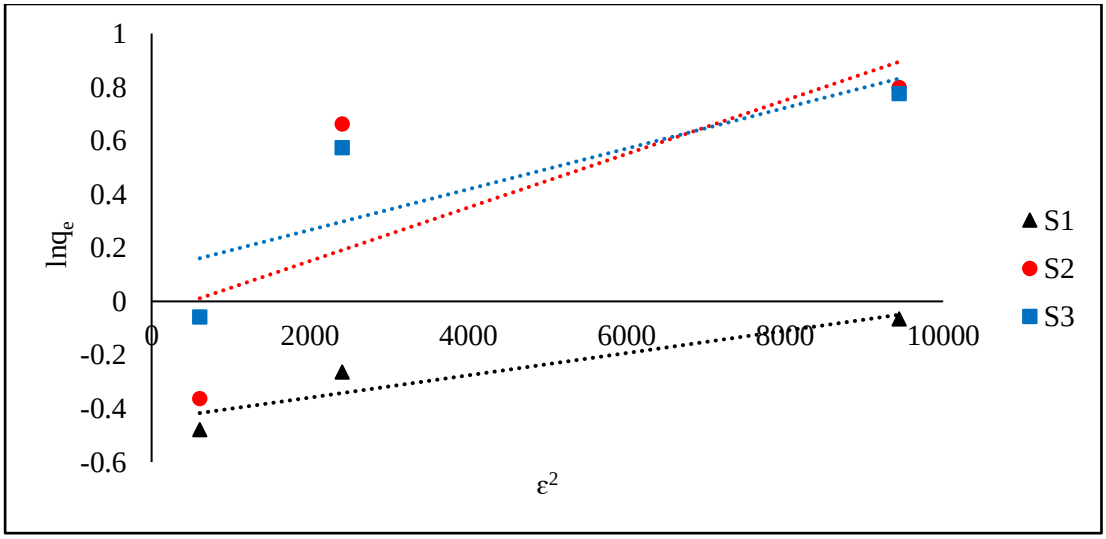

Figure 5.15: Dubinin-Radushkevich isotherm model for S1, S2 and S3.

In Dubinin-Radushkevich model, β which represents Dubinin-Radushkevich adsorption constant can be calculated from the trendline slope and Q which is the maximum amount of adsorbate per unit mass of the adsorbent represents the offset with reference to equation 3.12. Table 5.2 shows the parameters needed to plot Langmuir, Freundlich, Temkin and Dubinin-Radushkevich (D-R) isotherm and all the mentioned isotherm models' parameters respectively.

Table 5.2: Langmuir, Freundlich, Temkin and D-R isotherm parameters for all samples.

Isotherm Model	Isotherm Parameter	S1	S2	S3
Langmuir	q_m (g/g)	0.5774	0.6797	0.8991
	K_L	0.1001	0.05125	0.0617
	$R_{L\ (0.25)}$	0.2857	0.4384	0.3933
	$R_{L\ (0.5)}$	0.1667	0.2807	0.2448
	$R_{L\ (1.0)}$	0.0909	0.1633	0.1395
	R^2	0.9276	0.6298	0.7249
Freundlich	K_F (g/g)	2.4519	38.282	16.203
	1/n	0.2983	0.8383	0.6020
	R^2	0.9995	0.8368	0.9188
Temkin	A_t (L/g)	1.8016	14.477	7.9944
	B	0.0231	0.0901	0.0889
	b_T (kJ/mol)	107.25	27.498	27.869
	R^2	0.9987	0.7692	0.9599
Dubinin-Radushkevich	Q (mol/g)	1.5561	1.0505	1.1215
	β	4×10^{-5}	1×10^{-4}	8×10^{-5}
	E (kJ/mol)	111.80	70.710	79.056
	R^2	0.8805	0.5398	0.6636

Referring to Table 5.2. the Langmuir isotherm model describes the adsorption on homogeneous surfaces. It is based on the assumptions that there are a fixed number of active sites with the same energy on the adsorbent, and the activation energy is constant, and the adsorption occurs in the form of a single layer. It is also known that the R_L separation factor values are feasible in between $0<R_L<1$ (Ragadhita & Nandiyanto, 2022). The R_L separation factors for S1-0.25, S1-0.5, S1-1.0, S2-0.25, S2-0.5, S2-1.0, S3-0.25, S3-0.5 and S3-1.0 were 0.2857, 0.1667, 0.0909, 0.4384, 0.2807, 0.1633, 0.3933, 0.2448 and 0.1395 respectively. Since the R_L separation factors of all the adsorbents studied were in the range of $0<R_L<1$, it was determined that the Langmuir isotherm model was feasible for oil removal using any of the synthesized materials. In addition, the q_m monolayer capacities determined by the Langmuir isotherm model were found to be 0.5774 g/g, 0.6797 g/g and 0.8991 g/g for S1, S2 and S3 respectively, while the K_L surface binding energy values were found to be 0.1001, 0.05125, 0.0617 respectively. The model correlation coefficients R^2 are 0.9276, 0.6298, 0.7249 for S1, S2 and S3 respectively. Taking R^2, the correlation coefficients,

into account, it is believed that the Langmuir isotherm model provides a good fit for the removal of diesel with synthesized materials for S1 only.

The Freundlich model proposes a multilayer adsorption process with non-uniform adsorption enthalpy and affinity distribution over the heterogeneous adsorbent surface without lateral contact. The binding strength is predicted to decline sequentially with greater binding site coverage, starting with the energetically preferred binding sites being occupied first. The heterogeneity factor 1/n, which is the model parameter that provides information about the heterogeneity of the adsorbent surface, the suitability and capacity of the adsorbent/adsorbate system. In many cases, a value of $0<1/n<1$ indicates feasible adsorption (Shikuku, 2018; Ragadhita & Nandiyanto, 2022). According to Table 5.2., the heterogeneity factors of 1/n for S1, S2 and S3 were calculated as 0.2983, 0.8383 and 0.602 respectively. Given that the heterogeneity factor is between 0 and 1 for all three samples, it means that Freundlich isotherm model is suitable for explaining oil adsorption to the synthesized materials. In addition, the K_F model adsorption capacity were 2.4519 g/g, 38.282 g/g and 16.2032 g/g and R^2 correlation coefficients were 0.9995, 0.8368, 0.9188 for S1, S2 and S3 respectively. correlation coefficients ranging between 0.83-0.99 prove that the Freundlich isotherm model explains the adsorption mechanism better than Langmuir isotherm model.

The Temkin isotherm model assumes that the adsorption temperature (ΔH_{ads}) of all molecules in the layer will decrease linearly instead of logarithmically with the surface area. Physical adsorption occurs if b_T value is between 0-4 kJ/mol, if it's between 83-209 kJ/mol then the adsorption is a chemical and if it's between 4-83 kJ/mol then the adsorption is a mix of both chemical and physical (Ragadhita & Nandiyanto, 2022; Mohamed et al., 2022). Examining table 5.2., S1, S2 and S3's A_t, Temkin isotherm equilibrium binding constant it was found to be 1.8016 L/g, 14.4774 L/g and 7.9944 L/g respectively. While B, the constant related to heat of sorption were 0.0231, 0.0901 and 0.0889 respectively. b_T values for S1, S2 and S3 were calculated as 107.254 kJ/mol, 27.498 kJ/mol and 27.869 kJ/mol respectively which indicates that the adsorption for S2 and S3 is physical and chemical whereas the adsorption occurring for S1 is chemical. In addition, the correlation coefficients of R^2 was found to be 0.9987, 0.7692 and 0.9599 for S1, S2 and S3 respectively. The correlation coefficients, which are lower than Freundlich isotherm model, make the Temkin model less suitable for describing the adsorption mechanism specially for S2.

The Dubinin-Radushkevich isotherm model (D-R) assumes a multilayer physical adsorption mechanism on a heterogeneous surface. Module core E shows the average free energy of adsorption, E<8 kJ/mol indicates physical adsorption; 8 kJ/mol<E<16 kJ/mol indicates chemical adsorption and if E>16 kJ/mol then the adsorption is governed by particle diffusion (Nwodika & Onukwuli, 2017). According to the results of Dubinin Radushkevich isotherm model parameters, the average free energies of E for S1, S2 and S3 were determined as 111.803 kJ/mol, 70.710 kJ/mol and 79.0569 kJ/mol respectively. Since these results are above 16 kJ/mol, it is thought that the adsorption of oil to the synthesized materials is governed by particle diffusion. Furthermore, given that the correlation coefficients ranging between 0.53 and 0.88, it is unsafe to explain the adsorption mechanism by the Dubinin Radushkevich isotherm model.

In this part of the thesis, it was determined that the Freundlich isotherm model fits the process better than the Langmuir, Temkin, Dubinin Radushkevich isotherm models, which were evaluated to explain the adsorption mechanism in oil of ship origin removal with S1, S2 and S3 composites. Based on the results, it was determined that oil adsorption is a non-uniform multilayer adsorption process without lateral contact. It also implies that the binding strength is declining sequentially as the site coverage gets greater.

5.2.2 Adsorption kinetics

Pseudo first-order kinetic model, Pseudo second-order kinetic model, Weber-Morris intra-particle diffusion model and Elovich kinetic model were studied in order to evaluate the relationship of oil adsorption with respect to time when the equilibrium concentrations for S3 samples for 24h.

The pseudo-first order kinetic model obtained by graphing t versus $\ln(q_e-q_t)$ in oil adsorption with the synthesized composites concentrations shown in Figure 5.16.

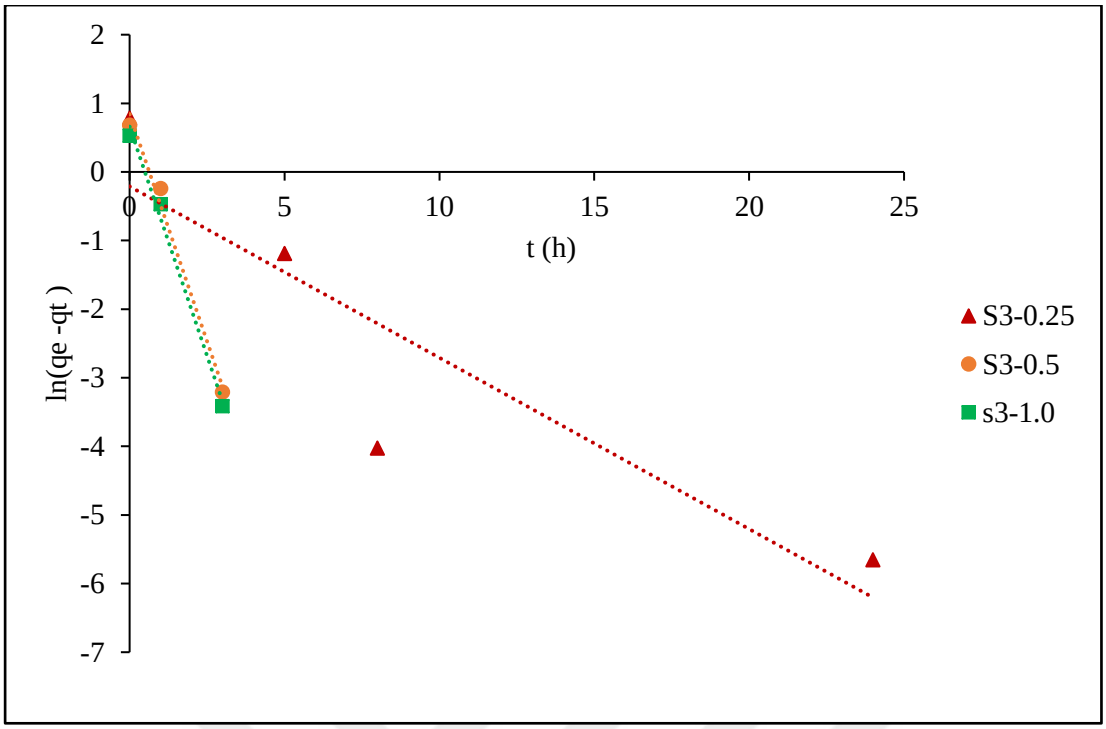

Figure 5.16: The pseudo-first order kinetic model.

The pseudo-first order kinetic model parameters for all the samples were studied using the slope lines obtained in Figure 5.12. where q_e is calculated from the trendline offset and the k_1 model velocity constants is obtained from the slope value. The calculated pseudo-first order kinetic model parameters are shown in Table 5.3.

The pseudo-second order kinetic model was graphed with t/qt against t. The pseudo-second order kinetic model is shown in Figure 5.17.

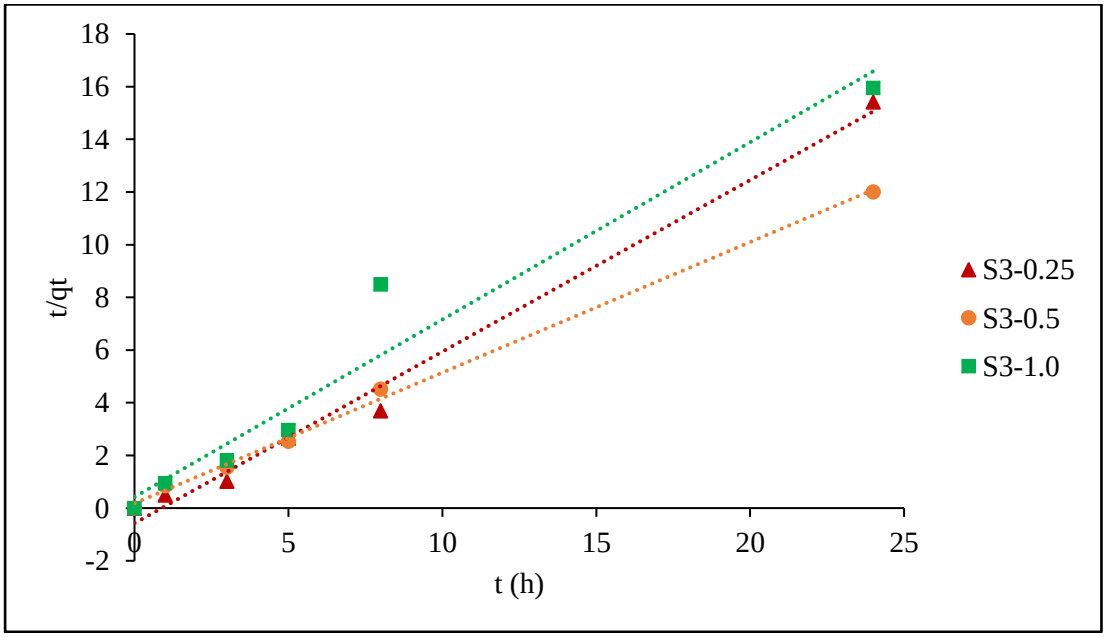

Figure 5.17: Pseudo-second order kinetic model.

Pseudo-second order kinetic model parameters; model constant k_2 and model adsorption capacity q_e were calculated from the trendlines' in Figure 5.17. offset and slopes, respectively. In addition, the h model velocity constants were calculated using equation 3.17. The model parameters of the synthesized composites are shown in Table 5.3.

Experimental data on oil adsorption with the synthesized composites were applied to the Elovich kinetic model by graphing q_t against ln(t) and are shown in Figure 5.18.

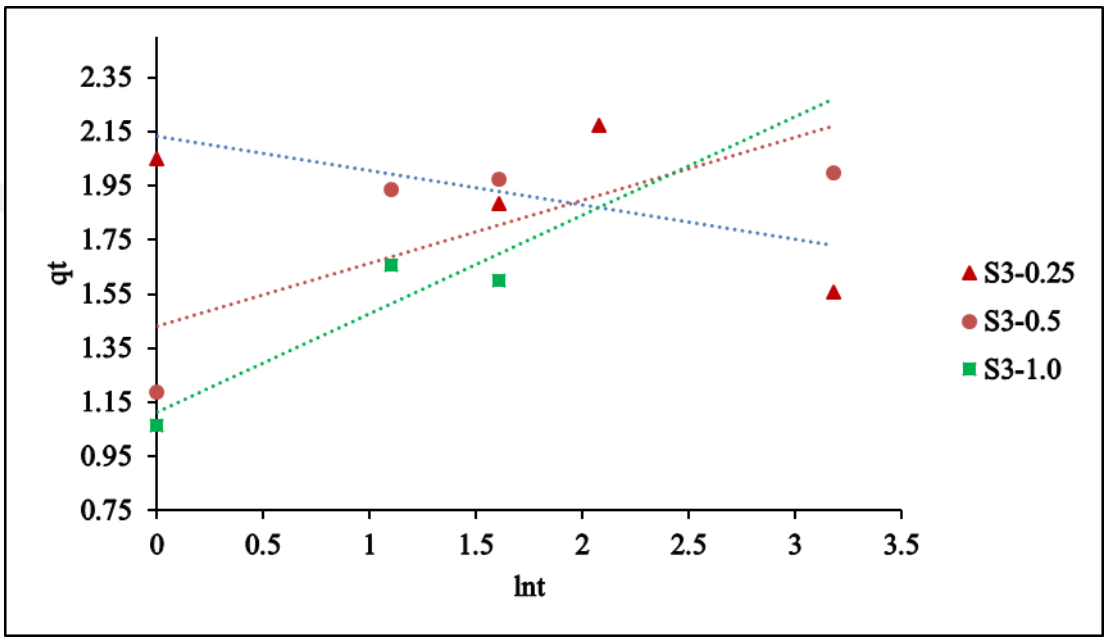

Figure 5.18: Elovich kinetic model.

The Elovich kinetic model parameters for all the composites were studied using the trendlines in Figure 5.18. where the slope is used to calculate β the desorption constant and the offsent is used to calculate the adsorption rate α. The calculated Elovich kinetic model parameters are shown in Table 5.3.

Regarding the evaluation of Weber-Morris intra-particle diffusion model in oil adsorption, q_t against $t^{0.5}$ was graphed and shown in Figure 5.19.

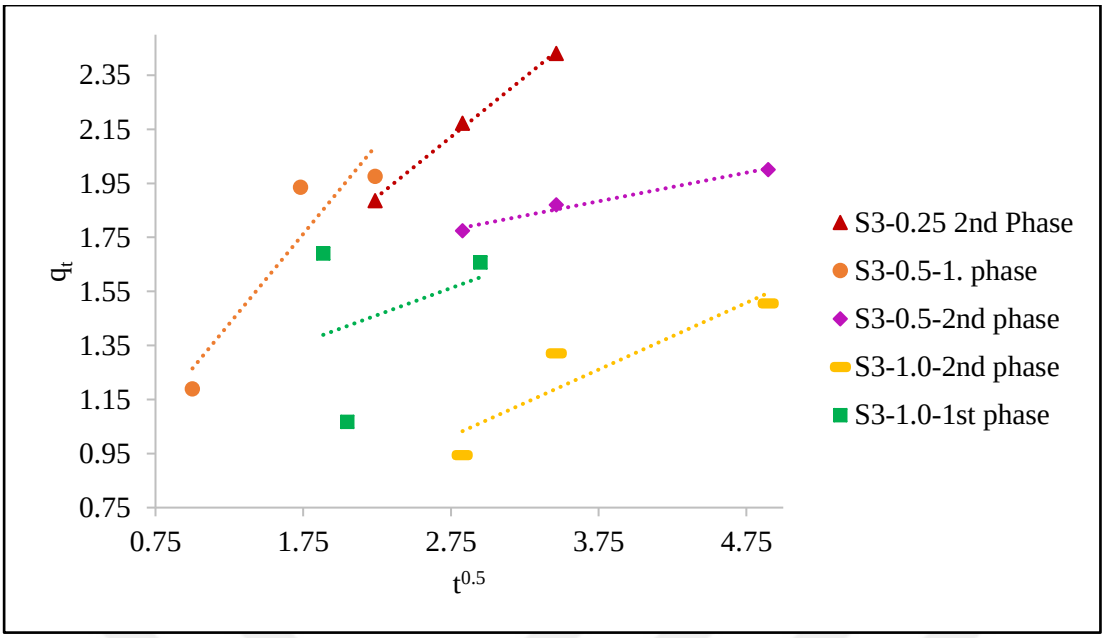

Figure 5.19: Weber-Morris intra-particle diffusion model.

The Weber-Morris intra-particle diffusion model parameter, k_{id} intra-particle velocity constant, was calculated from the slopes of the trendlines. The Weber Morris intra-particle diffusion model parameters of the synthesized composites were shown in Table 5.3.

Table 5.3: Pseudo-first order, pseudo-second order, Elovich kinetic models and Weber-Morris intra-particle diffusion model parameters for all samples.

Kinetics Model	Kinetics Parameter	S3-0.25	S3-0.50	S3-1.0
Pseudo-First Order	q_e (mg/g)	1.2356	2.3212	1.9352
	k_1 (h^{-1})	0.575	3.049	3.076
	R^2	0.8118	0.989	0.9924
Pseudo-Second Order	q_e (mg/g)	1.5349	2.0169	1.485
	k_2 (g/mg.h)	0.7357	1.3396	1.0740
	h (mg/g.h)	1.7333	5.449	2.3685
	R^2	0.9902	0.9977	0.9529
Elovich	β (mg/g)	7.9617	4.3159	2.7457
	α (mg/g.h)	2949828	113	7.7257
	R^2	0.3874	0.612	0.8457
Weber Morris	k_{id-1} ($mg/g.h^{0.5}$)	0.4431	0.6637	0.2001
	R^2	0.9974	0.8679	0.1071
	k_{id-2} ($mg/g.h^{0.5}$)	--	0.1059	0.2472
	R^2	--	0.9827	0.8379

The experimentally determined qe equilibrium adsorption capacities for S1-0.25, S2-0.5 and S3-1.0 at equilibrium were 1.5573 mg/g, 2.00 mg/g, and 1.504 mg/g, respectively, while the $q_{e,model}$ adsorption capacities calculated with the pseudo-first order kinetic model were 1.2356 mg/g, 2.3212 mg/g, and 1.9352 mg/g, respectively. According to these results, it was determined that the adsorption capacities calculated with the model were quite different from the adsorption capacities determined experimentally. Despite the high R^2 correlation coefficients ranging between 0.81-

0.99, the incompatible experimental and model adsorption capacities clearly show that this model is insufficient to explain the adsorption rate and parameters.

Regarding pseudo-second order kinetic model, Table 5.3, shows that when q_e is calculated, the adsorption capacities of S3-0.25, S3-0.50 and S3-1.0 were 1.5349 mg/g, 2.0169 mg/g and 1.94585 mg/g respectively. It is clearly seen that the model $q_{e,model}$ values and experimental q_e adsorption capacities overlap significantly. Examining R^2 correlation coefficients values falls in the range of 0.95-0.99, shows that this model provides a better explanation of the adsorption rate and parameters than the pseudo-first order model. The adsorption constants k_2 and model rate constants h were calculated as 0.7357 g/mgh and 1.7333 mg/gh for S3-0.25; 1.3396 g/mgh and 5.449 mg/gh for S3-0.5; 1.0740 g/mgh and 2.3685 mg/gh for S3-0.5, respectively. Based on these results, a pseudo-second order kinetic model is used to describe the relationship of adsorption over time in oil removal.

The Elovich kinetic model assumes that solid surfaces are energetically heterogeneous and that neither desorption nor interactions between adsorbate species can significantly affect the adsorption kinetics at a low surface area (Mercado-Borrayo et al., 2014).

Table 5.3 shows that the R^2 correlation coefficients for S3-0.25, S3-0.50 and S3-1.0 were 0.3874, 0.612 and 0.8457 respectively, while the initial adsorption rate α was 29.498 mg/g.h, 113 mg/g.h and 7.7257 mg/g.h respectively. Given that the correlation coefficient of Elovich model is considered low, it can be said that chemisorption is not the primary mechanism of adsorption.

Weber-Morris intraparticle diffusion is a kinetic model with multi-linearity correlation described by the diffusion of adsorbate molecules into pores in porous adsorbents. S3 and oil molecules were characterised by two distinct linear phases expressing different mass transfer mechanisms. In the first phase, rapid external surface sorption occurs, while in the second phase, slow intra-particle diffusion and gradual mass transfer are thought to occur.

For S3-0.5 and S3-1.0, the first-phase k_{d-1} intraparticle velocity constants and second-phase k_{d-2} intraparticle velocity constants were 0.6637 mg/g.$h^{0.5}$ and 0.1059 mg/g.$h^{0.5}$; 0.2001 mg/g.$h^{0.5}$ and 0.22472 mg/g.$h^{0.5}$, respectively. When the results are evaluated, the boundary layer mass transfer rates for S3-0.5 are calculated to be 6.29 times higher

than the intraparticle diffusion rates, respectively. For S3-1.0, the mass transfer rates did not change much. In addition, the R^2 correlation coefficients for the first phase were calculated to be between 0.99-0.10, while the R^2 correlation coefficients for the second phase were found to be in the range of 0.98-0.83. According to the Weber Morris model, since the correlation coefficient of the second order phase for the S3-1.0 sample is very low, we can say that intra-particular mass transfer was not achieved. In addition, For S3-0.25, the model indicates only rapid external surface sorption.

6. CONCLUSION

- The aerogel used during the course of thesis was successfully prepared by using the sol-gel method.
- The aerogel production yield was estimated by gravimetric analysis under the synthesis condition. The synthesized aerogel formation yield was estimated to be between 42% to 81%.
- The synthesized aerogel contained big open pores and small pores with widths ranging from 100 to 150 μm and 0.5 to 10 μm, respectively.
- The synthesized aerogel showed high thermal stability till 800 ^{o}C.
- Silica aerogel, the adsorption bond near 800 cm^{-1} showed symmetrical stretching vibrations of Si-O-Si bonds, the peak near 1022 cm^{-1} showed stretching vibration of free Si-OH groups. Peaks at 1647 cm^{-1} and 1392 cm^{-1} corresponded to O-H and Si-OH, respectively.
- For gum arabic, a broad absorption band was observed around 3000- 3600 cm^{-1} representing the characteristics of the glucosidic ring and for -OH stretching, 3000- 2800 cm^{-1} for -CH stretching of methyl groups, 1613 cm^{-1} for –C=O stretching and -NH bending, and 1100- 1050 cm^{-1} for -C-O-C stretching, vibrations.
- For maltodextrin, the band around 3330 cm^{-1} corresponded to O-H stretching vibration, 2900 and 2850 cm^{-1} corresponded to asymmetric and symmetric lipid C-H stretching vibration respectively. The area between 800 and 1200 cm^{-1} was called fingerprint region for carbohydrates.
- The specific peaks of maltodextrin, arabic gum and aeorogel in the adsorbents overlapped. In addition, it was clearly seen from the FTIR spectrum that the spectrum curves of samples S1 and S2 coincide with each other. Sample S3 was revealed at different transmittence values than S1 and S2.

- The thermal stabilities of the samples were investigated using TA Instruments TGA 55 thermogravimetric analyzers in an inert nitrogen environment at a heating rate of 10 °C/min.
- The main decomposition stage of S1, S2, and S3 were visible as a large signal on the DTG curve from 200 °C to 380 °C and it was associated with nearly 65% mass loss. At temperatures above 400 °C, a further slow mass losses were observed on TG curves as the temperature was increased. The residual mass values were determined to be nearly 20% for all samples at 500°C.
- The DTG curves of S1, S2, and S3 samples were analyzed, the difference in degradation rates can be clearly seen. While the lowest degradation rate was observed in S1, the highest degradation rate was determined in S3.
- A hump was observed for the amorphous matrix of SiO_2 at around $2\theta=22$ and 23^o for silica aerogel. Si-O peaks were seen on the XRD pattern of the raw aerogel between 25 and 60^o.
- In addition, due to the very low content of raw aerogel in the adsorbents, it was normal that no peak belonging to the crystalline phase was observed in the XRD pattern of samples S1, S2 and S3.
- The surfaces of S2 and S3, completely different and uniform structure were obtained.
- The smooth and homogenous structure was completely due to the maltodextrin and gum arabic structure. A smooth and homogenous surface was obtained due to the perfect mixture applied in adsorbent synthesis.
- When the surface was examined at high magnification, the point-like appearance of aerogels was also a proof of the synthesis.
- SEM results may be considered evidence of the successful introduction of both aerogel and gum arabic into maltodextrin. The large surface area of S2 and S3 where all potential binding sites were at receptive position were determined to contribute to a significant increase in the adsorption of oil spill.
- The specific surface areas of raw aerogel, S1, S2, and S3 samples were 12.19, 4.845, 5.278, and 8.631 m^2g^{-1}, respectively.

- The specific surface area was in the order of aerogel > S3> S2 > S1.
- S1-0.25 had an increasing removal percentage up to 3h and then started decreasing till it significantly dropped at 24h, whereas for S1-0.5 and S1-1.0 the removal percentage where about the same throughout the 24 hours span with slight increase around 5 and 24 hours.
- S3-0.25 had its peak at 3h reading and it remained somewhat stable for the rest of timespan. While S3-0.5 was shown stable results between 3 and 8 hours and peaked at 24 hours. S3-1.0 was shown similar readings at 3, 5, and 24 hours.
- S1 and S2 reached equilibrium around the third hour with removal percentage of 6.3% and 6.5% respectively.
- S3 reached to equilibrium in 8 hours with removal percentage of 9.4%
- According to the isotherm studies carried out to understand the adsorption mechanism in the adsorption of oil of ship origin with raw silica aerogel, Freundlich, Temkin and D-R models were found to explain the adsorption of petroleum derivatives well.
- The R_L separation factors for S1-0.25, S1-0.5, S1-1.0, S2-0.25, S2-0.5, S2-1.0, S3-0.25, S3-0.5 and S3-1.0 were 0.2857, 0.1667, 0.0909, 0.4384, 0.2807, 0.1633, 0.3933, 0.2448 and 0.1395 respectively. Since the R_L separation factors of all the adsorbents studied were in the range of $0<R_L<1$, it was determined that the Langmuir isotherm model was feasible for oil removal using any of the synthesized materials.
- According to R^2 values, the correlation coefficients, into account, Langmuir isotherm model provided a good fit for the removal of oil with synthesized materials for S1 only.
- The heterogeneity factors of 1/n for S1, S2 and S3 were calculated as 0.2983, 0.8383 and 0.602 respectively. Given that the heterogeneity factor is between 0 and 1 for all three samples, it means that Freundlich isotherm model was suitable for explaining oil adsorption to the synthesized materials.
- K_F model adsorption capacity were 2.4519 g/g, 38.282 g/g and 16.2032 g/g and R^2 correlation coefficients were 0.9995, 0.8368, 0.9188 for S1, S2 and S3 respectively.

- The correlation coefficients ranging between 0.83-0.99 mentioned that the Freundlich isotherm model explained the adsorption mechanism better than Langmuir isotherm model.
- The correlation coefficients, which were lower than Freundlich isotherm model, made the Temkin model less suitable for describing the adsorption mechanism specially for S2.
- It was determined that oil adsorption is a non-uniform multilayer adsorption process without lateral contact. It also implies that the binding strength is declining sequentially as the site coverage gets greater.
- Despite the high R^2 correlation coefficients ranging between 0.81-0.99 for pseudo first order kinetic model, the incompatible experimental and model adsorption capacities clearly showed that this model was insufficient to explain the adsorption rate and parameters.
- A pseudo-second order kinetic model was used to describe the relationship of adsorption over time in oil removal.
- The correlation coefficient of Elovich model was considered low, it can be said that chemisorption was not the primary mechanism of adsorption.
- Weber-Morris intraparticle diffusion is a kinetic model with multi-linearity correlation described by the diffusion of adsorbate molecules into pores in porous adsorbents. S3 and oil molecules were characterised by two distinct linear phases expressing different mass transfer mechanisms. In the first phase, rapid external surface sorption occurred, while in the second phase, slow intra-particle diffusion and gradual mass transfer were thought to occur.
- For S3-0.5 and S3-1.0, the first-phase k_{d-1} intraparticle velocity constants and second-phase k_{d-2} intraparticle velocity constants were 0.6637 mg/g.$h^{0.5}$ and 0.1059 mg/g.$h^{0.5}$; 0.2001 mg/g.$h^{0.5}$ and 0.22472 mg/g.$h^{0.5}$, respectively. When the results are evaluated, the boundary layer mass transfer rates for S3-0.5 are calculated to be 6.29 times higher than the intraparticle diffusion rates, respectively.

Supporting Person and Institution Information:

This study was carried out with the support of Istanbul Technical University Scientific Research Projects MYL-2022-43705.

REFERENCES

Abel, U. A., Habor, G. R., & Oseribho, O. I. (2020). Adsorption studies of oil spill clean-up using coconut coir activated carbon (CCAC). *American Journal of Chemical Engineering* 8(2), 36-47.

Aboul-Gheit, A. K., Khalil, F. H., & Abdel-Moghny, T. (2006). Adsorption of spilled oil from seawater by waste plastic. *Oil & Gas Science and Technology*, 61(2), 259-268.

Ahmed, S. S. (2023). Comparison of the properties of silica aerogel doped with two different laser dyes: Crystal violet and Rhodamine B. *Kuwa it Journal of Scie*nce, 50(3A).

Akhtar, K., Khan, S. A., Khan, S. B., & Asiri, A. M. (2018). Scanning electron microscopy: Principle and applications in nanomaterials characterization. Handbook of Materials Characterization, 113-145.

Akpan, U. F., & Akpan, G. E. (2012). The contribution of energy consumption to climate change: a feasible policy direction. *International Journal of Energy Economics and Policy*, 2(1), 21-33. (page 1)

AKTAŞ, E., Demir, Ö., & Deniz, U. Ç. A. R. (2020). Biodiesel production methods. *International Journal of Energy and Smart Grid*, 5(1-2), 3.

Akten, N. (2003). The Strait of Istanbul (Bosphorus): The seaway separating the continents with its dense shipping traffic. *Journal of Black Sea/Mediterranean Environment*, 9(3), 244.

Ali, A., Chiang, Y. W., & Santos, R. M. (2022). X-ray diffraction techniques for mineral characterization: A review for engineers of the fundamentals, applications, and research directions. Minerals, 12(2), 205.

Aljammal, N. (2020). *Modification and characterization of adsorbent materials and CNTs for oil spill cleanup from water* (Doctoral Dissertation). University of Pannonia, Doctoral School of Chemical Engineering and Material Sciences, VESZPRÉM.

Alleman, T.L., McCormick, R.L., Christensen, E.D., Fioroni, G., Moriarty, K. & Yanowitz, K. (2016). Biodiesel Handling and Use Guide-Fifth Edition. US Department of Energy. 3. Retrieved January 20, 2022, from https://afdc.energy.gov/files/u/publication/biodiesel_handling_use_guide.pdf

Ansell, D. V., Dicks, B., Guenette, C. C., Moller, T. H., Santner, R. S., & White, I. C. (2001). A Review of the Problems Posed By Spills of Heavy Fuel Oils. International Oil Spill Conference Proceedings, 2001(1), 591–596. https://doi.org/10.7901/2169-3358-2001-1-591

Ayasli, D. E., Yalcin, Y., Sahin, S., & Berument, M. H. (2023). Turkish Straits and an important oil price benchmark: Urals. *The Energy Journal*, 44(4), 1-14.

Aydogdu, Y. V. (2022). Utilization of full-mission ship-handling simulators for navigational risk assessment: a case study of large vessel passage through the Istanbul Strait. *Journal of Marine Science and Engineering*, 10(5), 659.

Bandura, L., Woszuk, A., Kołodyńska, D., & Franus, W. (2017). Application of mineral sorbents for removal of petroleum substances: a review. Minerals, 7(3), 37. 1-25.

Basuki, K. T., Hasnowo, L. A., & Jamayanti, E. (2019). Adsorption of uranium simulation waste using bentonite: titanium dioxide. Urania: *Jurnal Ilmiah Daur Bahan Bakar Nuklir*, 25(1). 22ç

Behnood, R., Anvaripour, B., Jaafarzadeh, N., & Farasati, M. (2016). Oil spill sorption using raw and acetylated sugarcane bagasse. *Journal of Central South University*, 23, 1618-1625.

Bejarano, A. C., Michel, J., Rowe, J., Li, Z., McCay, D. F., McStay, L., & Etkin, D. S. (2013). Environmental risks, fate and effects of chemicals associated with wind turbines on the Atlantic Outer Continental Shelf. US Department of the Interior, Bureau of Ocean Energy Management, Office of Renewable Energy Programs, Herndon, VA. OCS Study BOEM, 213. pp.76.

Biodiesel Spills Factsheet. (2019). Retrieved January 22, 2022, from https://response.restoration.noaa.gov/sites/default/files/Biodiesel.pdf

Blanco, I., & Siracusa, V. (2021). The Use of Thermal Techniques in the Characterization of Bio-Sourced Polymers. *Materials (Basel, Switzerland)*, *14*(7), 1686. https://doi.org/10.3390/ma14071686

Büyüksırıt, T., & Kuleaşan, H. (2014). Fourier dönüşümlü kizilötesi (FTIR) spektroskopisi ve gıda analizlerinde kullanımı. Gıda, 39(4), 235-241.

Chen, J., Zhang, W., Wan, Z., Li, S., Huang, T., & Fei, Y. (2019). Oil spills from global tankers: Status review and future governance. *Journal of Cleaner Production*, 227, 27.

Chilvers, B. L., Morgan, K. J., & White, B. J. (2021). Sources and reporting of oil spills and impacts on wildlife 1970–2018. *Environmental Science and Pollution Research*, 28(1), 758.

Çöken, N.Ö. (2021).Aktif Karbon Esasli Polimer Kompozitlerin Farmasötik Mikrokirleticilerin Gideriminde Kullanilmasi (PhD Thesis, Yalova University

Dada, A. O., Olalekan, A. P., Olatunya, A. M., & Dada, O. J. I. J. C. (2012). Langmuir, Freundlich, Temkin and Dubinin–Radushkevich isotherms studies of equilibrium sorption of Zn2+ unto phosphoric acid modified rice husk. *IOSR Journal of Applied Chemistry*, 3(1), 38-45.

Dai, L., Sun, C., Wei, Y., Mao, L., & Gao, Y. (2018). Characterization of Pickering emulsion gels stabilized by zein/gum arabic complex colloidal nanoparticles. *Food Hydrocolloids*, 74, 239-248.

Denatured Ethanol Factsheet. (2019). Retrieved January 25, 2022, from https://response.restoration.noaa.gov/sites/default/files/Denatured-Ethanol.pdf

Dielectric Fluids Factsheet. (2019). Retrieved January 24, 2022, from https://response.restoration.noaa.gov/sites/default/files/Dielectric-Fluids.pdf

Ebelegi, A. N., Ayawei, N., & Wankasi, D. (2020). Interpretation of adsorption thermodynamics and kinetics. *Open Journal of Physical Chemistry*, 10(03), 166-182.sity). 14-18.

Ebnesajjad, S. (2011). Surface and material characterization techniques. In Handbook of adhesives and surface preparation (pp. 31-48). William Andrew Publishing.

Fatahi, H., Claverie, J., & Poncet, S. (2022). Thermal characterization of phase change materials by differential scanning calorimetry: A Review. Applied Sciences, 12(23), 12019.

Feldberg, S., Taylor K., Baird, J., Casselman, J., Paetow, A., Miranda, E., Wilson, R., Iannone, R., McEwen, B., Hoshizaki, L., Kennedy, T., Carmichael, P., and C. Bettles. (2013). Lemon Creek Spill Response Environmental Impact Assessment. Pp. 9-17. Report prepared for Executive Flight Center and BC Ministry of Environment. 92p. + Appendices.

Fingas, M. (2014). Vegetable oil spills: Oil properties and behavior. Handbook of Oil Spill Science and Technology, 79-91.

Fingas, M. (2021). Introduction to Oil Spills and their Clean-up. In Petrodiesel Fuels (pp. 875-889). CRC Press.

Fingas, M. (2021). Introduction to Oil Spills and their Clean-up. 10.1201/9780367456252-4.

Fingas, M., & Brown, C. E. (2017). A review of oil spill remote sensing. sensors, 18(1), 91. 2-15.

Frahm, E. (2014). Scanning electron microscopy (SEM): Applications in archaeology. Encyclopedia of global archaeology, 6487-6495.

Fritt-Rasmussen, J., Wegeberg, S., Gustavson, K., Sørheim, K. R., Daling, P. S., Jørgensen, K., ... & Holst-Andersen, J. P. (2018). Heavy Fuel Oil (HFO): A review of fate and behaviour of HFO spills in cold seawater, including biodegradation, environmental effects and oil spill response. Pp.13-16.

Gad, S. C. (2014). Diesel Fuel. Encyclopedia of Toxicology, 115–118. https://doi.org/10.1016/b978-0-12-386454-3.00837-x

García-Borboroglu, P., Boersma, P. D., Reyes, L., & Skewgar, E. (2008). Petroleum pollution and penguins: marine conservation tools to reduce the problem. Marine pollution: new research. Nova Science Publishers, New York, 340.

Hakami, A. A. (2020). *Evaluation of Natural and Synthetic Sorbents for Oil Spill Clean-up Applications* (Master's thesis). University of Waterloo, Chemical Engineering, WATERLOO.

Heavy Fuel Oil Spills Factsheet. (2019). Retrieved February 3, 2022, from https://response.restoration.noaa.gov/sites/default/files/Heavy-Fuel-Oil.pdf

Hebbar, R., Isloor, A., & Ismail, A. (2017). Contact Angle Measurements. Membrane Characterization, 219–255. https://doi.org/10.1016/b978-0-444-63776-5.00012-7

Ho, S. (2022). Low-cost adsorbents for the removal of phenol/phenolics, pesticides, and dyes from wastewater systems: A Review. Water, 14(20), 3203. 2.

Hodgson, E., Chambers, J. E., Mailman, R. B., & Roe, R. M. (2015). In Dictionary of toxicology (Third, pp. 199–200). essay, Academic Press.

Inyinbor, A. A., Adekola, F. A., & Olatunji, G. A. (2016). Kinetics, isotherms and thermodynamic modeling of liquid phase adsorption of Rhodamine B dye onto Raphia hookerie fruit epicarp. Water Resources and Industry, 15, 14-27.

İstikbal, C. (2020). Strait of Istanbul, major accidents and abolishment of left-hand side navigation. Aquatic Research, 3(1), 42.

ITOPF. (2023). Oil Tanker Spill Statistics 2022. ITOPF Ltd, London, UK.

Jing, A. J., Zhang, A., & Wu, Z. (2002). Thermal analysis of polymer fibers. Handbook of Thermal Analysis and Calorimetry, 3, 409-490.

Kalam, S., Abu-Khamsin, S. A., Kamal, M. S., & Patil, S. (2021). Surfactant adsorption isotherms: A review. ACS Omega, 6(48), 32345-32346.

Kang, Y. R., Lee, Y. K., Kim, Y. J., & Chang, Y. H. (2019). Characterization and storage stability of chlorophylls microencapsulated in different combination of gum Arabic and maltodextrin. Food Chemistry, 272, 337-346.

Kass, M. D., Sluder, C. S., & Kaul, B. C. (2021). Spill Behavior, Detection, and Mitigation for Emerging Nontraditional Marine Fuels (No. DTMA91X20A65). United States. Department of Transportation. Maritime Administration. 10-11.

Kerosene and Jet Fuel Spills Factsheet. (2019). Retrieved February 7, 2022, from https://response.restoration.noaa.gov/sites/default/files/Kerosene-Jet-Fuel.pdf

Lam, N. L., Smith, K. R., Gauthier, A., & Bates, M. N. (2012). Kerosene: a review of household uses and their hazards in low-and middle-income countries. *Journal of Toxicology and Environmental Health*, Part B, 15(6), 398-399.

Li, F., Dong, H., & Liang, M. (2018, August). Analysis, treatment and countermeasures on oil spills at sea. In IOP Conference Series: Materials Science and Engineering (Vol. 397, No. 1, p. 012086). IOP Publishing.

Light Shale Oil Spills Factsheet. (2019). Retrieved February 10, 2022, from https://response.restoration.noaa.gov/sites/default/files/Light-Shale-Tight-Oil.pdf

Majd, M. M., Kordzadeh-Kermani, V., Ghalandari, V., Askari, A., & Sillanpää, M. (2022). Adsorption isotherm models: A comprehensive and systematic review (2010− 2020). *Science of The Total Environment*, 812, 151334. 3-5.

Massachusetts Department of Environmental Protection. (2011). Large Volume Ethanol Spills–Environmental Impacts and Response Options pp. 8.

Matekenya, W., & Ncwadi, R. (2022). The impact of maritime transport financing on total trade in South Africa. *Journal of Shipping and Trade*, 7(1), 1-17.

Medicine, N. A. O. S. E. A., Studies, D. O. E. A. L., Technology, B. O. C. S. A., & Environment, C. O. T. E. O. D. B. O. T. (2016). Spills of Diluted Bitumen from Pipelines. National Academies Press. 21-22.

Mercado-Borrayo, B., Schouwenaars, R., Litter, M., Montoya-Bautista, C., & Ramírez-Zamora, R. (2014). Metallurgical Slag as an Efficient and Economical Adsorbent of Arsenic. Water Reclamation and Sustainability, 95–114. https://doi.org/10.1016/b978-0-12-411645-0.00005-5

Mohamed, F., Shaban, M., Zaki, S. K., Abd-Elsamie, M. S., Sayed, R., Zayed, M., ... & Soliman, N. K. (2022). Activated carbon derived from sugarcane and modified with natural zeolite for efficient adsorption of methylene blue dye: Experimentally and theoretically approaches. Scientific Reports, 12(1), 18031.

Mohamed, M., Jaafar, J., Ismail, A., Othman, M., & Rahman, M. (2017). Fourier Transform Infrared (FTIR) Spectroscopy. Membrane Characterization, 3–29. https://doi.org/10.1016/b978-0-444-63776-5.00001-2

Mohammadi, A., & Moghaddas, J. (2015). Synthesis, adsorption and regeneration of nanoporous silica aerogel and silica aerogel-activated carbon composites. Chemical Engineering Research and Design, 94, 475-484.

Mohammed, A. and Abdullah, A. (2018) Scanning Electron Microscopy (SEM): A Review. Proceedings of 2018 International Conference on Hydraulics and Pneumatics-HERVEX, Baile Govora, Romania, 7-9 November 2018, 1-9**.**

Moheman, A., Bhawani, S. A., & Tariq, A. (2021). Aerogels for waterborne pollutants purification. Advances in Aerogel Composites for Environmental Remediation, 109–124. https://doi.org/10.1016/b978-0-12-820732-1.00007-2

Musah, M., Azeh, Y., Mathew, J. T., Umar, M. T., Abdulhamid, Z., & Muhammad, A. I. (2022). Adsorption kinetics and isotherm models: a review. CaJoST, 4(1), 20-26.

Narin van Court, W. A., LaRock, J., & van Leeuwen, S. (2017). Important Considerations For First Responders To Large Volume/High-Concentration Ethanol Spills. In International Oil Spill Conference Proceedings (Vol. 2017, No. 1, pp.10-11). International Oil Spill Conference.

Nasrollahzadeh, M., Atarod, M., Sajjadi, M., Sajadi, S. M., & Issaabadi, Z. (2019). Plant-Mediated Green Synthesis of Nanostructures: Mechanisms, Characterization, and Applications. Interface Science and Technology, 199–322. https://doi.org/10.1016/b978-0-12-813586-0.00006-7

Neff, J.M., S. McKelvie and R.C. Ayers, Jr. (2000). Environmental impacts of synthetic based drilling fluids. Report prepared for MMS by Robert Ayers & Associates, Inc. U.S. Department of the Interior, Minerals Management Service, Gulf of Mexico OCS Region, New Orleans, LA. OCS Study MMS 2000- 064. 8-10.

Netto, S. A., Gallucci, F., & Fonseca, G. (2009). Deep-sea meiofauna response to synthetic-based drilling mud discharge off SE Brazil. Deep Sea Research Part II: Topical Studies in Oceanography, 56(1-2), 41.

Non-Petroleum Oil Spills Factsheet. (2019). Retrieved January 25, 2022, from https://response.restoration.noaa.gov/sites/default/files/Non-Petroleum-Oil.pdf

Non-Petroleum Oils. (2022). US Environmental Protection Agency (EPA). Retrieved January 15, 2022, from https://www.epa.gov/emergency-response/non-petroleum-oils

Notes on The Turkish Straits. (n.d). Republic of Turkiye, Ministry of Foreign Affairs. Retrieved January 12, 2022, from https://www.mfa.gov.tr/the-turkish-straits.en.mfa

Nwodika, C., & ONUKWULİ, D. O. (2017). Adsorption study of kinetics and equilibrium of basic dye on kola nut pod carbon. *Gazi University Journal of Science*, 30(4), 86-102.

Oil Spills. (n.d.). The International Charter Space and Major Disasters. Retrieved January 15, 2022, from https://disasterscharter.org/web/guest/disaster-types/-/article/oil-spills

Oil Types. (2020). US National Oceanic and Atmospheric Administration (NOAA). Retrieved January 5, 2022, from https://response.restoration.noaa.gov/oil-and-chemical-spills/oil-spills/oil-types.html

Ozcan, N., Saygi Yalcin, B., Bilgin Simsek, E., & Saloglu, D. (2022). Removal of naproxen from wastewater using chitosan–aerogel–activated carbon biocomposites: Theory, equilibrium, kinetics, thermodynamics, and process optimization. Water Environment Research, 94(3), e10699.

Patalano, A., Villalobos, F., Pena, P., Jauregui, E., Ozkan, C., & Ozkan, M. (2019). Scaling sorbent materials for real oil-sorbing applications and environmental disasters. MRS Energy & Sustainability, 6. 1-11.

Pratson, L. F. (2023). Assessing impacts to maritime shipping from marine chokepoint closures. Communications in Transportation Research, 3, 100083.

Qian, H., Lin, Y. L., Xu, B., Wang, L. P., Gao, Z. C., & Gao, N. Y. (2018). Adsorption of haloforms onto GACs: Effects of adsorbent properties and adsorption mechanisms. *Chemical Engineering Journal*, 349, 849-859.

Qiu, H., Lv, L., Pan, B. C., Zhang, Q. J., Zhang, W. M., & Zhang, Q. X. (2009). Critical review in adsorption kinetic models. *Journal of Zhejiang University-Science A*, 10(5), 716-724.

Ragadhita, R. I. S. T. I., & Nandiyanto, A. B. D. (2022). Curcumin adsorption on zinc imidazole framework-8 particles: Isotherm adsorption using Langmuir, Freundlich, Temkin, and Dubinin-Radushkevich models. *Journal of Engineering Science and Technology*, 17(2), 1078-1089.

Raja, P. B., Munusamy, K. R., Perumal, V., & Ibrahim, M. N. M. (2022). Characterization of nanomaterial used in nanobioremediation. Nano-Bioremediation : Fundamentals and Applications, 57–83. https://doi.org/10.1016/b978-0-12-823962-9.00037-4

Raju, A., Rao, B. S., Madhukar, K., Reddy, K. R., Sadhu, V., & Chouhan, R. (2022). Effect irradiation on physicochemical and mechanical properties of polymers and polymer blends. Green Sustainable Process for Chemical and Environmental Engineering and Science, 147–163. https://doi.org/10.1016/b978-0-323-99643-3.00011-5

Raya, S. A., Mohd Saaid, I., Abbas Ahmed, A., & Abubakar Umar, A. (2020). A critical review of development and demulsification mechanisms of crude oil emulsion in the petroleum industry. *Journal of Petroleum Exploration and Production Technology*, 10, 1711-1728.

Razavi, Z., Mirghaffari, N., & Rezaei, B. (2014). Adsorption of crude and engine oils from water using raw rice husk. *Water Science and Technology*, 69(5), 947-952.

Rengasamy, R. & Das, Dipayan. (2011). Oil spill cleanup by structured fibre assembly. *Indian Journal of Fibre and Textile Research*. 36.190-200.

Rezvankhah, A., Emam-Djomeh, Z., Safari, M., Salami, M., & Askari, G. (2022). Investigating the effects of maltodextrin, gum arabic, and whey protein concentrate on the microencapsulation efficiency and oxidation stability of hemp seed oil. *Journal of Food Processing and Preservation*, 46(6), e16554.

Rodrigue, J.-P. (2020). The Geography of Transport Systems (5th ed.). Routledge. P171-172. https://doi.org/10.4324/9780429346323

Saadatkhah, N., Carillo Garcia, A., Ackermann, S., Leclerc, P., Latifi, M., Samih, S., ... & Chaouki, J. (2020). Experimental methods in chemical engineering: Thermogravimetric analysis—TGA. *The Canadian Journal of Chemical Engineering*, 98(1), 34-43.

Sahoo, T. R., & Prelot, B. (2020). Adsorption processes for the removal of contaminants from wastewater. Nanomaterials for the Detection and Removal of Wastewater Pollutants, 161–222. https://doi.org/10.1016/b978-0-12-818489-9.00007-4

Saleh, T. A. (2022). Isotherm models of adsorption processes on adsorbents and nanoadsorbents. Interface Science and Technology, 99–126. https://doi.org/10.1016/b978-0-12-849876-7.00009-9

Sayed, K., Baloo, L., & Sharma, N. K. (2021). Bioremediation of total petroleum hydrocarbons (TPH) by bioaugmentation and biostimulation in water with floating oil spill containment booms as bioreactor basin. *International Journal of Environmental Research and Public Health*, 18(5), 2226. 1-26.

Shikuku, V. O., Kowenje, C. O., & Kengara, F. O. (2018). Errors in parameters estimation using linearized adsorption isotherms: sulfadimethoxine adsorption onto kaolinite clay. *Chemical Science International Journal*. 29, 1-6.

Small Diesel Spills Factsheet. (2006). Retrieved February 02, 2022, from https://dec.alaska.gov/spar/ppr/response/sum_fy10/100111201/NOAA Factsheet_Diesel.pdf

Small Diesel Spills Factsheet. (2020). Retrieved January 21, 2022, from https://response.restoration.noaa.gov/sites/default/files/Small-Diesel-Spills.pdf

Smith, B. C. (2011). Fundamentals of Fourier transform infrared spectroscopy. CRC press. 8-8

Speight, J. G. (2014). The chemistry and technology of petroleum. CRC press. 3-3.

Stefan, M., & Romanescu, G. (2010). Problems Of Seagoing Navigation In Bosphorus Strait. Aerul Si Apa.Componente Ale Mediului, , 178-187. Retrieved from https://www.proquest.com/scholarly-journals/problems-seagoing-navigation-bosphorus-strait/docview/1335068800/se-2

Synthetic-Based Drilling Mud Spills Factsheet. (2019). Retrieved February 18, 2022, from https://response.restoration.noaa.gov/sites/default/files/Synthetic-Drilling-Mud.pdf

Tan, K. L., & Hameed, B. H. (2017). Insight into the adsorption kinetics models for the removal of contaminants from aqueous solutions. *Journal of the Taiwan Institute of Chemical Engineers*, 74, 25-48.

Taufik, T., Jalil, Z. A., & Mursal, M. (2020). Use of SiO2 Rice Husk Ash and Ni in Materials Solid Hydrogen Storage Based on MgH2. *Journal of Aceh Physics Society*, 9(1), 9-12.

Tran, H. N. (2022). Improper Estimation of Thermodynamic Parameters in Adsorption Studies with Distribution Coefficient KD (qe/Ce) or Freundlich Constant (KF): Considerations from the Derivation of Dimensionless Thermodynamic Equilibrium Constant and Suggestions. *Adsorption Science & Technology*, 2022, 1–23. https://doi.org/10.1155/2022/5553212

Union of Concerned Scientists. (2016). The Truth about Tight Oil: Methane from Unconventional Oil Extraction Poses Significant Climate Risks. Union of Concerned Scientists.

United Nations Conference on Trade and Development (UNCTAD). (2020). Review on Maritime Transportation: Navigating Stormy Waters. United Nations. Retrieved January 10, 2022, from https://unctad.org/system/files/official-document/rmt2022_en.pdf

Usluer, H. B., & Oğuzülgen, S. (2018). Oil spill along the Turkish Straits Sea Area ; Accidents , Environmental pollution , Socio-Economic Impacts and Protection

Vegetable Oils and Animal Fats. (2023). US Environmental Protection Agency (EPA). Retrieved January 15, 2022, from https://www.epa.gov/emergency-response/vegetable-oils-and-animal-fats

Wang, J., & Guo, X. (2020). Adsorption kinetic models: Physical meanings, applications, and solving methods. Journal of Hazardous Materials, 390, 122156.

Williams, D. N., Gold, K. A., Holoman, T. R. P., Ehrman, S. H., & Wilson, O. C. (2006). Surface modification of magnetic nanoparticles using gum arabic. *Journal of Nanoparticle Research, 8*, 749-753.

Wolok, Eduart, Jamal Barafi, Navneet Joshi, Rossella Girimonte, and Sudip Chakraborty. (2020). "Study of bio-materials for removal of the oil spill." *Arabian Journal of Geosciences* 13, 1-11.

Yurdun, T. (2018). Effects of oil spills on human health. Oil Spill along the Turkish Straits, 313.

Zamparas, M., Tzivras, D., Dracopoulos, V., & Ioannides, T. (2020). Application of sorbents for oil spill cleanup focusing on natural-based modified materials: A review. Molecules, 25(19), 4522. 3.

Zhong, X., Li, P., Lin, X., Zhao, Z., He, Q. S., Niu, H., & Yang, J. (2022). Diluted Bitumen: Physicochemical Properties, Weathering Processes, Emergency Response, and Recovery. *Frontiers in Environmental Science*, 10. https://doi.org/10.3389/fenvs.2022.910365

CURRICULUM VITAE

Name Surname **:** Noor Khader Hussain HUSSAIN

EDUCATION **:**

B.Sc. **:** 2015, University of Basrah, Engineering Faculty, Mechanical Engineering Department

PROFESSIONAL EXPERIENCE AND REWARDS:

- 2015 winner of the 4th best graduation project award at Engineering Faculty, University of Basrah
- 2015-2017 AutoCAD Plant 3D trainer at ARATC
- 2017-2018 Technical Assistant at Majnoon Oilfield

PUBLICATIONS, PRESENTATIONS AND PATENTS ON THE THESIS:

- **Hussain N.K.H. ,** Saloğlu Dertli D. and Aydın A.A. 2023. Deniz Suyundan Gemi Kökenli Petrol Kirliliğinin Silika Aerojel ile Giderilmesi. 15. Ulusal Kimya Mühendisliği Kongresi, 4-7 Eylül 2023 Çanakkale, Türkiye.

OTHER PUBLICATIONS, PRESENTATIONS AND PATENTS:

- **Hussain N.K.H. ,** Saloğlu Dertli D. 2022. Beirut Explosion: One of The Largest Non-Nuclear Explosions in History. Research in Natural and Engineering Sciences, Volume III. Duvar Yayınevi. 5-17.
- **Hussain N.K.H.,** 2023. The Future Scenarios for Air Quality and Climate Change. Air pollution, Air Quality, and Climate Change. Elsevier. (submitted).